DYNAMIC CHARACTERIZATION OF RIGID POLYURETHANE FOAM

USED IN FEA SOFTBALL SIMULATIONS

By

SCOTT D. BURBANK

A thesis submitted in partial fulfillment of
the requirements for the degree of

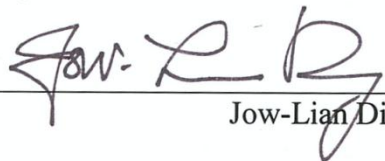MASTER OF SCIENCE IN MECHANICAL ENGINEERING

WASHINGTON STATE UNIVERSITY

Department of Mechanical and Materials Engineering

MAY 2012

To the Faculty of Washington State University:

The members of the Committee appointed to examine the thesis of SCOTT D. BURBANK find it satisfactory and recommend that it be accepted.

<div style="text-align: right">

_____
Lloyd V. Smith, Ph.D., Chair

_____
Jow-Lian Ding, Ph.D.

_____
William Cofer, Ph.D.

</div>

Acknowledgement

DYNAMIC CHARACTERIZATION OF RIGID POLYURETHANE FOAM

USED IN FEA SOFTBALL SIMULATIONS

Abstract

by Scott D. Burbank, M.S.
Washington State University
May 2012

Chair: Lloyd V. Smith

Numerical simulation of sport ball impacts is challenging due to the varied contact conditions involved and the difficulty in characterizing nonlinear materials at high strain rates. The following considers rigid polyurethane (PU) foam used in softballs. Past works have shown that load displacement curves from viscoelastic material models do not completely agree with experiment, suggesting incorrect mechanisms of compressive deformation. Additionally, dynamic testing using a pressure bar apparatus was unable to achieve strain rates low enough and dynamic mechanical analysis was unable to achieve strain magnitudes large enough to represent play conditions.

A method was developed to impact PU foam samples over a range of displacement rates and magnitudes representative of play conditions. A single, rate-independent master curve describing the stress-strain loading response was experimentally developed and implemented into LS-DYNA's Mat #57 foam material model. Five constant-rate loading curves were also derived experimentally and incorporated into a second foam material with rate-dependent formulation (Mat #83). Comparison of experimental and numerical load-displacement curves

produced agreeable results for both materials. Lack of temporal formulation for Mat #57 resulted in low rebounding rate dependence while Mat #83 showed penetration between contacting surfaces which led to nonlinear rebounding trends.

Both foam material models were implemented into a simulated softball which impacted flat and cylindrical surfaces at speeds between 60 and 120 mph. Mat #57 showed excellent correlation with both the shape and magnitude of experimental load-displacement curves, predicting softball deformation mechanisms better than previous linear-viscoelastic models both as a function of speed and surface geometry. Mat #83 characterized rebound behavior on both flat and cylindrical impact surfaces within 2% of experiment, which was better than any comparable model.

Table of Contents

List of Tables

List of Figures

1   Introduction

1.1   Introduction

Finite element analysis (FEA) has been widely implemented in sport ball simulations including golf, cricket, baseball, tennis, and softball. As technology and competition in the field of sports equipment increases, numerical modeling and simulation becomes a more viable and economical option in research and development. Numeric models that reliably simulate the performance of sports equipment before manufacturing would result in increased design optimization, and reduced time and cost associated with testing and manufacturing prototypes. An accurate ball impact model may be used, for instance, to simulate sport equipment performance, protective equipment or personal injury.

Softballs are difficult to model due to the dynamic environment of operation and the material sensitivity to temperature, humidity composition and rate of impact. Previous methods used to model softballs have been primarily phenomenological. These models incorporated a viscoelastic material model based on the rate dependent nature of the polyurethane (PU) ball core. Results, however, showed that load displacement curves from viscoelastic material models do not completely agree with experiment, suggesting incorrect mechanisms of compressive deformation. As the core of a softball consists of rigid structural foam, a foam material model, rather than viscoelastic, was used for this study.

Numerical foam material models require input of experimentally-derived compressive loading curves to describe the nonlinear response typical of foam. As a softball's PU foam matrix is rate dependent, the nonlinear compressive response necessitates development at strain rates typical of play (1000 to 2500 s^{-1}).

Softball performance is typically characterized by stiffness and liveliness which can be measured by standardized procedures. Performance, however, changes according to the ball speed and the geometry of the surface impacted. Accuracy of numerical ball models can be quantified by comparison with experimental impact performance.

The objective of this study was to develop a FEA softball model which could accurately emulate instrumented ball impact behavior both as a function of speed and surface geometry. New instrumentation was developed to characterize the PU foam at rates typical of play. Two numerical foam material models were developed with experimentally derived material loading responses and phenomenologically developed unloading responses. These materials were then applied to softball simulations and compared to previous material models to show performance improvement.

2   Background

2.1   Softball Composition

Predominantly, modern softballs consist of a rigid polyurethane (PU) foam core wrapped in a stitched leather cover which is colored either white or yellow (Fig. 2.1). ASTM standards for softballs used in bat certification testing limit the ball weight to between 6.25 oz and 6.75 oz. Circumference is also restricted to between 12.0 and 12.25 in (ASTM F1890, 2009).

Figure 2.1 Softball cross section showing the PU foam core.

The rigid polyurethane foam core is made by the reaction of polyisocyanates and polyols in the presence of catalysts, surfactants and blowing agents. Softballs are constructed by mixing the polyisocyanates and polyols in a large mixing tank. The batter, in the consistency of pancake mix is poured into the molds and then rotated while it cures over three minutes. Variation in cure time, chemical composition and temperature all lead to differences in foam properties (Bryson, 2009).

2.2   Ball Properties

2.2.1   Introduction

In an effort to keep the offense and defense sides of play fair, regulating agencies have placed limits on how well softball bats and balls can perform. Bats with high performance and balls with extra liveliness will shift the game balance in favor of the offense. This puts the defense at a disadvantage, increases the number of home runs, and reduces the skill required to excel in the sport. Because properties of both bat and ball contribute to the resultant batted ball speed (BBS), certification testing methods have been implemented to regulate bat and ball performance. The following will discuss the calculations, tolerances, and methods associated with softball performance properties.

2.2.2   COR and CCOR

The coefficient of restitution (COR) or e, which is a measure of the elasticity of an impact, is defined as the ratio of the relative normal velocity of two objects after impact to that before impact, as

$$e = -\left(\frac{v_1 - v_2}{V_1 - V_2}\right),$$
(2.1)

where v_1 and v_2 are the post impact rebound speeds and V_1 and V_2 are the incident speeds of objects 1 and 2 (Barnes, 1957). The chosen coordinate system is such that V_1 is negative. A perfectly elastic collision results in e = 1, while a perfectly inelastic collision sets e = 0 (Cross, 2000). The ASTM standard test method for measuring the COR of baseballs and softballs, as shown in Fig. 2.2, requires the ball to contact a massive rigid, flat wall of either wood or metal (ASTM F1887, 2009).

4
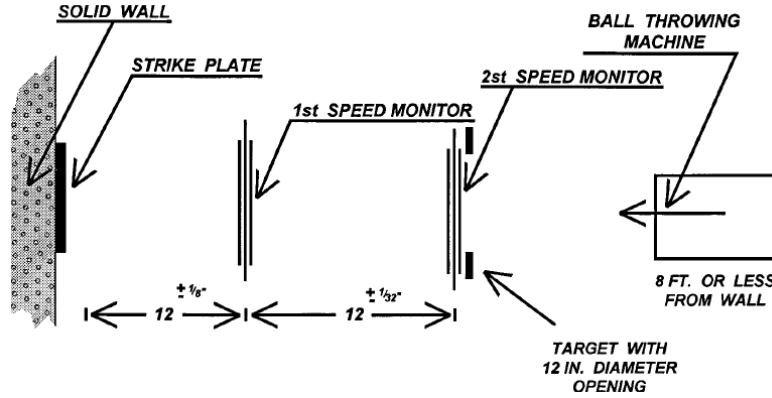
Figure 2.2 Schematic for measuring softball COR from ASTM F1887.

A stationary impact surface simplifies Eq. 2.1 to the ratio of the incident (v_i) and rebounding (v_r) ball speeds as

$$e = \frac{v_r}{v_i}\,.$$

(2.2)

Softballs used in bat certification testing have COR values ranging between 0.45 and 0.47 (ASTM F1890, 2009).

Because baseball and softball bats have cylindrical shapes, the cylindrical coefficient of restitution or CCOR is a useful property in defining ball impact behavior. CCOR is lower than COR due to a reduction in contact area which increases both ball deformation and dissipated energy. Equation 2.2 is used throughout this paper to calculate COR and CCOR.

Experimental results published elsewhere show a linear correlation between incident softball velocity and COR at speeds typical of play (Duris, 2004), (Biesen, 2006). The dependence of COR on speed was observed as early as the 19th centrury (Hodgkinson, 1835), and also applies to baseballs (Russel, 2005), and other sports balls (Cross, 2000) (Miller, 2006).

2.2.3   Static Compression

Ball compression is a measure of the quasi-static stiffness of a ball (ASTM F1888, 2009). The softball is compressed 0.25 inches between two flat surfaces as shown in Fig. 2.3, and ball

compression is the corresponding peak force. Softballs used in bat certification testing have compression values between 350 and 375 lbs.
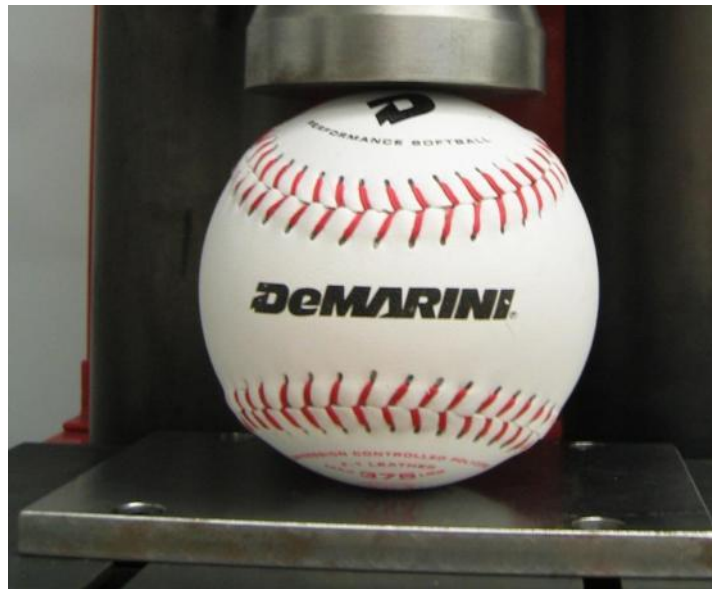
Figure 2.3 Static compression test setup.

Compression is an important property in determining general ball performance and establishing consistency in standardized bat testing. However, the rate of compression is about 10,000 times lower than what occurs in play (Duris, 2004).

2.2.4 Dynamic Stiffness

Dynamic stiffness (DS) quantifies ball stiffness for impacts at high speeds. The setup for measuring DS (Fig. 2.4) is also used to measure CCOR (ASTM F2845, 2010). Load cells mounted to a cylindrical surface capture the force exerted by the ball on the impact surface while speed monitors determine the incident and rebounding ball velocities.
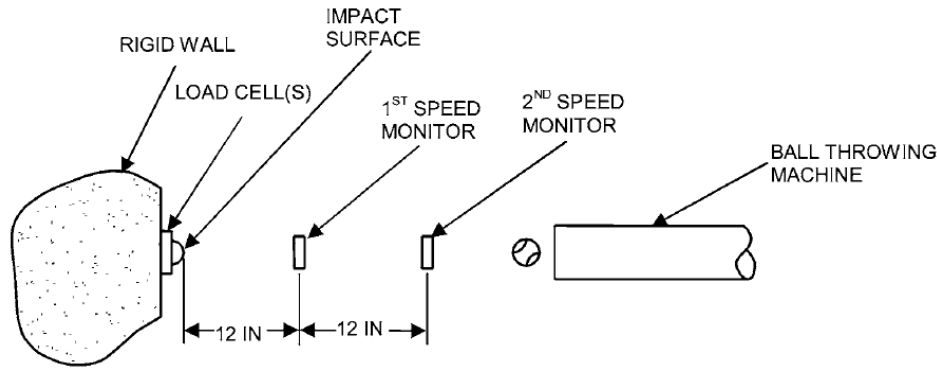
Figure 2.4 Schematic of Dynamic stiffness and CCOR measurement from ASTM F2845.

Smith compared quasi-static softball compression to DS and found bat performance to have a much stronger dependence on DS (Smith, 2008). Hendee, Greenwald, and Crisco tried unsuccessfully to correlate baseball compression to dynamic properties obtained by firing balls from an air cannon onto a rigidly mounted force plate. They found that energy losses during quasi-static compression differed from the dynamic energy losses (Hendee, 1998). Chauvin and Carlson also investigated the correlation between compression and dynamic impact response. They used pressure sensitive film to record the impact pressure distribution of baseballs and softballs. No correlation between compression and dynamic impact pressure was shown (Chauvin, 1997). These studies conclude that the dynamic impact behavior of sports balls is best characterized by dynamic properties, not static properties.

For dynamic stiffness and CCOR to effectively describe a bat-ball collision, the incoming velocity must account for a forward bat swing and backward bat recoil which occurs during play. Smith compared the dynamic stiffness of balls impacting a rigid half cylinder and free cylinders of differing mass that recoiled upon impact. When the speeds were matched correctly, Smith found the force-displacement curves to be similar. A dynamic stiffness speed of 95 MPH was found to represent the relative speed of a 110 MPH softball-bat collision (Smith, 2008).

To calculate dynamic stiffness, the ball is assumed to behave like a linear spring with stiffness k according to

$$f(t) = k\, x(t) \tag{2.3}$$

where f(t) and x(t) are force and displacement respectively. This assumption is justified as the loading stiffness of a typical softball, shown in Fig 2.5, is linear. Setting the incident kinetic energy of the ball equal to the potential energy of a linear spring at maximum deflection results in

$$\frac{1}{2}m_b v_i^{\,2} = \frac{1}{2}kx^2 \tag{2.4}$$

where m_b and v_i are respectively ball mass and initial velocity. Using Newton's second law,

$$f(t) = m_b \frac{d^2 x}{dt^2} \tag{2.5}$$

displacement x(t) of the ball center of mass (COM) is found by dividing the load signal by ball mass and integrating twice.

$$x(t) = \int_0^t \left(v_i - \int_0^t \frac{f(t)}{m_b}\,dt \right) dt \tag{2.6}$$

Combining Eq. 2.3-2.6 and evaluating at maximum force results in the equation for dynamic stiffness.

$$k = \frac{1}{m_b}\left(\frac{F_{max}}{v_i}\right)^2 \tag{2.7}$$
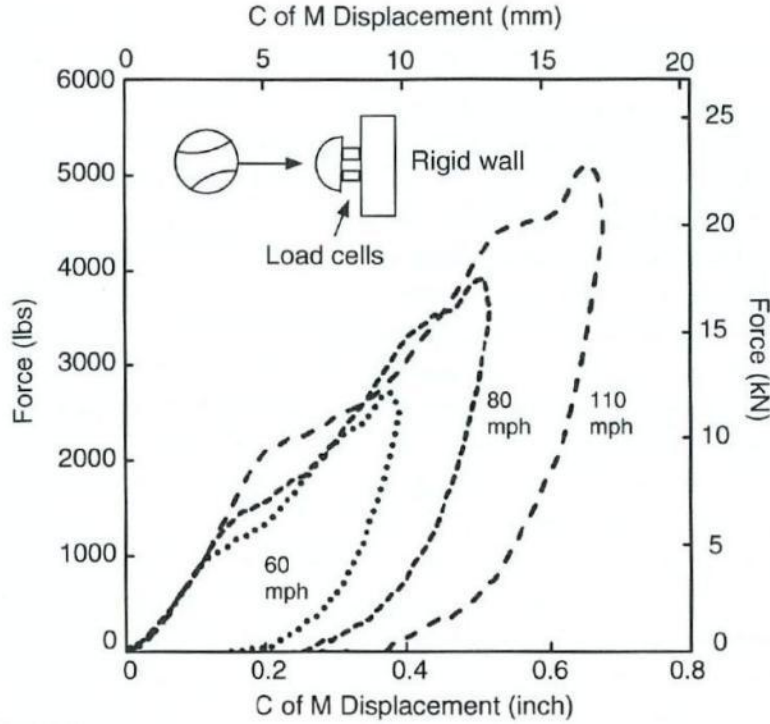
Figure 2.5 Typical load-displacement curves of a softball impact from Cross (Cross, 2000).

2.2.5 Impulse

The momentum of a translating object is a function of both mass and velocity. Impulse, or the change in momentum due to a collision, is calculated by integrating the load signal over the duration of impact (from t_0 to t_1).

$$I = \int_{t_0}^{t_1} F(t)dt \tag{2.8}$$

The impulse calculated in Eq. 2.8 can also be used to verify the measured initial and rebounding ball speeds by performing a momentum balance,

$$v_i m_b = I - v_r m_b \tag{2.9}$$

solving for impulse,

$$I = m_b(v_i + v_r) \tag{2.10}$$

and applying the instrumented velocity measurements where rebound speed is negative. An ideal collision will result in identical impulse values from Eq. *2.8* and *2.10*.

2.3 Conditioning

Polyurethane, being a viscoelastic polymer, is sensitive to temperature and humidity. Experimental testing which minimizes variation in environmental variables will enhance accuracy in measuring dynamic ball response. ASTM standards for measuring ball properties requires softballs to be conditioned at 50% (±10%) relative humidity (RH) at 72°F (±4°F) for a minimum of 14 days prior to testing (ASTM F1887, 2009), (ASTM F1888, 2009), (ASTM F2845, 2010). Duris monitored the weight gain of softballs transitioning from 30% to 50% RH and found the moisture saturation to be reached at 14 days (Duris, 2004). He also found the difference in COR of a ball conditioned at 30% RH and 55% RH to be less than 1%, whereas the static compression decreased 21% over the same humidity range. This suggests that rate effects may depend on moisture content.

Drane investigated the effects of temperature on baseball COR. Baseballs which were conditioned at 25, 40, 70 and 120°F and then impacted at 60mph were found to have statistically significant differences in COR. For 100 mph impacts (more representative of play conditions) the COR was unaffected by temperatures above freezing. The subfreezing temperature, however, significantly reduced the ball COR (Drane, 2004).

Duris performed a durability test on softballs to determine the effects of repeated impacts on ball performance. Three softballs were impacted 100 times at 90 mph continuously (within 120 minutes). Surface temperature of the ball increased 10°F over 100 impacts, and the data suggested that COR significantly changed. A second test, in which the balls were intermittently hit 100 times, allowed the ball temperature to stabilize after 10 consecutive hits. The COR remained relatively independent to the impact number. This suggests that ball temperature as

well as testing frequency affects ball performance. This also shows that damage to the ball's foam core as a result of repetitive impacting is minimal up to 100 impacts.

2.4   Polymeric Foam

The compressive response of closed cell foam, like the foam core of a softball, is governed by its cellular microstructure and is characterized by three regions of behavior shown in Fig. 2.6. At small strains the foam behaves elastically as the inherent stiffness of the material controls compression with minimal energy absorption. At a critical strain, the structure can no longer support loading and the cell walls begin to collapse. In the stress-strain curve a plateau region, in which the cells collapse at a relatively constant stress, continues until the cells are near full compression. Irrecoverable damage to the foam structure may occur during compression as the result of a brittle matrix, excessively high stresses, or degradation. As the cells fully collapse, stiffness rapidly increases in a densification region where the foam behaves much like the matrix material. Rate insensitive compressive response is often represented as a single master curve.
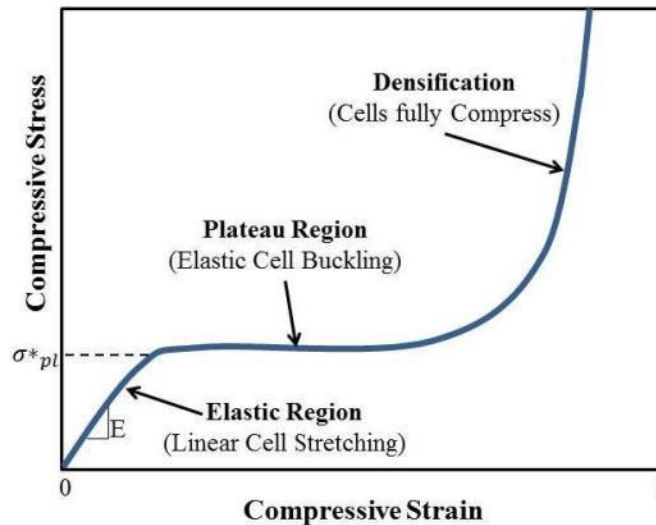
Figure 2.6 Typical Stress-strain loading response of polymeric foam under compression.

Because PU foam is viscoelastic, the compressive response is rate dependent. The plastic collapse strength of a foam (σ^*_{pl}), or the stress at which cell collapse begins, is directly

proportional to the yield strength of the solid of which it is made (Gibson, 1999). Increasing

strain rate ($\dot{\varepsilon}$) causes a slight increase in yield strength. Multiple studies listed by Gibson have

shown a linear increase in yield strength with increasing $\log \dot{\varepsilon}$. This behavior is shown for rigid

polystyrene foam in Fig. 2.7.
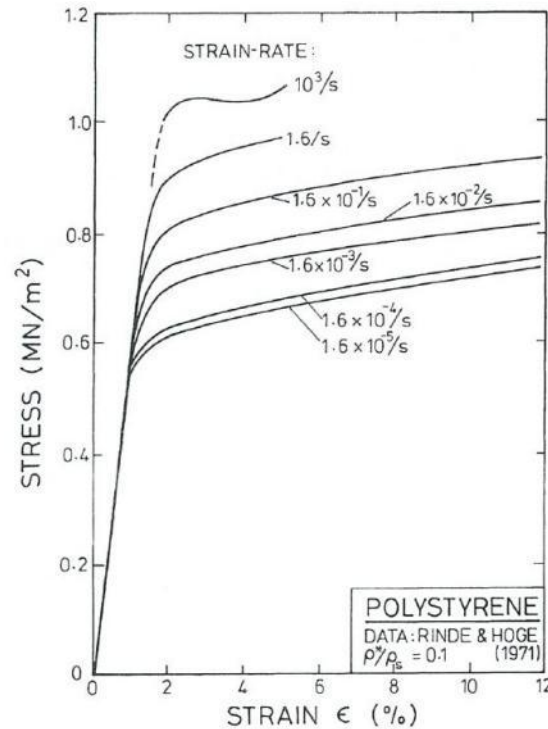
Figure 2.7 Rate dependent compressive stress-strain response of rigid Polystyrene foam at strain rates between 10^{-5} and 10^3 s^{-1} from Gibson.

Differences in σ^*_{pl} between the quasi static and high rate (2780 s^{-1}) stress-strain response of PU

softball foam have been shown both experimentally and numerically by Bryson. (Bryson, 2009).

Even more so than strain rate, the behavior of foam is dependent on temperature.

Compressive strength of rigid PU foam has shown a strong decreasing correlation with

increasing temperature (Traeger, 1967). Compressive Young's modulus of the same foam was

also shown to depend on temperature. The compressibility of the gas inside closed cell foams is

dependent on temperature. As the gas temperature lowers, its molecules vibrate slower and the

gas is more easily compressed. It is clear that the properties of a foam softball core will change

with temperature. Environmental conditioning is necessary to acquire consistent and accurate impact data.

Foam density contributes heavily to compressive response. Gibson defines relative density as the density of the cellular material divided by that of the solid from which the cell walls are made (Gibson, 1999). Increasing the relative density of foam increases Young's modulus, raises the plateau stress and reduces the strain at which densifcation starts. As relative density increases, the cell walls thicken and the pore spaces shrink. Gibson also stated that foams above a relative density of 0.3 are considered to be more of a solid which contains isolated pores. This distinction is highlighted in other experimentation (Chen, 2001). It was found that for PU foam with relative densities of 0.065, 0.128 and 0.249 at high enough rates (between 950 s^{-1} and 5300 s^{-1}), the viscous nature of the foam became saturated, and the mechanisms creating rate dependence were ineffectual, causing rate insensitivity for stress-strain curves below the densification region. Foam samples of higher relative density (0.37) over a similar strain rate range were observed to be strain rate dependent. The relative density of the foam used in this study is 0.33.

Goga investigated the impact response of PU foam as a function of density. A free falling 13.45 lb. weight was dropped onto foam specimens (3.15 x 3.15 x 2 inches) from a height of 30 inches. It was found that although the plateau region of the stress-strain curve was initiated at similar strain magnitudes (~.08) the corresponding plastic collapse strength was proportional to foam density. Density was also shown to have a substantial effect on deceleration during impact, as well as impact duration (Goga, 2010). It is clear that composition effects foam behavior during impact. Later discussion will highlight methods to minimize variation of foam composition.

Polymeric foam behavior is evident in the response mechanisms of a softball impact. Figure 2.5 shows a typical softball load-displacement curve with displacement being that of the ball COM. During compression, the plastic deformation of the foam due to cell collapse absorbs some of the impact energy. Hysteresis, or energy lost during impact, is represented as the area under the load-displacement curve. Increasing hysteresis in a softball model will decrease COR. After maximum compression, a softball continues recovering to its original shape even after the ball has separated contact. By the time a softball leaves contact with the bat it has recovered only about half of the deformation (Faber, 2010). Minimal displacement recovery is shown after peak deformation and throughout the unloading phase. The slow recovery is caused by the creep response of the viscoelastic PU matrix.

2.5   Instrumentation

Experimental foam impacts must occur at strain rates representative of play. The peak strain rate during an impact occurs just as the collision begins, which for bat-ball impacts is between 1000 and 2500 s^{-1} (Bryson, 2009). Few devices exist which are capable of measuring foam properties at these rates. Universal testing machines (UTM) have peak strain rates well below this range (25 s^{-1}).

Drop towers have been used to characterize polymeric foams, but not for the purpose of sports ball modeling (Goods, 2003), (Serifi, 2003). Maximum speed ranges of a typical drop tower are around 15 ft/s, which is well below the speed of a bat-ball collision (Instron, 2009). Optional features, such as springs can be added to increase the potential energy of the drop weight to achieve strain rates similar to play. The cost of a specialized drop tower, however, is not justified.

Previous studies investigating the impact response of PU foam have used Split Hopkinson pressure bar (SHPB) devices (Bryson, 2009), (Chen, 2001). The device uses strain gages to measure the difference in reflected and transmitted compression waves propagating through two axially aligned, long, metal bars with a foam sample suspended between the two. A striker bar, propelled by compressed air, causes a compression wave by colliding with one of the bars. By adjusting either the initial striker bar velocity, or material sample thickness, strain rate can be adjusted. Bryson achieved a minimal strain rate of 2780 s^{-1} in PU foam samples by using a 9 inch long, 0.5 inch diameter aluminum rod, with an average foam specimen thickness of .08 inches. Chen measured strain rates from 950 s^{-1} to 5300 s^{-1} in PU foam samples by using a 12 inch long, 0.75 inch diameter aluminum striker bar to impact samples of thicknesses between .067 and .19 inches.

Besides the ability to measure foam properties at rates typical of play, significant problems exist in a traditional SHPB. The first is that the magnitude of the transmitted wave is often small and difficult to distinguish from the baseline electrical noise. PU foam, being a relatively soft material, has low elastic impedance, which results in a slower transmitted compression wave. While many of the challenges of the SHPB can be overcome, the minimum strain rate cannot (Bryson, 2009).

2.6   Ball Modeling

Numerical modeling of softballs has received limited attention compared to the baseball, which has been the focus of previous work by Mustone & Sherwood, Shenoy, and others (Munstone, 2000), (Shenoy, 2000). Softballs have been previously modeled as isotropic and homogeneous, with mass and diameter equal to a standard softball. The contribution of the cover is often neglected as justified by Duris (Duris, 2004). He tested softballs with and without covers

at various speeds and observed a 4.2% increase in COR and a 16.6% decrease in maximum

impact force without the cover. Normalizing the results with ball momentum increased the

maximum force by 4.4%, suggesting the large change in maximum force was due to loss of the

cover mass. Removing the cover was also found to have a minimal effect on rate dependence, as

the COR slope with respect to pitch speed with and without a cover was observed to remain

approximately constant.

An early softball model by Sandmeyer used a three parameter power law viscoelastic

material model with a time dependent shear modulus defined by

$$G(t) = G_\infty + (G_0 - G_\infty)e^{-\beta t} \tag{2.11}$$

where G_∞ and G_0 were the long term and instantaneous shear moduli, and β was the decay

constant (Sandmeyer, 1994). In the power law model, stiffness is governed by the long term

modulus for loading conditions of extended duration, while brief time intervals are governed by

the short term modulus. The decay constant controls how quickly the resultant modulus

transitions between the two moduli. Sandmeyer's softball model was implemented into a

simulated bat-ball collision. The numerical ball COR was systematically adjusted to match

experimental COR values obtained from 58 mph impacts with a 2.5 in thick, rigidly mounted

wood plank.

Duris also investigated a power law model as well as a general viscoelastic model based

on a six term Prony series. The Prony series was based on a spring-damper system and used a

series of Voight elements as shown in Fig. 2.8.
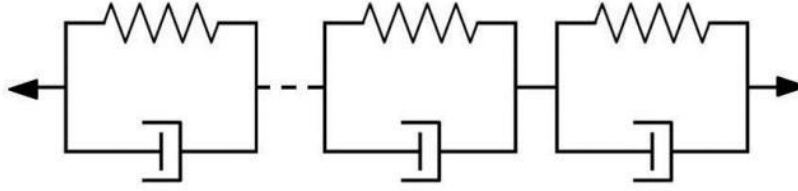
Figure 2.8 Schematic of a Prony series material model characterized by multiple Voight elements in series.

The time dependent shear modulus *G(t)* is defined as the summation of multiple Voight elements,

$$G(t) = \sum_{i=1}^{N} g_i e^{-\beta_i t} \tag{2.12}$$

each having an individual shear modulus g_i and decay constant β_i. Duris defined six shear moduli and decay constants from dynamic mechanical analysis (DMA) of a polyurethane softball core sample. The softball model was developed in LS-DYNA and was modeled as an isotropic, homogeneous sphere using eight-noded, solid elements. Both power law and Prony series viscoelastic models were applied to a simulated impact on cylindrical and flat surfaces and were compared to experimental data. Duris concluded that the Prony series model did not match well with experiment because material deformation during DMA testing was low compared to deformation created in the model. Good characterization was found in the power law models, which were developed phenomenologically. Ten models with differing power law parameters were found to fit experimental COR and maximum impact force data for a 60 mph impact. Two of those showed fair agreement with experimental force-time curves at speeds ranging between 60 and 110 mph. None of the models, however, were able to fit experimental cylindrical impact data. A high Poisson's ratio (0.5) was observed in the model, which is uncharacteristic of an actual ball (≈ 0.1 as stated by Duris). It was suggested that future work focus on a different material model which could better capture the low Poisson effect and improve response to varied impact surface geometry.

A numerical bat-ball collision was developed by Biesen to describe the plastic deformation of aluminum softball bats (Biesen, 2006). The softball was modeled in LS-DYNA as a solid, isotropic sphere. Tuning of the model was accomplished by simulating a dynamic stiffness test and comparing the results to instrumented measurements of softball CCOR and DS at speeds between 60 and 130 mph. Viscoelastic parameters from Eq. 2.11 were adjusted at each speed to produce good agreement. The model was able to accurately describe ball hardness and energy loss for a number of speeds; however the desired accuracy was only achieved by tailoring the ball's parameters at each impact speed.

Faber developed an FEA bat-ball collision in LS-DYNA (Faber, 2010). A power law viscoelastic material model was applied to a modeled dynamic stiffness test (Fig. 2.4). Numerical force-time and force-displacement curves were compared to experiment and are shown in Fig. 2.9 and 2.10.
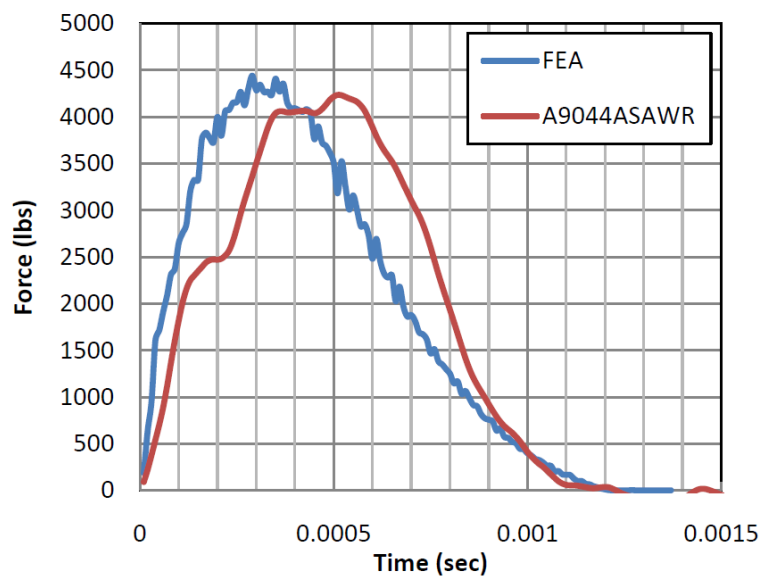
Figure 2.9 Force-time curve comparison of experiment and FEA softball impacts at 95 mph from Faber.
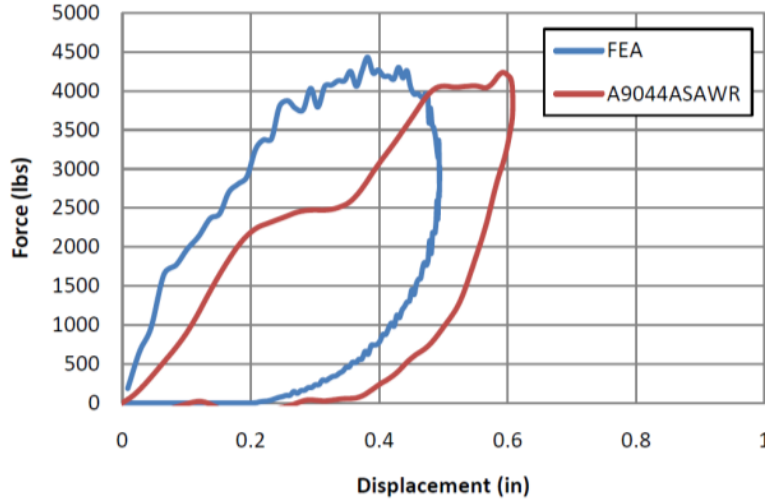
Figure 2.10 Force-displacement curve comparison of experiment and FEA softball impacts at 95 mph from Faber.

FEA ball stiffness was shown to be greater than experiment, which resulted in a lower displacement. A difference in load-displacement curve shape in Fig. 2.10 suggests an incorrect material characterization. Despite the difference in load curves, the model did agree with experimental CCOR and DS for a 95 mph impact with viscoelastic material parameters of $G_0=20$ ksi, $G_\infty=1.0$ ksi and $\beta = 6.8 \times 10^4$ from Eq. 2.11.

A split Hopkinson pressure bar (SHPB) device was used by Bryson in an effort to characterize PU softball foam at high strain rates (Bryson, 2009). Stress-strain curves from experimental testing were compared to mathematical viscoelastic models defined by equations 2.13 and 2.14.

$$\sigma(t) = 2R(1 + v)\left(G_\infty t + \frac{G_0 - G_\infty}{\beta}(1 - e^{-\beta t})\right) \tag{2.13}$$

$$\varepsilon(t) = RtH(t) \tag{2.14}$$

A constant strain rate, *R,* was assumed where v was Poisson's ratio and the step function *H(t)* was defined as 0 for t < 0 and 1 for t > 0. The shear moduli were obtained from finite element models created by Faber (Faber, 2010), which had the same DS as the foam samples tested in the SHPB. An over-prediction of stiffness in the mathematical model was attributed to collecting

data at excessively high strain rates (2780 s^{-1}). Strain rates could not be lowered as an increased sample thickness caused high signal to noise ratios, and bar velocity was already minimized.

2.7   Summary

Standardized procedures to test softball impact properties which incorporate environmental conditioning have been established to obtain accurate and consistent experimental data. Measureable properties like COR and DS are obtained from high speed impacts and are used to quantify ball performance.

The behavior of a softball during impact is governed by its composed material. The closed-cell foam microstructure produces a unique three-phase compressive loading response while the viscoelastic PU matrix causes rate dependence. The behavior of foam is also affected by its density and external factors like humidity and temperature. Neglecting the cover does not significantly change performance if the cover weight is accounted for.

Current instrumentation setups are not well suited to impact foam samples at rates typical of play. Devices such as a UTM, drop towers and SHPB devices each have shortcomings inherent in their design which limit testing capabilities. New instrumentation is needed to achieve the necessary strain rates and magnitudes.

Previous work in softball modeling has produced promising results, but there still remains room for improvement. Characterizations matching experimental COR and DS have been shown at a single speed, but rate dependence as well as correct response to variation in surface geometry have not been accurately simulated. While implementation of viscoelastic material models has been typical, no work has yet treated the softball as structural foam. High Poisson ratios and misshaped load-displacement curves suggest that softballs have a different mechanism of deformation than what has been characterized previously.

2.8   References

ASTM F1887. 2009. Standard test method for measuring the coefficient of restitution of baseballs and softballs. West Conshohocken, PA : s.n., 2009.

ASTM F1888. 2009. Standard test method for compression-displacement of baseballs and softballs. West Conchohocken, PA : s.n., 2009.

ASTM F1890. 2009. Standard test method for measuring softball bat performance factor. West Conshohocken. PA : s.n., 2009.

ASTM F2845. 2010. Measuring the Dynamic Stiffness (DS) and Cylinderical Coefficient of Restitution (CCOR) of Baseballs and Softballs. s.l. : American Society of Testing and Materials, 2010.

Barnes, G. 1957. Study of Collisions. *Am. J. Phys.* 1957. Vol. 26, p. 9.

Biesen, E. D. 2006. Prediction of plastic deformation in aluminum softball bats using finite element analysis. *Master's Thesis, Washington State University.* 2006.

Brody, H. 1997. The physics of tennis. III. The ball racket interaction. s.l. : American Journal of Physics, 1997. Vol. 65, 10, p 981-987.

Bryson, A. J. 2009. Impact response of polyurethane. *Master's thesis, Washington State University.* 2009.

Chauvin, D. J. and Carlson, L.E. 1997. A comparative test method for dynamic response of baseballs and softballs. *International symposioum on safety in baseball/softball.* 1997. p. 38-46.

Chen, W. Lu,F. Winfree, N. 2001. High-strain-rate compressive behavior of a rigid polyurethane foam with various densities. *Experimental Mechanics.* 2001. p. 65-73.

Cross, R. 2000. The coefficient of restitution for collisions of happy balls, unhappy balls, and tennis balls. *Am. J Phys.* 2000. Vol. 68, p. 1025-1031.

Drane, P.J., Sherwood, J.A. 2004. Characterization of the effect of temperature on baseball COR performance. *Proceedings from the Eng. of Sport 5.* 2004. p. 59-65.

Duris, J. and Smith, L.V. 2004. Evaluating test methods used to characterize softballs. *5th International Conference on the Engineering of Sport,.* 2004. Vol. 2, p. 80-86.

Duris, J. G. 2004. Experimental and numerical characterization of softballs. *Master's Thesis, Washington State University.* 2004.

Faber, W. L. 2010. Reducing the effect of ball variation in bat performance measurements. *Master's thesis, Washington State University.* 2010.

Gibson L, Ashby M. 1999. *Cellular Solids.* Cambridge, MA : Cambridge University Press, 1999. ISBN: 0521499119.

Gibson, L. Ashby, M. 1999. *Cellular Solids.* Cambridge, MA : Cambridge University Press, 1999. ISBN: 0521499119.

Goga, Vladimir. 2010. Measurement of the energy absorption capability of polyurethane foam. *Portal pre odborne publikovanie ISSN 1338-0087.* 2010.

Goods, S. H. Dentinger, P. M. Whinnery, L. L. 2003. Flashfoam: A triboluminescent Polymer Foam for Mechanical Sensing. *Sandina National Laboratories Report.* 2003.

Hendee, S.P., Greenwald, R. M., and Crisco, J. J. 1998. Static and Dynamic Properties of Various Baseballs. *Journal of Applied Biomechanics.* 1998. Vols. 14, p. 390-400.

Hodgkinson, E. 1835. Rept. *Brit. Assoc. Advance. of Sci. 4th meeting.* 1835.

Instron. 2009. Drop Weight Impact Testing Systems. [Online] 2009. [Cited: October 24, 2011.] http://www.instron.us/wa/product/Drop-Weight-Impact-Testing-Systems.aspx.

LSTC. 2010. LS-DYNA Keyword User's Manual Volume II Material Models. *Version 971/ Rev 5.* 2010.

Miller, S. 2006. Modern tennis rackets, balls and surfaces. *J. Sports Med.* 2006. Vol. 40(5), p. 401-405.

Munstone, T. Sherwood, J. 2000. Using LS-DYNA to develop a baseball bat performance and design tool. Detroit, MI : s.n., 2000.

Russel, D. A. 2005. Physics and Acoustics of Baseball and softball bats. *Kettering University Website.* [Online] 2005. [Cited: 8 26, 2011.] http://www.kettering.edu/physics/drussell/bats-new/nonlinear-ball.html.

Sambamoorthy, B. Halder, T. 2001. Characterization and Component Level Correlation of Energy Absorbing (EA) Polyurethane Foams (PU) using LS-DYNA Material Models. *LS_DYNA Eurpoean Conference.* 2001.

Sandmeyer, B.J. 1994. Simulation of bat/ball impacts using finite element analysis. *Master's Thesis, Oregon State University.* 1994.

Serifi, E. Hirth, A. Matthaei, S. Mullershon, H. 2003. Modelling of Foams using MAT 83-Preparation and Evaluation of Experimental Data. *4th European LS-Dyna Users Conference.* 2003.

Shenoy, M. M. 2000. Numerical simulation of baseball bat performance. *Master's Thesis, Washington State University.* 2000.

Smith, L.V. 2008. Measuring the hardness of softballs. *IMAC-XXVI.* Orlando, FL : s.n., 2008.

Traeger, R K. 1967. Physical Properties of Rigid Polyurethane Foams. s.l. : Journal of Cellular plastics, 1967. Vol. 3, 405.

3   Foam Testing

3.1   Introduction

The FEA foam material models used in this study required experimentally developed compressive loading curves to govern the model's compressive response. Obtaining compressive foam properties at rates typical of play is not trivial. Limitations and disadvantages in established instrumentation has led to the development of a new device ideally suited to measure the impact response of soft materials over a wide range in strain rates.

The following will present the new device setup, and the methods used to obtain experimental foam impact data. As PU foam is viscoelastic, and thus has rate dependent behavior, the effect of loading rate was also explored.

3.2   Apparatus

3.2.1   Device Hardware

The device used a small, horizontally-mounted air cannon to fire a striker bar that could achieve a larger range in speed than is possible with a standard drop tower (7 to 46 mph). Foam samples were mounted to a stationary load cell and impacted by the striker bar as shown in Fig. 3.1. Bar speed and impact force were measured to calculate impact properties and produce stress-strain curves. These measurements enabled a more direct calculation of stress and strain in the tested material compared to a pressure bar device.
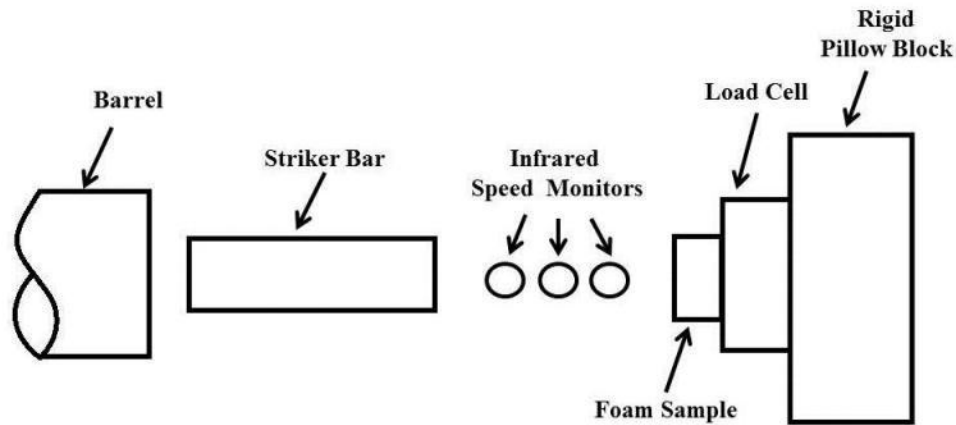
Figure 3.1 Schematic of the new device used to impact softball foam samples.

The device, as shown in Fig. 3.2, consisted of 45x45 Bosch aluminum structural framing which was reinforced by ninety degree gussets. The main horizontal member was a 3 foot piece of 45x90 Bosch framing on which was mounted the barrel, fiber optic sensors, and load cell. The cannon and the load cell were each secured to the frame using pillow blocks. Set screws in each pillow block enabled the cannon and load cell to be aligned.
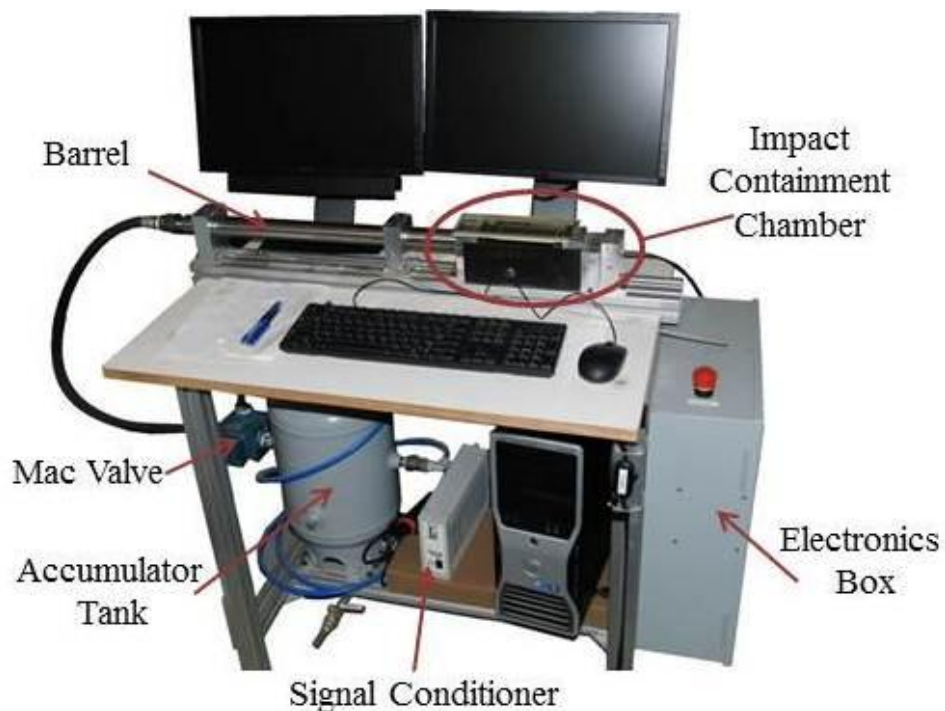
Figure 3.2 Instrumentation used to impact foam samples.

The foam samples were mounted with a thin coating of synthetic lubricating grease to a load cell which measured the force of impact. The load cell (PCB model 208C03) was designed for dynamic loading applications and had a compressive rating of 500 lbs. Load measurements were taken at a sample rate of 1.0 MHz. The load cell was connected to a signal conditioner (PCB model 482A21) by a 10-32 Coaxial to BNC cable. To securely attach the load cell to the device frame, a threaded steel cylinder was machined and securely thread onto the load cell using a thread locking adhesive. The steel insert was fit inside of a pillow block and aligned with set screws. Once aligned, additional pillow blocks were wedged behind the steel cylinder to prevent set screw slippage.

Three fiber optic sensors (Banner D10) were used to measure incident striker bar speed. Each sensor was set to a response time of 50 μs and had a detection range of 6 inches. Cables leading from each sensor were mounted to an aluminum plate which had three holes spaced 1.5 inches apart (Fig. 3.3). The cables were designed to both transmit and receive light. As the striker bar passed in front of a cable, the emitted light would reflect back into the cable and be measured by the sensor. Adaptive light thresholds for each sensor were set so as to trigger an analog signal when the striker bar passed by.
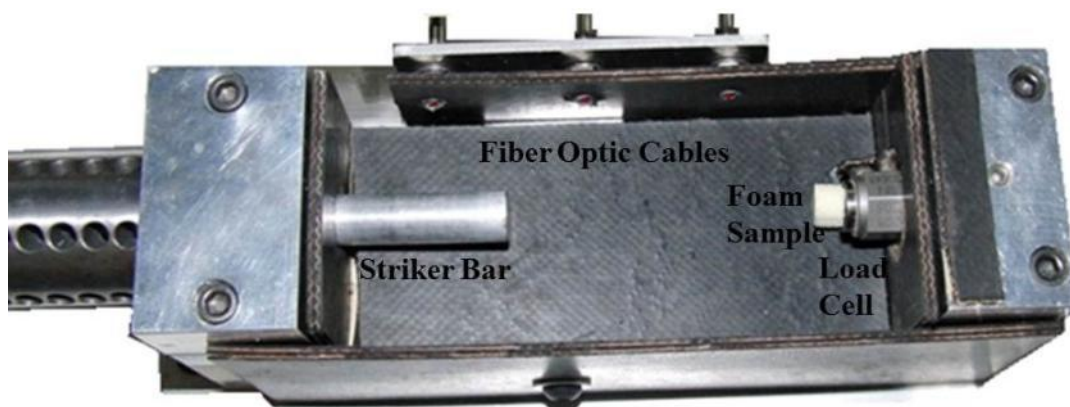
Figure 3.3 Visual layout of the impact containment chamber.

Striker bar speed was measured by dividing the distance between sensors by the difference in time between triggers. The arrangement of three fiber optic sensors produced three speed measurements: one measurement from sensors one and two (v_{12}), from sensors two and three (v_{23}), and from sensors one and three (v_{13}). This enabled each speed measurement to be verified by the other two. As v_{23} was the speed measurement taken closest to impact, it was used as the initial striker bar speed for calculating impact properties.

The source of propulsion for the striker bar was compressed air. The device was supplied with compressed air which was stored in a five gallon accumulator tank. The tank pressure was controlled using a digital regulator (SMC ITV3050-31N3CL4) shown in Fig. 3.4. Connected to the tank was a pneumatic valve (MAC 57D-32-110AA) which released the air to propel the striker bar. The barrel was attached to the valve using a 0.5 inch diameter high pressure hose. Measuring 24 inches long with a 0.5 inch bore, the steel barrel had vent holes drilled radially along the last 6 inches. The vent holes allowed compressed air within the barrel to be released as the striker bar exited the barrel, producing a more consistent bar speed.

Figure 3.4 Pressure Regulator.

The load cell, pressure regulator and MAC valve were wired to a Dell T3500 desktop computer using a connection block SCB-68 made by National Instruments (NI). The connection

block was wired to a NI analog-to-digital PCI-6111 board capable of sampling at 5 mega-

samples per second. The MAC valve was activated by a 24V signal supplied through a solid state

relay. It was given its own power supply to minimize signal spikes observed when the valve

opened and closed. The two analog channels on the PCI-6111 board were connected to the load

cell and pressure regulator, so a NI CB-68LP I/O connector block and NI PCI-6602 board were

installed to attach the fiber optic sensors to analog channels.

3.2.2   Device Operation

All electronic functions, calculations and data logging for the device were controlled

using NI's LabVIEW software. A screen image of the user interface is shown in Fig. 3.5 and

detailed operating instructions of the device are listed in Appendix B. Before the striker bar was

fired, accumulator tank pressure and load cell sampling frequency could be adjusted. Foam

sample diameter d, and length l_0 were input by the user as well as the mass of the striker bar m_b.

After a foam sample was mounted to the load cell and the striker bar was pushed to the breach of

the barrel using a small rod, the fire button was pushed. The MAC valve then opened, releasing

the pressurized air within the accumulator tank to the barrel which forced the striker bar out.

After measuring striker bar speed and impact force, impact properties were calculated and logged

along with tabulated load-displacement and stress-strain data.
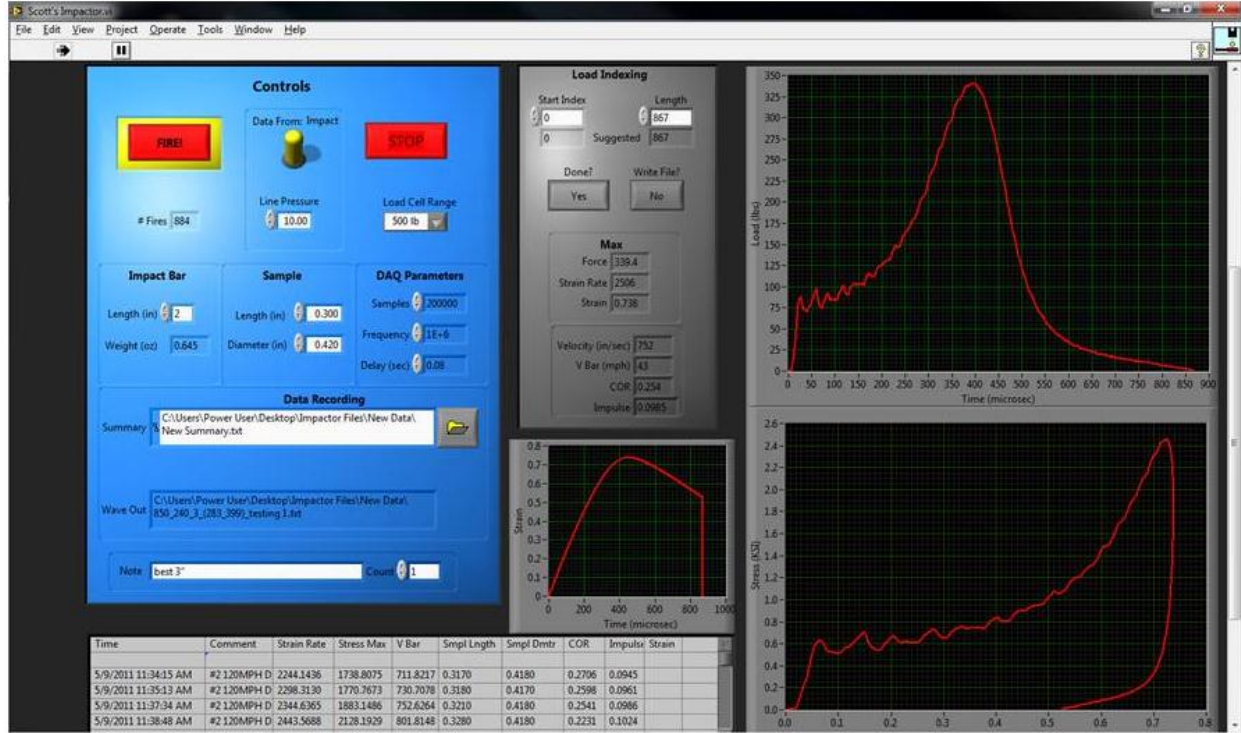
Figure 3.5 Screen shot of the LabVIEW vi used to operate the impactor device. Plots of strain (center), load-time (top right) and a stress-strain curve (lower right) were output for each impact.

Calculations of foam sample impact properties performed in LabVIEW were very similar

to the equations used for softball impact testing discussed in Chapter 2. The initial bar velocity

v_{23}, and user-defined mass m_b of the striker bar, along with the load signal were used to calculate

the displacement of the striker bar COM during impact (Eq. 2.6). Foam sample displacement was

assumed to be equal to the striker bar displacement. Because rebound speed was not measured,

COR was calculated from Eq. 2.2 where rebound speed was calculated as

$$v_r = v_i - \int_0^t \frac{f(t)}{m_b} dt \, .$$ (3.1)

Average engineering strain in the foam sample was calculated by dividing the user defined

sample thickness by the calculated displacement.

$$\varepsilon(t) = \frac{x(t)}{l_0}$$ (3.2)

29

Engineering stress was calculated by dividing the load signal by the cross sectional area A.

$$\sigma(t) = \frac{f(t)}{A} \tag{3.3}$$

Eq. 2.8 was used to calculate impulse. Substitution of the calculated rebound velocity from Eq. 3.1 into Eq. 2.10 would result in Eq. 2.8. Thus, the method of speed and force measurement verification by means of calculating impulse described in Chapter 2 cannot be done for this device.

3.3   Foam Samples

In an effort to maintain consistency in softball composition and size, a single ball model was used for all experimental testing as shown in Fig. 2.1 (DeMarini A9044). The ball was ASA certified with a rated COR of 0.44 and a nominal compression of 375 lbs.

The diameter of the foam samples used for impact testing was selected based on the consideration of several factors. If the specimen diameter were larger than the striker bar diameter, an undesirable non-uniform load distribution would result. If the specimen diameter were to decrease, higher stresses would be developed for a given striker bar speed. Smaller specimens are disadvantaged in that small imperfections, such as surface finish or inhomogeneous foam, produce more significant changes in experimental results. Inspection of the foam under a microscope showed the average cell size to be about two orders of magnitude smaller than the specimen dimensions (0.004 inches), as shown in Fig 3.6. It was determined that a specimen diameter slightly smaller than the striker bar (0.42 inches), would ensure uniform load distribution and provide sufficient stress levels, while minimizing the effects of possible surface defects or foam inhomogeneity.
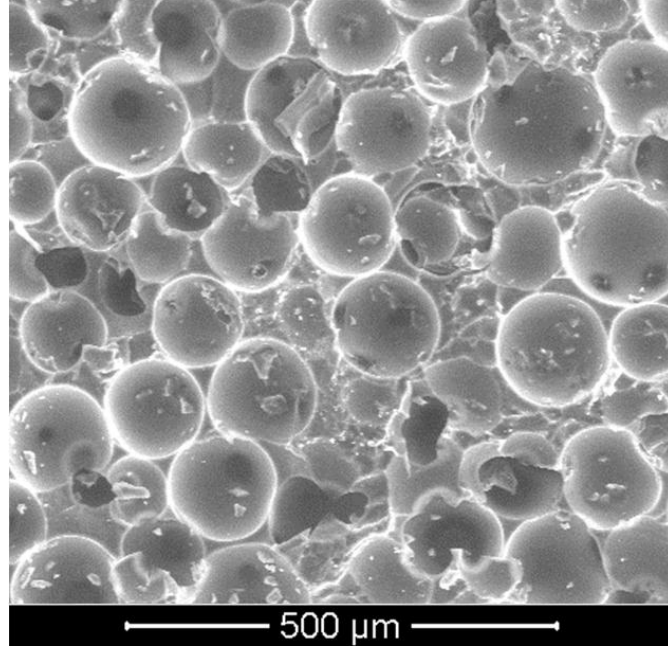
Figure 3.6 SEM image of softball foam cross section.

Specimen length also had limitations based on several factors. Longer foam samples are harder to accurately manufacture. A shorter foam sample would allow less stopping distance for the striker bar at a given speed. This would increase the bar's deceleration and impact force. Using a thinner sample would reduce the striker bar speed which would exceed the capacity of the load cell (500 lbs). The same effect would result from impacting samples made of stiffer materials like solid plastics or metals.

Specimen length also directly affected strain rate. Maximum strain rate in the sample occurred just as the impact began and was calculated as

$$\dot{\varepsilon}_{max} = \frac{v_{23}}{l_0}.$$ (3.4)

Dividing the striker bar speed which caused a 500 lb. impact force (45 mph) by the desired maximum strain rate of 2500 s^{-1} resulted in a sample length of 0.3 inches.

The foam samples were all machined from new softballs which had been impacted once on a dynamic stiffness test apparatus at 60 mph. Each softball was tested to ensure COR, and ball

weight were typical for the model (discussed in Chapter 4) and that the load curves looked similar. Only one impact was performed to limit possible damage effects. The evolution of the samples from a softball is shown in Fig. 3.7. After removing the leather cover, two wafers were cut from each ball using a 12 inch miter saw. The wafers were then sanded to 0.3 inches to produce a smooth, flat surface and to achieve the correct thickness. Bryson, in making softball foam samples, used a hole punch to stamp out specimens from 0.08 inch thick wafers (Bryson, 2009). Using a hole punch to make samples from 0.3 inch wafers produced jagged edges. It was also difficult to use the hole punch to make samples with perpendicular edges. A new approach was needed to produce clean, square samples.

Figure 3.7 Step by step machining of a softball to obtain samples: I. Removal of the cover. II. Cutting wafers out of the ball. III. Drilling the samples using a custom hole saw.

Standard hole saws were considered but were found to have several downsides. The smallest hole saw sold in a standard hardware set had a 0.5 inch diameter, which was too large. The teeth of standard hole saws were too course and would rip the soft PU foam as the holes were made. The blade material was also too thick. This caused the saw to not stay in the same place as penetration started, which damaged the foam surface.

A custom hole saw was developed which resolved the problems encountered with standard hole saws. A section of aluminum tubing with an outside diameter of 0.5 inches was sanded on the inside to a custom diameter of just over 0.4 inches. Square teeth were cut into the end to prevent the foam from ripping. The teeth were tapered as shown in Fig 3.8, to decrease the initial contact surface area which increased hole saw stability as penetration started. When mounted in a drill press, the hole saw produced straight and square samples with excellent surface smoothness (Fig. 3.9). The nominal dimensions of the foam samples used in this study were 0.42 inches in diameter and 0.3 inches long with ±1% tolerance.
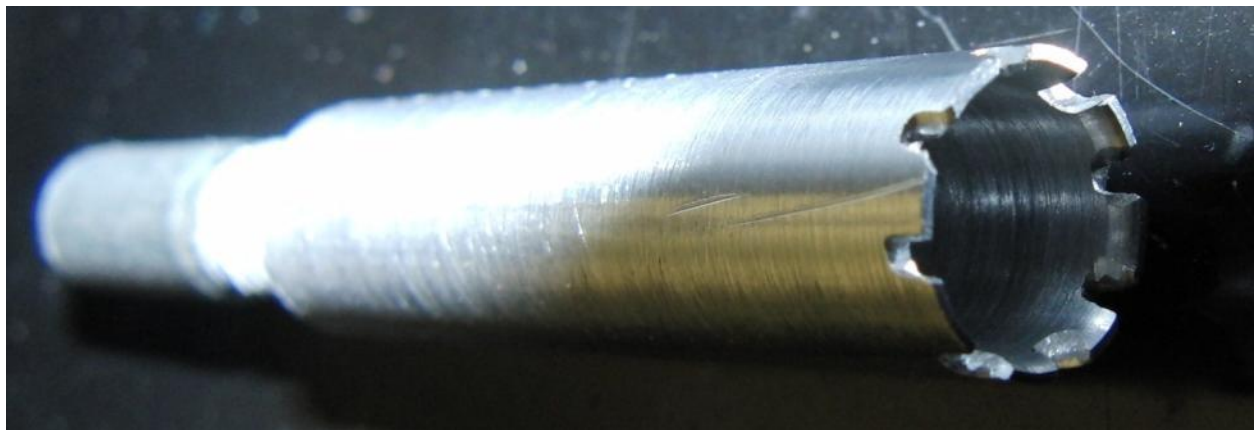
Figure 3.8 Custom hole saw used to machine foam samples from wafers.

Figure 3.9 Standard foam sample used for impact testing.

3.4   Verification

To verify velocity and displacement measurements for the new device, a Phantom V711 high speed camera was placed directly above the foam sample as shown in Fig. 3.10. Videos of ten impacts at high (> 40 mph) and low (< 23 mph) speeds were taken at 60,000 frames per second. ProAnalyst motion tracking software was used to measure initial and rebounding striker bar velocities as well as foam sample displacement.

Figure 3.10 Setup for velocity and displacement verification using a high speed camera.

Figures 3.11-3.13 show the comparison of measurement methods at the lower impact speed. Incoming velocity was quite accurate with an average difference of 1.6% at low speeds and 1.7% at high speeds. Sample displacement was also very similar with an average difference of 2% at low speeds and 1.5% at high speeds. Rebound velocity did not match as well, with the fiber optic sensors measuring low by an average of 9.8% (low speeds) and 13.9% (high speeds) compared to the high speed videos.
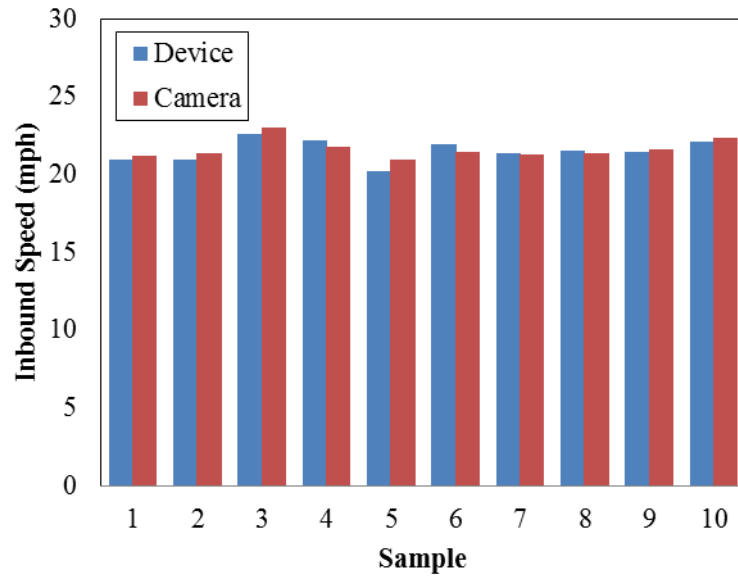
Figure 3.11 Comparison of initial striker bar speed as measured by the impactor device and the high speed camera.
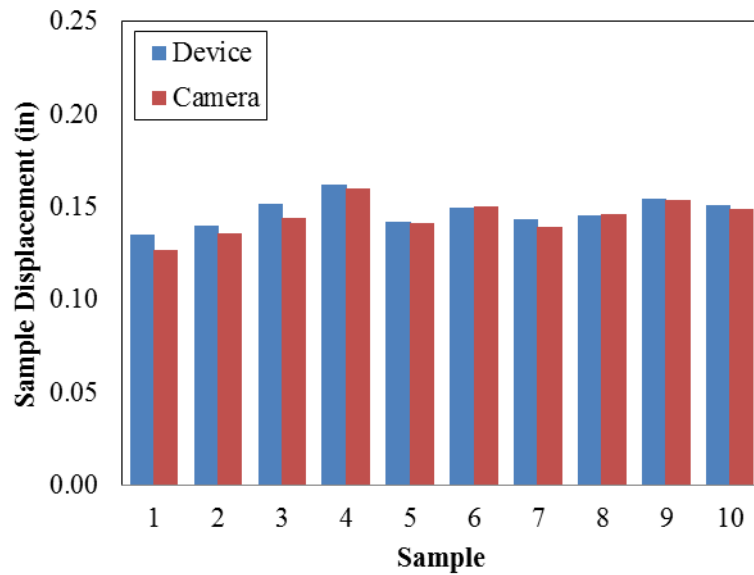
Figure 3.12 Comparison of sample displacement as measured by the impactor device and the high speed camera.
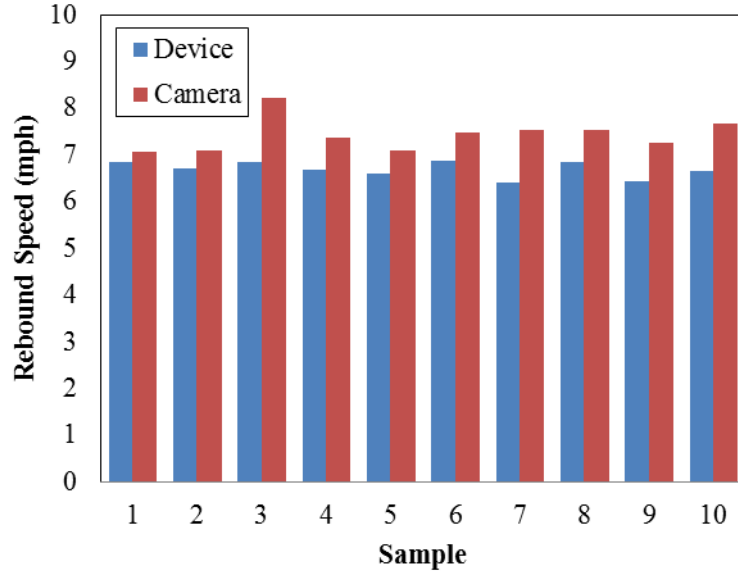
Figure 3.13 Comparison of rebound speed as measured by the impactor device and the high speed camera.

A second method used to verify instrumented measurements involved impacting a 1 inch helical metal spring. The collision between the striker bar and metal spring was modeled as a simple mass spring system represented as the differential equation

$$m_b \ddot{x}(t) + kx(t) = 0 \tag{3.5}$$

where k was the linear spring stiffness measured by a UTM. The solution to Eq. 3.5, with initial conditions of $x(0) = 0$ and $\dot{x}(0) = v_{23}$, is shown in Eq. 3.6.

$$x(t) = \frac{\sqrt{km_b} \, v_{23} \, Sin\left(\sqrt{\frac{k}{m_b}} \, t\right)}{k} \tag{3.6}$$

Spring displacements were calculated for six impacts at low speeds (10 mph). The results in Fig. 3.14 show good agreement with an average displacement difference of 2%. The device measured COR an average of 10.8% lower than the model.
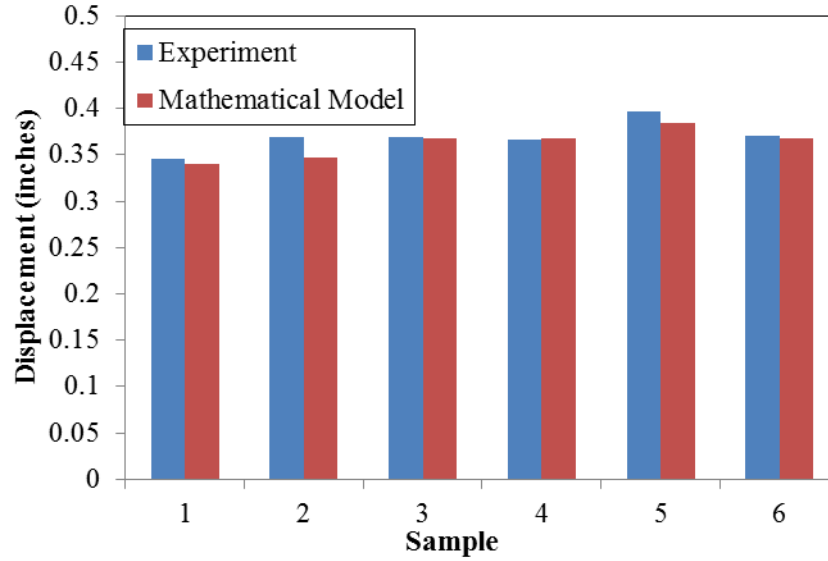
Figure 3.14 Displacement Comparison between the device and differential model.

Both external methods of measurement verification showed that the device measured COR between 10% and 14% low. This error in device measurement was either due to errors in the infrared sensors or the load cell. Because the high speed video verified correct speed measurements from the infrared sensors, the load cell likely caused the low COR values.

Theoretical force of impact was calculated by differentiating Eq. 3.6 twice to get acceleration and then multiplying by striker bar mass (f = m a). A comparison with the load cell measurements showed the load cells measuring 9.8% low on average. Measurements of static loads on the load cell could not be done because as time elapsed, the force value decreased. This behavior was described in the load cell operation manual as the discharge time constant. The decay of load value was found to have a half-life of approximately 6 seconds. Using the equation for half-life decay,

$$f(t) = f_0 * \left(\frac{1}{2}\right)^{t/t_{1/2}} \qquad 3.7$$

where $t_{1/2}$ is the half-life, f_0 is the actual force and $f(t)$ is the measured force at time t, the measured force would only be 0.01% lower than the actual force after the time interval of

interest (0.001 s). There is some confidence, however, in the load cell accuracy as it was newly purchased for this study and came with a calibration certificate stating that calibration procedures were in compliance with ISO 10012-1.

3.5   Results

All experimental testing was performed at the Sports Science Laboratory at Washington State University. To reduce the effect of environmental conditions, the temperature and humidity of the tests were regulated by a Stability Environment, Inc. environmentally controlled walk-in chamber number 1332401. The environmental chamber was 429 square feet and 8-10 feet high and space was sufficient to both acclimatize materials and conduct tests. The chamber was set to conditioning parameters defined in ASTM F2845 (72 ± 4 °F, $50 \pm 10\%$ RH). The environmental consistency over the period of experimental testing is shown in Fig. 3.15 and 3.16. Two weeks were allowed for the foam samples to acclimatize prior to testing.
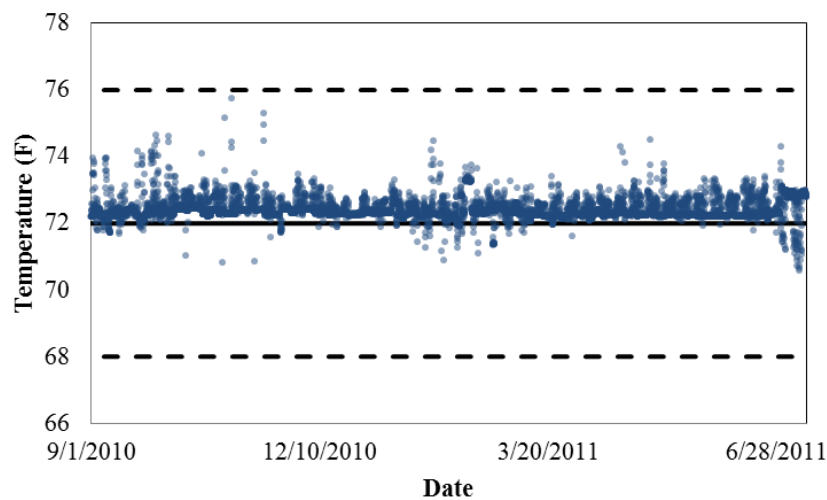
Figure 3.15 Logged temperature over the duration of experimental testing.
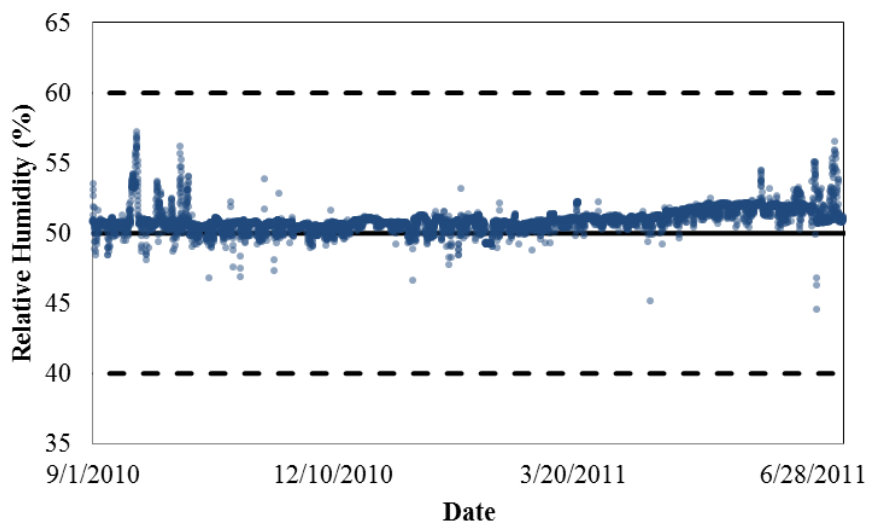
Figure 3.16 Logged humidity over the duration of experimental testing.

After being environmentally acclimatized, thirty foam samples were impacted by a 2 inch long striker bar at speeds ranging from 17 to 45 mph which resulted in peak strain rates between 1000 and 2700 s^{-1}. Each sample was tested once so that the results would not be influenced by potential damage from cell wall collapse. The stress-strain curves of each impact, along with the master compressive loading curve are shown in Fig. 3.17. The three phases of polymeric foam compression were evident. Foam collapse occurred at approximately 0.1 ε, and continued until the densification region at approximately 0.4 ε. This is consistent with the dynamic compressive behavior of PU foam published elsewhere (Chen, 2001).
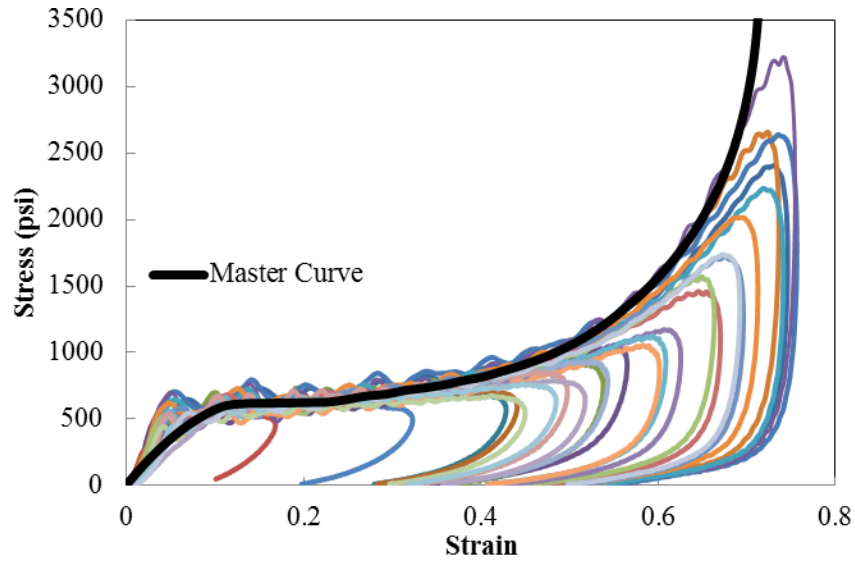
Figure 3.17 Dynamic compressive response of softball foam at various rates and the corresponding master curve.

The master curve was developed to represent compressive response as a single rate-independent curve. Many of the stress-strain curves in Fig. 3.17 depart from the master curve as peak strain is approached and the strain rate nears zero. This is consistent with viscoelastic effects where creep tends to increase as strain rate decreases. The master curve was used as a parameter to control compressive response in a numerical foam material model discussed in Chapter 5.

Oscillations in the stress-strain curves, consistent with elastic wave propagation, may be observed at low strain magnitudes in Fig. 3.17. The oscillation in the stress-strain response is a result of measuring load at the fixed end of the sample and deriving strain from the displacement at the free end of the sample. Fortunately, the magnitude of the oscillations is relatively small, so that the average material stress-strain response could be readily discerned. Elastic wave propagations were also observed in numeric simulations discussed in Chapter 5.

The speed of a wave in any medium is dependent on the medium's density. While the foam structure will increase density during compression due to cell collapse, the PU matrix, which transmits the compression wave, maintains a constant density. As further verification that

elastic wave propagation was the source of the oscillations in Fig. 3.17, the load signals of three

impacts at differing speeds were magnified in Fig. 3.18. The alignment of the oscillations

indicates a constant compression wave speed which is independent of collision conditions.
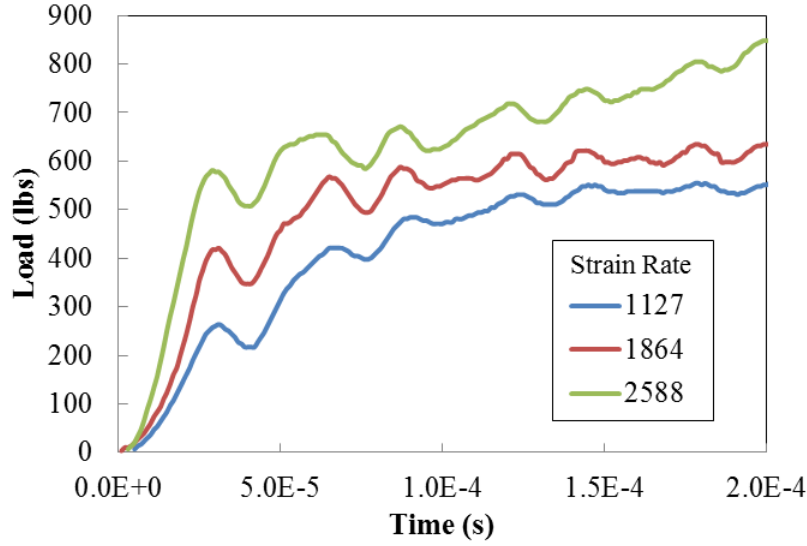
Figure 3.18 Magnification of load signals at differing speeds shows similar oscillatory behavior.

One advantage of the device was the ability to use striker bars of varying mass. Testing

bars of differing mass at similar velocities can produce variation in strain magnitude while

maintaining a constant strain rate. Using classical kinematics, and neglecting frictional effects,

the energy of the striker bar can be expressed as

$$\frac{1}{2}m_b v_b{}^2 = PA_b(l - l_b) \tag{3.8}$$

where v_b is bar velocity at the end of the barrel, P is constant barrel pressure, A_b is the bar cross-

sectional area, l is barrel length and l_b is the bar length. Pressure of the barrel is unknown as the

striker bar is being fired. However the tank pressure, which is measured before firing, will be

slightly higher than barrel pressure and is a good estimate. Eq. 3.8 was used in comparisons

between bar lengths to achieve similar speeds.

To verify that the master curve was independent of sample dimensions, a second round of testing was performed. Samples with an average thickness of 0.205 inches were impacted with a 3 inch striker bar at strain rates ranging between 950 and 2600 s^{-1}. The results were plotted along with the master curve developed from impacting 0.3 inch thick samples in Fig. 3.19. The master curve closely aligned, indicating its independence from foam sample thickness.
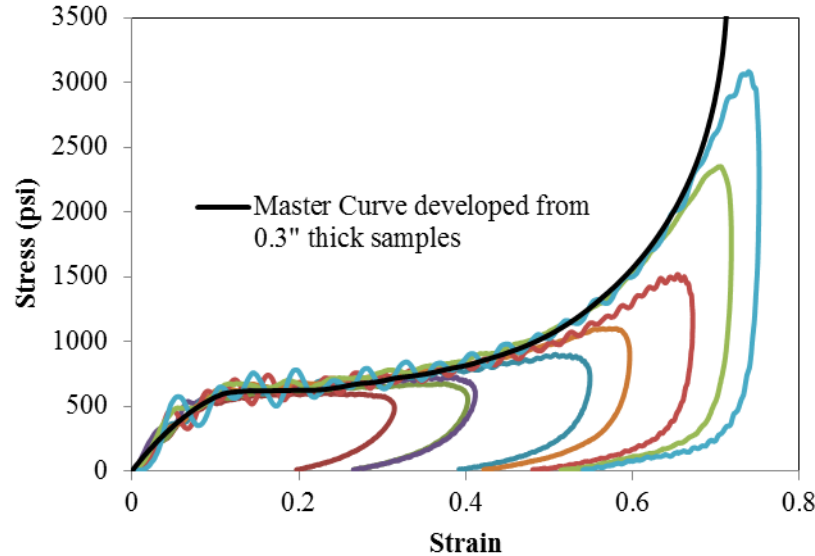
Figure 3.19 Stress-strain response of 0.2" thick samples plotted with the master curve developed from impacting 0.3" thick samples.

The relationship between striker bar speed and the corresponding strain rate and magnitude induced in the foam sample is shown for the 3 inch bar in Fig 3.20. Strain rate increased linearly with striker bar speed. Strain magnitude also increased but with decreasing gains at higher speeds.
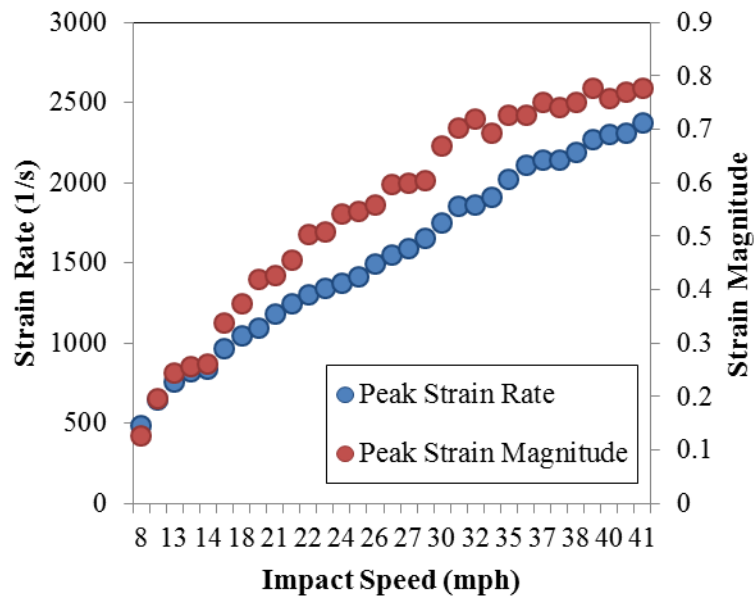
Figure 3.20 The effect of striker bar speed peak strain rate and magnitude in the foam sample.

An investigation was conducted to reveal whether impact response was dependent on the the mass of the striker bar. Aluminum striker bars 2, 3, 6 and 9 inches in length, with weights of 0.645, 0.955, 1.83 and 2.76 oz. respectively, were used to impact foam samples over the range of operable speeds (up to the maximum load cell range of 500 lbs for each bar). Results comparing impact properties for differing bar lengths are shown in Figs. 3.21-24.
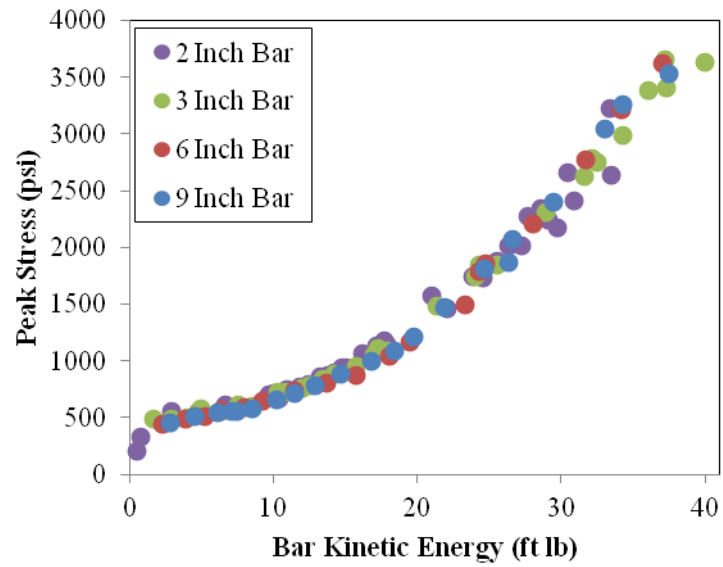
Figure 3.21 Comparison of peak stress in foam samples impacted with striker bars of varying length.
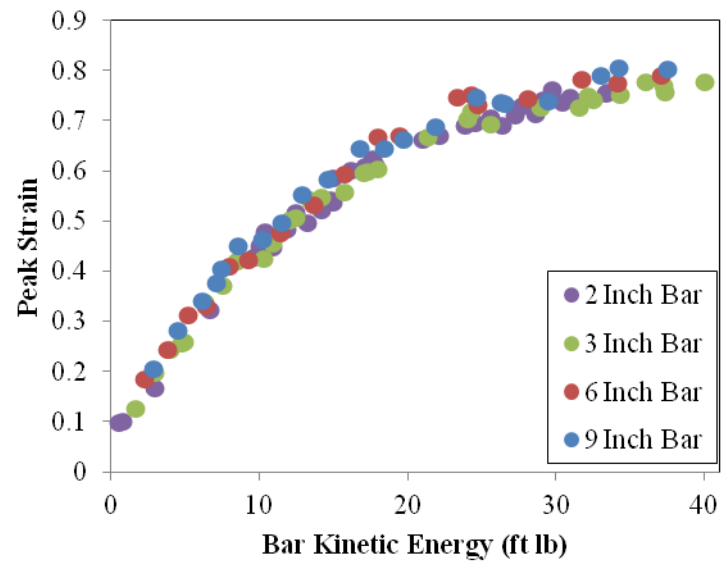
Figure 3.22 Comparison of peak strain in foam samples impacted with striker bars of varying length.
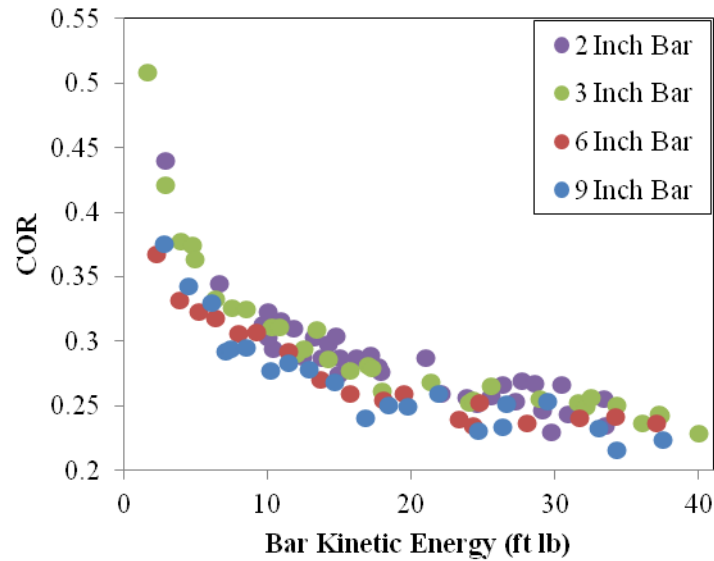
Figure 3.23 Comparison of COR in foam samples impacted with striker bars of varying length.
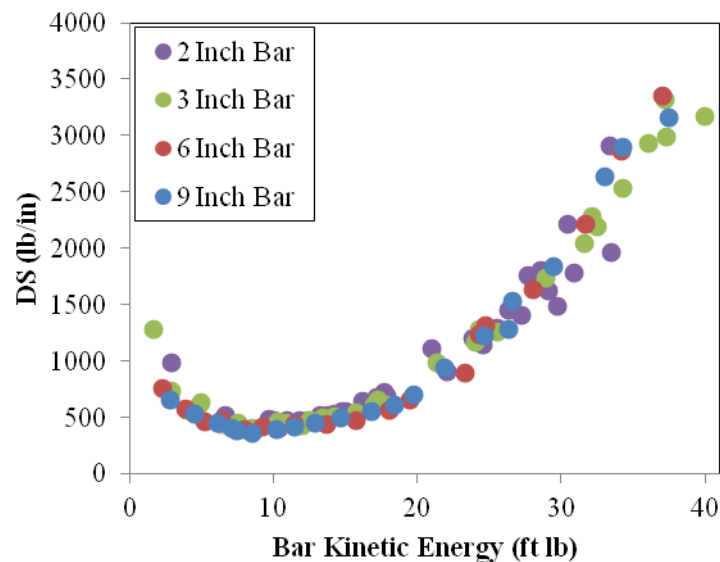
Figure 3.24 Comparison of DS in foam samples impacted with striker bars of varying length.

Figure 3.24 showed an interesting response. It would be expected that stiffness would increase with the energy of collision, however the opposite is shown for impacts below 10 ft lb of kinetic energy. Referring to Fig. 3.22, impacts below 10 ft lb had peak strain magnitudes in the cell collapse region of compressive foam response according to Fig. 3.17. An increase in

striker bar velocity, without a corresponding increase in force of impact, due to cell collapse, will reduce DS as defined by Eq. 2.7.

A strong correlation with inbound striker bar kinetic energy ($\frac{1}{2}mv^2$) was observed for peak stress, peak strain, and DS across bars of differing lengths. The aligning results of differing bar lengths suggest that dynamic results obtained from the device are independent of both the physical dimensions and mass of the striker bar. COR, Impact duration and impulse were similarly compared and were found to be dependent on the mass of the striker bar. This was expected, as these variables would be affected by the bar momentum. These results are promising for other potential uses of the device to investigate or compare the effects of energy absorption on foams or other soft materials.

All of the data from impacts with differing bar lengths at various speeds was used to further investigate the effect of strain rate on PU foam. Strain rate was calculated as the derivative of Eq. 3.2, which could be evaluated throughout each collision as shown in Fig. 3.25. From 100 different impacts, coupled stress and strain values were collected at strain rates closest to 250, 750, 1250 and 2000 s^{-1} (but no more than $\pm$ 50 s^{-1}). Stress-strain values at similar rates were combined to produce the constant strain rate curves shown in Fig. 3.26. The temporal dependence of the viscoelastic foam is evident, as an increase in stiffness was observed in both the cell collapse and densification regions. A trend of increasing deviation between strain rates was also observed as strain magnitude increased. When the master curve from Fig. 3.17 was plotted alongside curves from Fig 3.26, it closely followed the 2000 s^{-1} strain rate data.
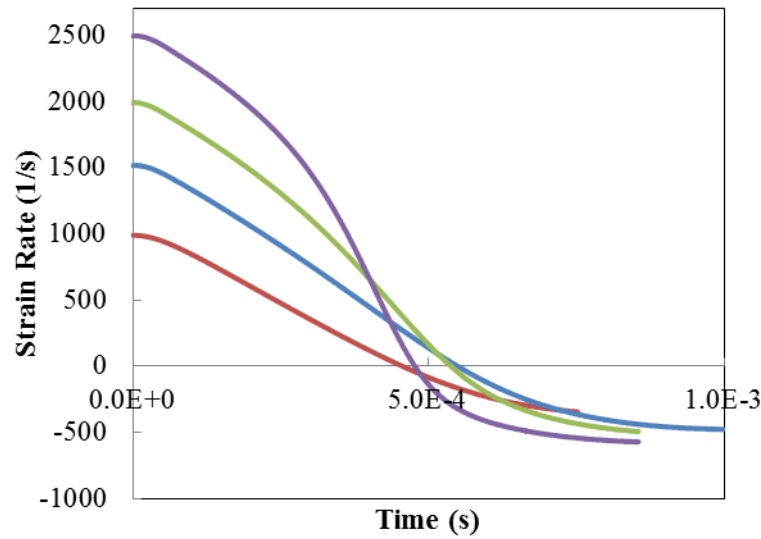
Figure 3.25 Strain rates plotted throughout impacts from a 2 inch striker bar.
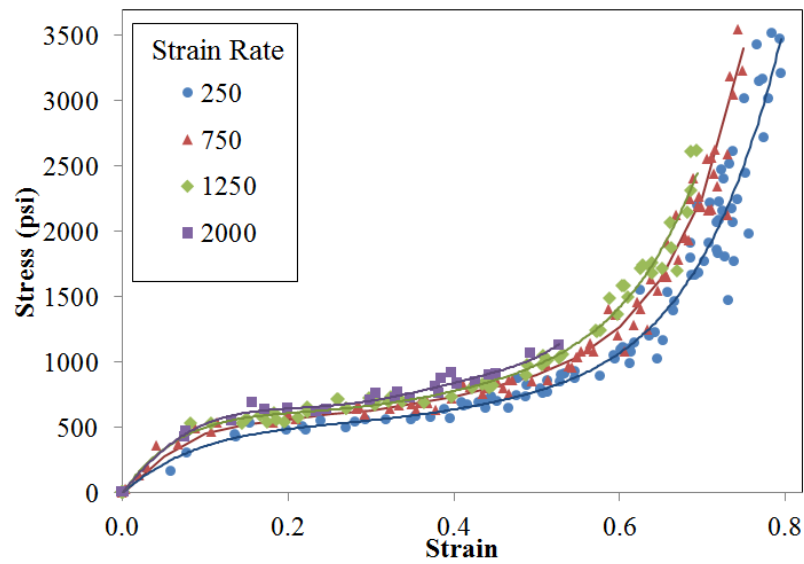
Figure 3.26 Constant strain rate curves derived from impact testing.

Duris stated that the Poisson ratio of softball foam is approximately 0.1 (Duris, 2004). To quantify the Poisson ratio, five high speed videos of impacted PU foam samples were taken at 60,000 frames per second. The average Poisson ratio was 0.28 with a standard deviation of 0.02.

47

3.6   Quasi Static Data

In conjunction with the dynamic results obtained from the impactor device, low rate uniaxial compressive foam tests were performed on a customized load frame (Fig 3.27). The screw-driven device, made by ADC, was capable of measuring displacement to an accuracy of 1×10^{-4} inches at a sample rate of 1 kHz. The samples were placed between two flat surfaces and then compressed as both force and displacement were measured to produce stress-strain curves using Eqs. 3.2 and 3.3.

Figure 3.27 Load Frame used to conduct low rate compressive testing.

Foam samples of two different thicknesses (0.2 and 0.3 inches) were compressed at a constant rate (0.01 s^{-1}) to determine if sample thickness affected compressive response. Samples of each thickness were compressed at uniformly-incremented strain magnitudes ranging from 0.2 to 0.8 ε to compare unloading behavior. The results in Fig. 3.28 show excellent agreement in both loading and unloading behavior of the 0.2 and 0.3 inch samples.
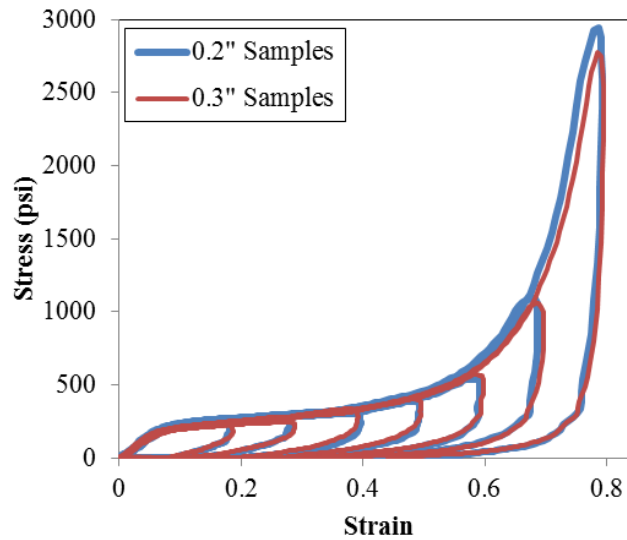
Figure 3.28 Comparison of low rate loading and unloading behavior of samples of differing thickness.

According to Gibson, the effect of loading rate on foam compression is significant when scaled by decades (Fig. 2.8). Because a softball experiences low strain rates near maximum deflection, the compressive response of softball foam was tested across decades of low strain rates. Six foam samples were compressed at constant strain rates of 0.01, 0.33 and 3.33 s^{-1}. The average response at each loading rate, along with the lower and upper constant-rate curves from Fig 3.26 are shown in Fig 3.29. Results from the load frame were similar to those of the impactor device, showing an overall stiffer behavior at higher loading rates. Besides the 250 s^{-1} strain rate curve slightly overlapping the 3 s^{-1} strain rate curve at densification strains, the data from the load frame and the impactor device correlated well, showing good transition across the strain rate spectrum.
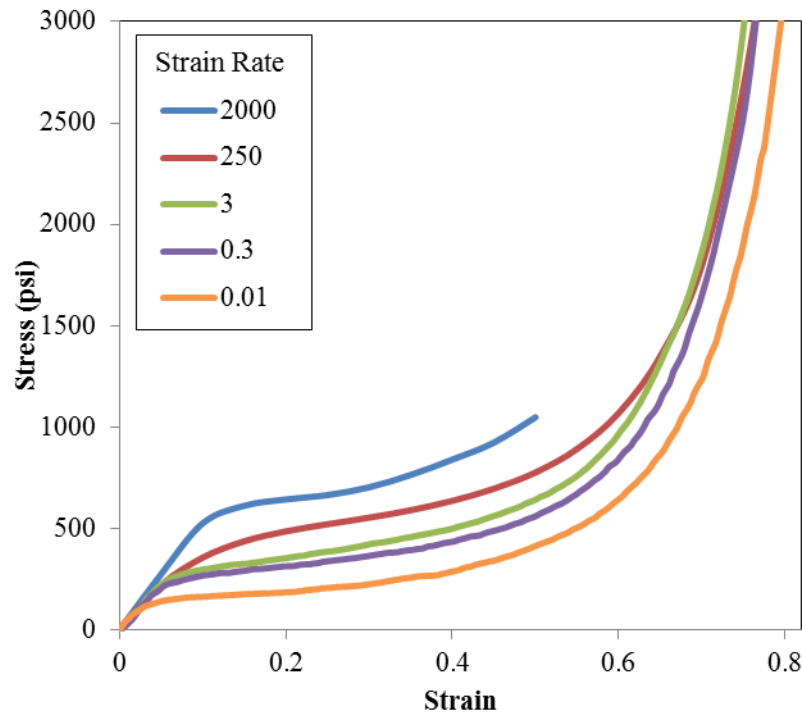
Figure 3.29 Constant strain rate curves from the load frame (0.01, 0.33, 3.3 s^{-1}) and impactor device (250, 2000 s^{-1}).

3.7   Damage Effects

The damage to a foam structure due to deformation is specific to the material and its structure. Open celled foams are frequently designed for applications involving large strain magnitudes, yet no damage occurs because the polymer is flexible and air easily penetrates the open-celled structure. Some crushable foams are designed to have no recovery. If a foam is composed of a brittle matrix, fracture will occur at large strains and permanently damage the structure. 3M produces a crushable foam with voids created by soda lime glass bubbles which act as a mechanical fuse to collapse at specific pressures (3M, 2011). Bubble wrap, when excessively compressed, also suffers catastrophic and irrecoverable damage.

To study the effects of damage in softball foam, both 0.2 and 0.3 inch thick samples were compressed at a quasi-static strain rate (0.01 s^{-1}) with strain magnitudes ranging from 0.2 to 0.8

ε. The thickness of each sample was then monitored to see how the samples recovered over time. It was found that the sample thickness did not change after one week of recovering.

Figure 3.30 shows the permanent residual strain after allowing sufficient time for recovery. Damage to the foam structure increased with strain magnitude. Full recovery was shown for samples compressed up to 0.3 ε.
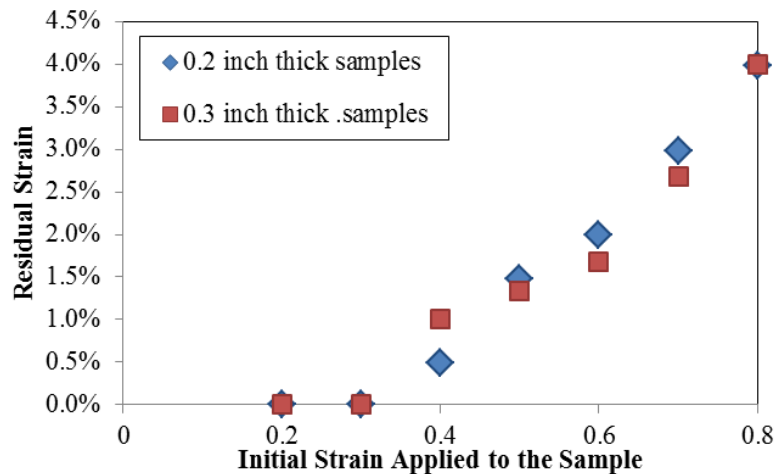
Figure 3.30 Structural foam damage indicated by permanent residual strain from quasi-static loading.

When comparing the effect of deformation on softballs, Smith observed that quasi-static loading was more severe than impact loading (Smith, 2008). To determine how a dynamic impact induces structural damage in softball foam, permanent residual strain was monitored for 0.3 inch samples impacted over a range of strain magnitudes. Sample recovery stopped after one week. The results in Fig. 3.31 are comparable to quasi-static loading, with samples strained up to 0.3 ε showing full recovery. While an exponential increase in residual strain was shown for increasing initial strain, residual strains from impact were approximately half that of quasi-static loading.
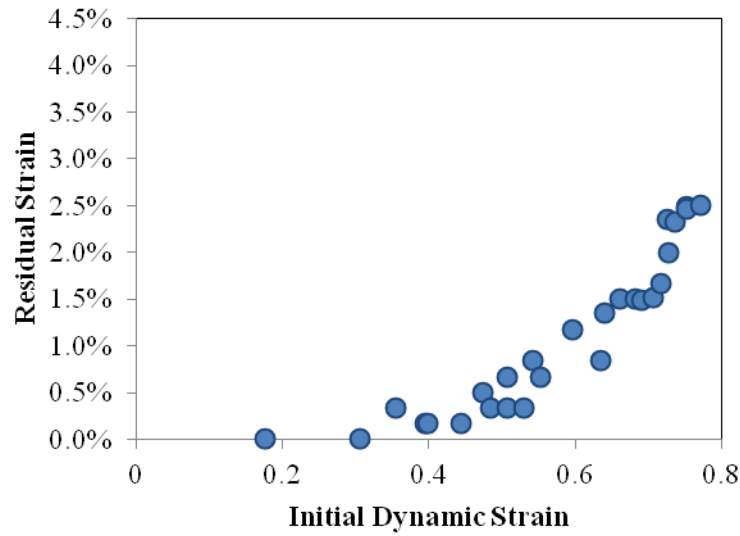
Figure 3.31 Damage to the foam structure indicated by permanent residual strain for high rate impacts.

While it was shown that structural damage occurs to softball foam during both quasi-static and dynamic loading, the effect of damage on impact performance was still unknown. Six foam samples were impacted repeatedly at differing speeds while an effort was made to keep peak strain for each sample relatively constant. Repeating specific strain magnitudes was difficult on the impactor device because a constant tank pressure produced striker bar speeds ranging an average of 3.6 mph. Sufficient time was allowed between impacts for sample recovery.

According to Fig. 3.22 and 3.23, the relationship between COR and impact speed was linear for impacts with peak strains above 0.3 ε. To negate the effects of differing impact speeds for a single foam sample, COR was divided by impact speed as shown in Fig 3.32. Samples impacted below densification strains showed an increase in COR for a given impact speed. This effect diminished with increasing strain such that COR remained constant for the most severely impacted samples. The opposite was shown for DS in Fig. 3.33. Samples impacted at lower strains maintained stiffness while increasing the severity of impact also increased sample stiffness.
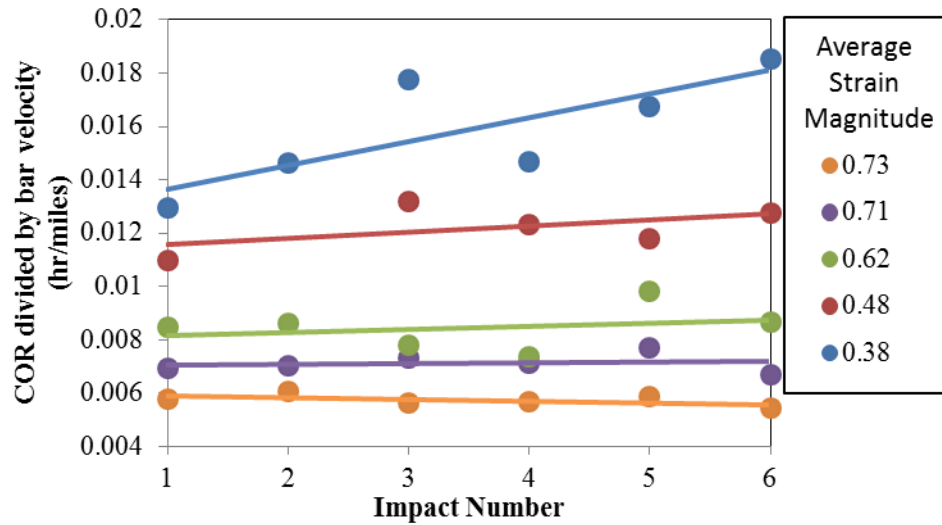
Figure 3.32 Change in COR due to repeated impacting as a function of strain magnitude.
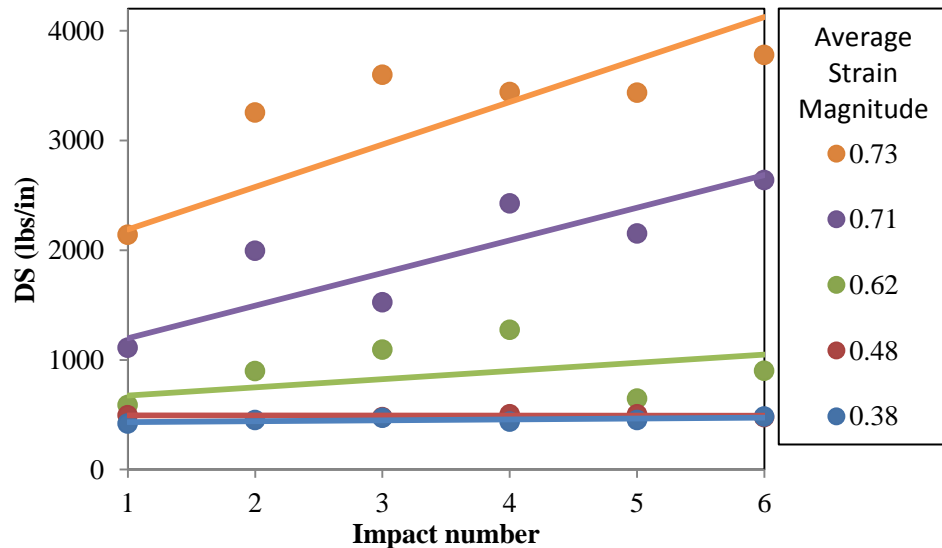
Figure 3.33 Change in DS due to repeated impacting as a function of strain magnitude.

If a foam structure was damaged, less energy could be absorbed by the matrix and the structure would more easily yield to an applied load. An increase in both COR and DS indicate the development of damage in the foam samples. Increases in COR and DS after a single impact further support the fact that permanent structural damage is caused by compressing the material at the strains tested.

Strain magnitudes along the cross section of a softball during impact cannot be measured directly. Thus it is difficult to apply these results to softballs. Numerical simulations of softball impacts discussed in Chapter 6 will highlight cross-sectional strain distributions.

3.8   Summary

A new device was developed to impact samples of softball foam at rates similar to play. It was found that inbound striker bar speed and foam sample displacement measurements were quite accurate when compared to linear helical spring impacts at low rates ($< 2\%$) and high speed cameras at both high and low rates ($< 2\%$). A custom hole saw was manufactured to successfully produce uniform foam samples with square, smooth surfaces.

Impacts with a two inch striker bar resulted in peak strain rates ranging between 1000 and 2700 s^{-1} which is the range typical of play conditions. A single master curve was developed to describe the compressive response of the foam. Impacts of foam samples with differing thickness fit well with the master curve. Impacts with striker bars of four different lengths produced similar results when compared as a function of striker bar kinetic energy. These results are promising for possible future studies into dynamic energy absorption and rate effects of various types of foam.

The device's ability to use striker bars of differing length or mass allowed strain rate and magnitude to be independently adjusted. This proved useful in the development of constant-rate, stress-strain curves. As would be expected of a viscoelastic material, an increase in stiffness at higher loading rates was shown. The high rate curves merged well with slower, constant-rate curves obtained from a load frame.

Permanent damage to the foam structure was shown to occur at strains above 0.3 ε at both low and high compression rates. Repeatedly impacting the samples caused an increase in both COR and DS.

3.9   References

3M, 2011. Crushable Foam. [Online] 2011. [Cited: Dec 22, 2011.]
http://solutions.3m.co.uk/wps/portal/3M/en_GB/OilGas/Industry/Solutions/Drilling/CrushableFo
am/

Bryson, A. J. 2009. Impact response of polyurethane. Master's thesis, Washington State
University. 2009.

Chen, W. Lu, F. Winfree, N. 2001. p. 65-73. High-strain-rate compressive behavior of a rigid
polyurethane foam with various densities. Experimental Mechanics. 2001, p. 65-73.

Duris, J. G. 2004. Experimental and numerical characterization of softballs. *Master's Thesis,
Washington State University.* 2004.

Smith, L.V. 2008. Measuring the Hardness of Softballs. IMAC-XXVI, Orlando, FL. Society of
Experimental Mechanics: Bethal, CT, 2008.

4   Ball Testing

4.1   Introduction

Instrumented softball performance data was needed for both development and validation of the numerical softball models. Performance, measured as a function of speed and impact surface geometry, was of primary interest. The following will discuss the methods and results of experimentally measuring dynamic softball performance. Damage to the ball's foam core, due to repeated impacting, was also studied to determine if such effects were significant. All testing was performed in the environmental chamber described in Chapter 3 and all balls were acclimatized for two weeks prior to testing.

4.2   Instrumentation

Instrumented ball impacts were performed on a dynamic stiffness test apparatus shown in Fig. 4.1 (ASTM F2845, 2010). The test consisted of firing a ball from an air cannon against either a fixed solid-steel half cylinder 2.25 inches in diameter, or a 0.5 inch thick steel plate. Light gates and load cells measured ball speed and the force of impact which were used to calculate impact properties and develop load displacement curves.
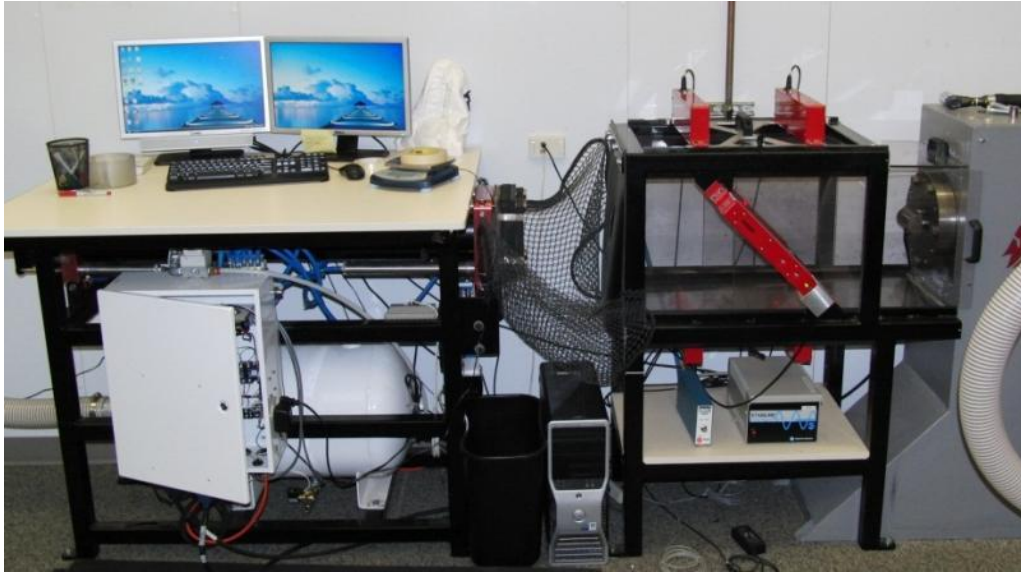
Figure 4.1 Setup of the dynamic stiffness test apparatus.

The softballs were fired from a four foot long, 5.5 inch diameter air cannon using compressed air stored in an accumulator tank (Fig. 4.2). The desired pitch speed was obtained by adjusting the pressure in the accumulator tank with a pressure regulator. When fired, a MAC valve released air from the accumulator tank. All device components and measurement sensors were wired to a connection board and controlled by a PC using labVIEW software (National Instruments Austin, TX).
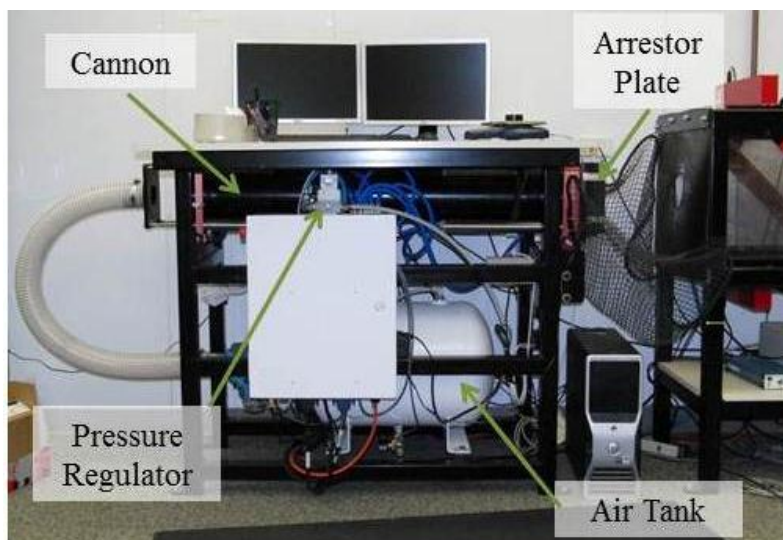
Figure 4.2 Air cannon used to fire softballs and baseballs.

While inside the cannon barrel, the ball was cradled by a polycarbonate sabot (Fig 4.3). The sabot was used to center the ball, control speed, and launch the ball without rotation. This allowed testing at specific locations on the ball.

Figure 4.3 Sabot used to cradle the ball as it travels through the cannon.

Previous sabot designs were constructed of ultra-high molecular weight polyethylene (Duris, 2004). These would yield upon impact with the arrestor plate and require re-shaping. It was found that polycarbonate sabots withstood impacts far better. Older sabot designs were one solid bowl-shaped piece machined from a cylindrical piece of polymer using CNC mills and lathes. The solid base had a large mass and cracked quickly. A re-design included a light weight fiberglass disk to replace the solid base, reducing the weight, and allowing cheaper replacements.

The sabot was placed in the breech end of the barrel before firing. Pneumatic cylinders closed the breach plate so when air was released, the full pressure was behind the sabot, ensuring consistent speed. After traveling the length of the cannon, the sabot was captured by an arrestor plate (Fig. 4.4), while the ball continued forward to the light gates. The arrestor plate consisted of a series of leather, foam and aluminum plates bound together. Pneumatic cylinders were connected to the arrestor plate that extended out just after the cannon was fired to catch the sabot and lessen its impact.
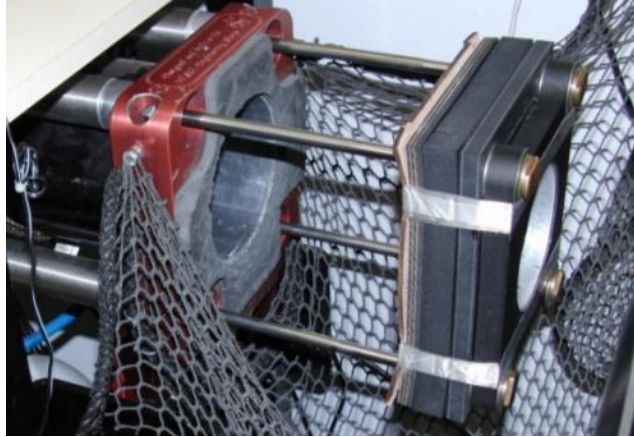
Figure 4.4 Arrestor plate used to catch the sabot after exiting the barrel.

The ball traveled past light gates (Fig 4.5), impacted the control surface, and then rebounded back through the light gates. Two sets of ADC iBeam light gates measured ball speed similar to the device in Chapter 3. Ball speed was adjusted such that only shots within ± 1 mph were accepted as valid test shots. A diagonal pair of light gates determined ball rebound angle. Vertical cannon alignment with respect to the impact surface was adjusted so that only rebounds within ±10° of the inbound path were considered valid shots. Ball rebound trajectory was verified using high speed videos operating at 250 fps. Interestingly, the distance between the light gates and impact surface was previously found to be measureable due to the effects of drag (Smith, 2006).
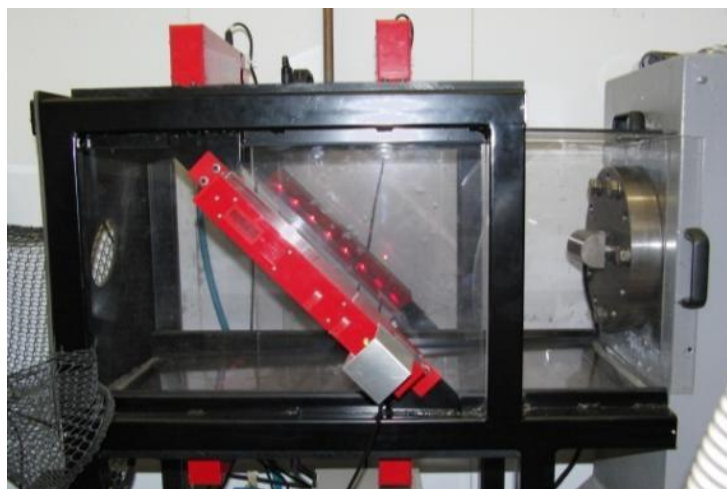
Figure 4.5 Light gates (red) and cylindrical impact surface mounted to the rigid surface (right).

The impact surfaces were mounted to three load cells designed for dynamic loading applications and rated to 5 kips each (PCB, model 208C05). The load cells were arranged in a two-inch equilateral triangle and were mounted to a massive support from behind (Fig. 4.6). Load measurements were taken at a sample rate of 100 kHz.

Figure 4.6 Maximum deformation of a softball impacting a cylindrical surface at 100 mph.

4.3   Results

Various authors have conducted experimental testing on softballs. Biesen impacted 42 softballs at speeds of 60, 80, 95, 105, 110, 120 and 130 mph on a cylindrical surface (Biesen, 2006). Each ball was tested once, and 6 balls were used for each speed. CCOR and DS were both found to be linearly dependent on speed. Damage to the balls tested at 130 mph was found to be negligible as the COR and DS of the original 80 mph test group and the 130 mph group tested again at 80 mph were similar.

Faber tested DeMarini A9044 softballs as part of his work in normalizing softball bat performance (Faber, 2010). The CCOR and DS at 95 mph were found to be 0.373 and 5716 lb/in respectively. Load displacement curves showed a peak force of 4300 lbs and a peak displacement of 0.6 inches.

Duris performed softball tests investigating the effects of rate and surface geometry. (Duris, 2004). A decreasing trend of COR and CCOR as well as increasing trends of peak force with respect to ball speed was observed. A flat impact surface was found to have a greater peak force, lower impact time and an increased COR compared to a cylindrical surface.

Even among softballs of an identical model (DeMarini A9044), some variation in performance was shown. Figure 4.7 shows a qualitative comparison of load curves from 100 different DeMarini A9044 softballs impacting a cylindrical surface at 95 mph. The greatest spread occurred at the impact apex. According to Eq. 2.7, this would also cause spread in DS.
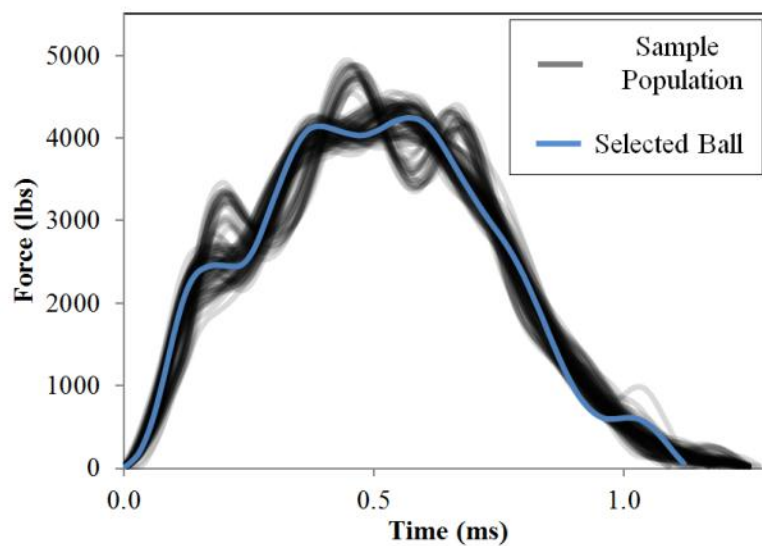
Figure 4.7 Load curves from 100 different DeMarini A9044 softballs impacting a cylindrical surface at 95 mph along with the selected ball.

To quantify the average ball response, ASTM standard procedures were used to measure the COR, DS and CCOR of 200 new balls (ASTM F2845, 2010), (ASTM F1887, 2009). The results summarized in Table 4.1 show a good level of consistency in performance with a standard deviation of less than 1% for ball mass, COR, and CCOR. DS had a higher standard deviation (9%), which is likely due to the spread of peak force shown in Fig. 4.7.

Table 4.1 Comparison of ball properties for a 200 ball population and the selected ball (Average ± SD).

Ball	Mass (oz)	COR (60 mph)	DS (lb/in)	CCOR (95 mph)
200 Ball Sample	6.97 ± 0.05	0.445 ± 0.003	6196 ± 571	0.377 ± 0.003
Selected ball	6.99	0.442 ± 0.002	6026 ± 514	0.375± 0.003

A single ball was selected to quantify experimental performance. The ball was selected based on both its similarity to the average loading curve in Fig. 4.6 and its performance values listed in Table 4.1. The ball was impacted six times at 60, 95 and 120 mph on both flat and cylindrical surfaces. The impact properties shown in Table 4.2 were calculated using the equations from Chapter 2, and agree with trends and values of previous works (Duris, 2004), (Faber, 2010).

Table 4.2 Performance measures as a function of impact speed and surface geometry (Average ± SD).

Impact Speed (mph)	Surface	COR/CCOR	Peak Load (lbs)	Impulse (lb s)	Peak Disp. (in)	DS (lb/in)
60.1 ± 0.3	Flat	0.442 ± 0.002	2995 ± 52	1.79 ± 0.005	0.378 ± 0.007	7235 ± 213
94.8 ± 0.2	Flat	0.390 ± 0.003	4805 ± 60	2.72 ± 0.006	0.568 ± 0.012	7319 ± 185
120.2 ± 0.6	Flat	0.357 ± 0.002	6285 ± 90	3.34 ± 0.016	0.687 ± 0.032	7828 ± 170
60.2 ± 0.2	Cylinder	0.418 ± 0.003	2575 ± 22	1.74 ± 0.020	0.425 ± 0.013	5487 ± 88
94.7 ± 0.5	Cylinder	0.375 ± 0.003	4132 ± 177	2.67 ± 0.017	0.631 ± 0.007	6026 ± 514
120.0 ± 0.5	Cylinder	0.350 ± 0.002	5297 ± 242	3.28 ± 0.027	0.780 ± 0.012	6192 ± 527

Compared to the flat surface, the cylindrical surface had an inherently smaller contact region. This increased the total deformation of the ball by 11%. Greater deformation resulted in more energy absorption by the ball's foam core. This lowered the COR by 4% and also lowered peak force by 17%. The difference between peak force and displacement were evident in the load-displacement curves in Fig 4.8. DS changed significantly, with cylindrical stiffness being 27% lower than that of the flat surface. The time to reach peak force was longer with the cylindrical surface, taking an extra 0.01 seconds as shown in Fig 4.9. The change in impact

surface affected impulse the least (2% average). The increase in energy dissipation for the

cylindrical surface properly resulted in a lower impulse as shown in Fig 4.10.
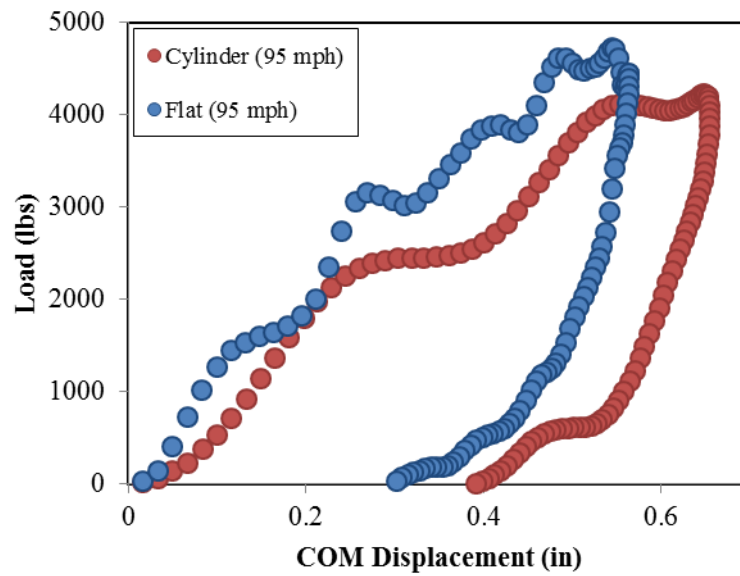
Figure 4.8 Load-displacement curves highlighting the impact behavioral differences between a cylinder and flat plate.
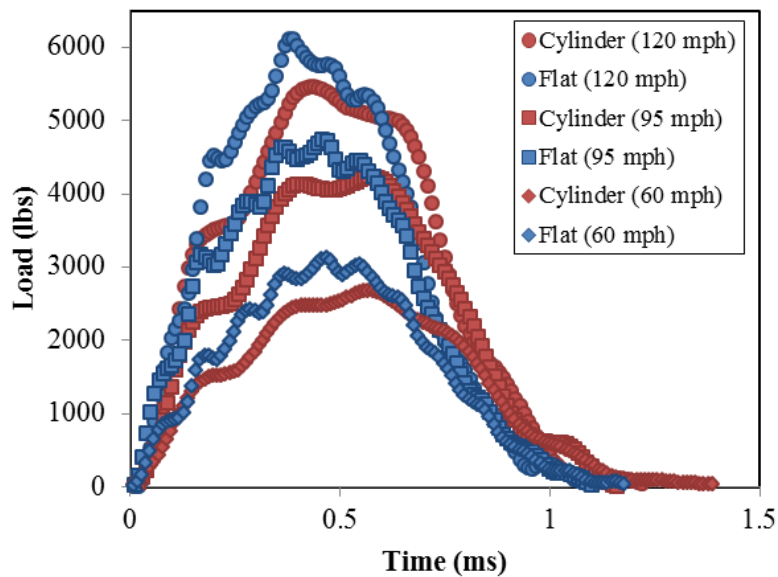
Figure 4.9 Load vs. time measurements of softball impacts at speeds of 60, 95 and 120 mph. Comparison of flat and cylindrical impact surfaces highlight the differences in impact response caused by the surface geometry.
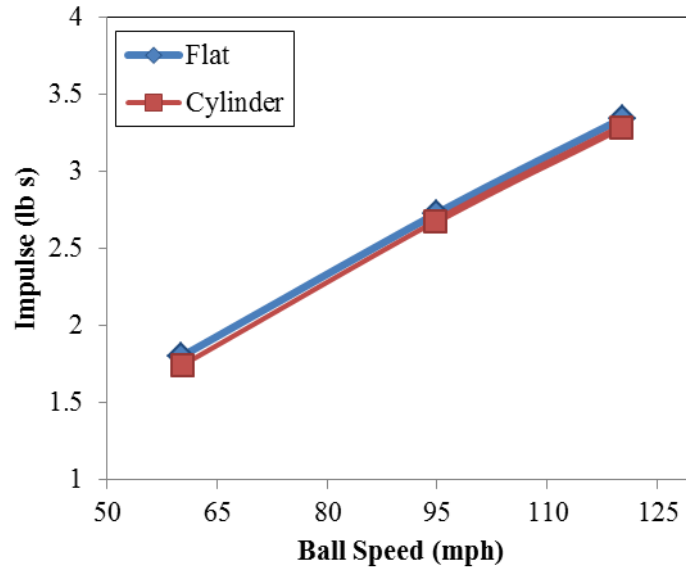
Figure 4.10 Impulse as a function of both speed and surface geometry.

The effect of speed on impact properties was significant for both cylindrical and flat impact surfaces as shown in Fig 4.11 and 4.12 respectively. COR was observed to linearly decrease with increasing ball speed, while impulse, peak force and peak displacement increased with speed. DS behaved similarly to peak force, although showing a smaller dependence on ball speed and a greater dependence on surface geometry.
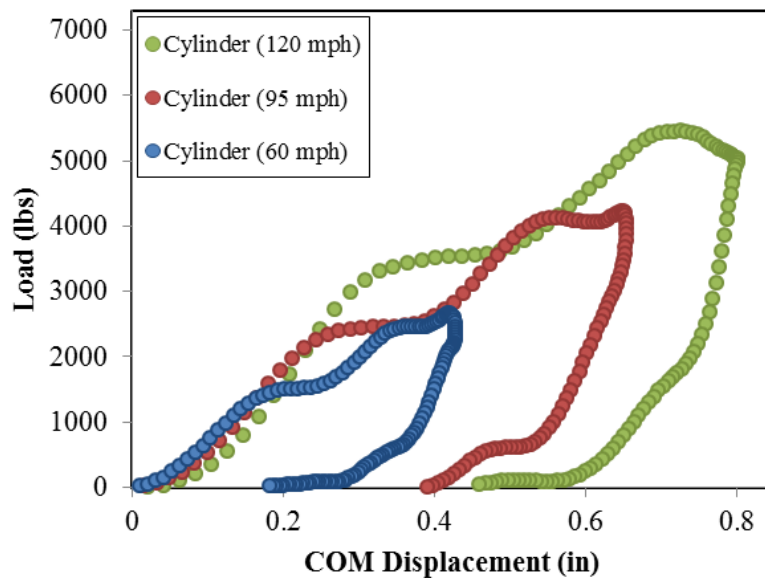
Figure 4.11 Load-displacement curves for cylindrical impacts at 60, 95 and 120 mph.

64
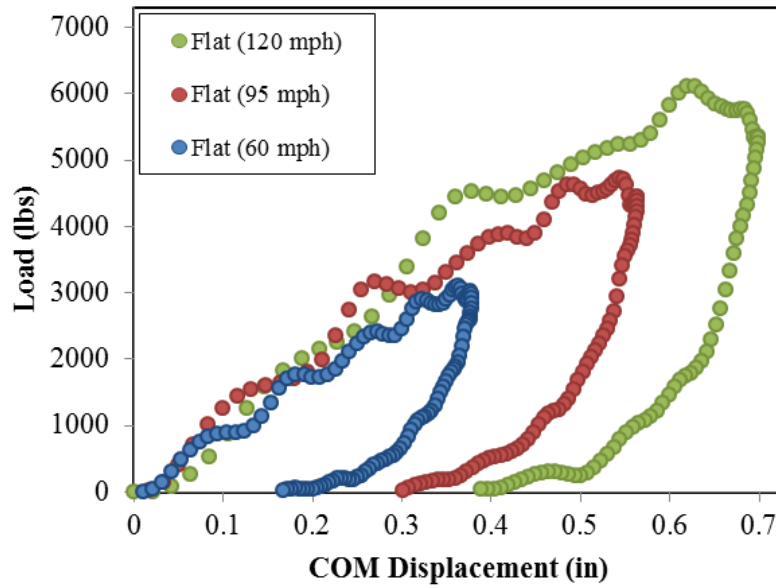
Figure 4.12 Load-displacement curves for flat surface impacts at 60, 95 and 120 mph.

As discussed in Chapter 2, impulse can be calculated by integrating the load signal (Eq. 2.8) or by performing a momentum balance (Eq. 2.10). The two impulse measurements were denoted as L_f and L_s respectively. The ratio of the impulse values ($K=L_s/L_f$) is an indication of measurement accuracy which, according to Fig 4.13, slightly decreased as speed increased for both surface types.
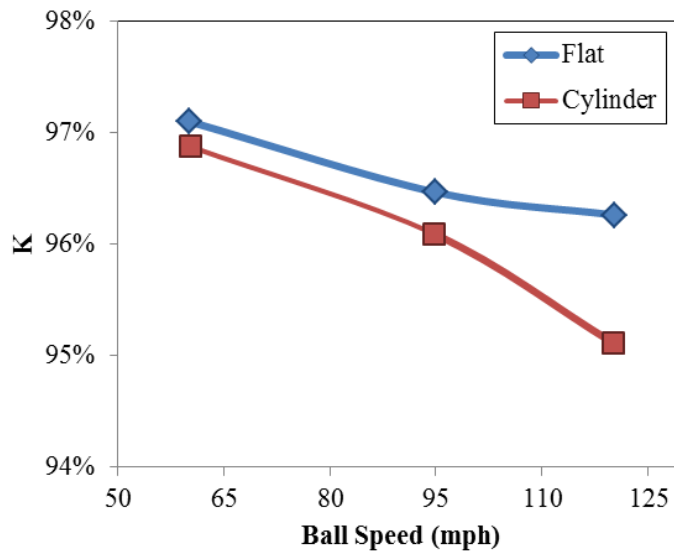
Figure 4.13 The ratio of impulse measurements as a function of ball speed. Trends indicate a decrease in instrumentation accuracy as speed increased.

4.4   Damage Effects

Limited work has been done to quantify the effect of repeated impacts on softball performance. As discussed in Chapter 2, Duris found that ball COR and peak force remained constant through 100 impacts (Duris, 2004). This however, applies to the entire ball, and not to a single impact location. Current softball bat performance testing methods do not stipulate a limit on the number hits a softball can take (ASTM F1890, 2009). However, softballs used for Amateur Softball Association (ASA) certification testing are limited to ten impacts on each ear.

Regarding the recovery time allowed between impacts, Duris suggested that balls be impacted no more than 10 times in one hour or more than one impact per minute. He also suggested that balls which are to be reused should be given a minimum of one hour in standard laboratory conditions to recover following a sequence of impacts before re-use. In ASA bat certification testing, impact frequency is no more than one impact per minute per ball, while all four ears of the ball are sequentially impacted.

To better understand changes in impact performance due to repeated testing, a durability test was performed. Three balls were repeatedly impacted 50 times on the same ear at 95 mph. While monitoring surface temperature, it was found that a single 95 mph impact raised the ball surface temperature by 2°F. To keep ball temperature within the ASTM F2845 limit of ± 4° F, only two hits were made on each ball before allowing temperature to stabilize for an hour. Five minutes was allowed between the two hits to allow foam structure recovery.
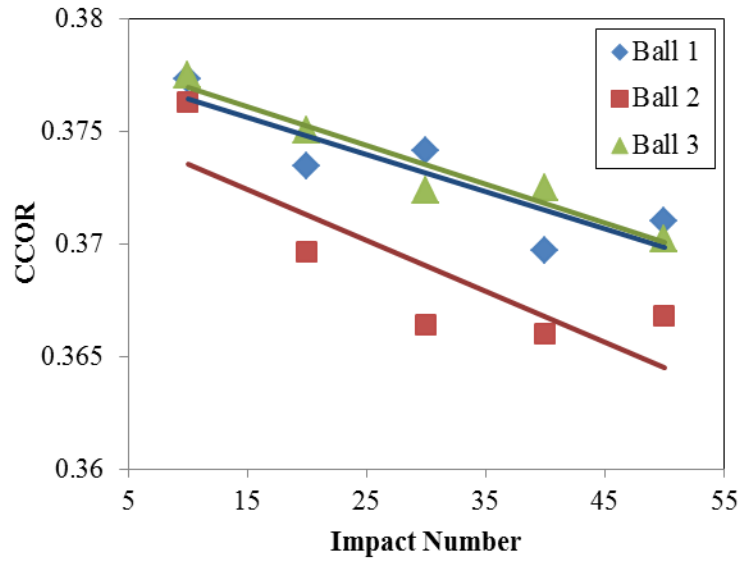
Figure 4.14 CCOR as a function of repeated impacts.
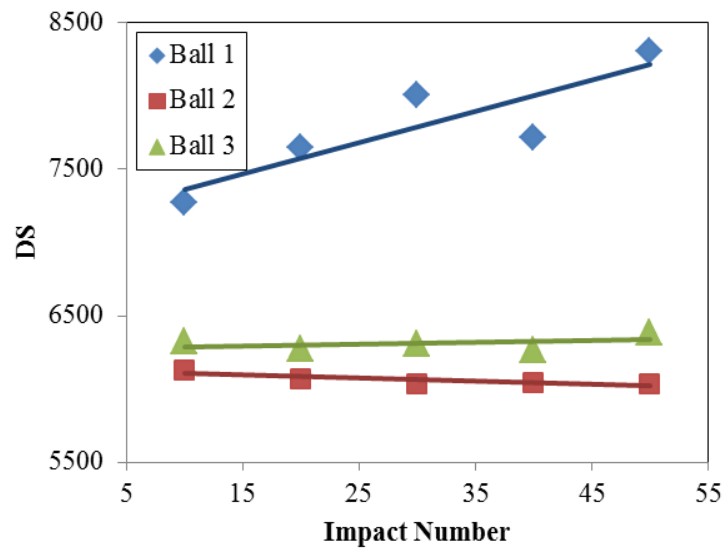
Figure 4.15 DS as a function of repeated impacts.

The results in Fig. 4.14 show a 2% decrease in CCOR for balls 1 and 3 and a 3% decrease for ball 2. The change in CCOR was likely due to the repeated impacting as the decrease in performance occurred over time. DS for balls 2 and 3 remained constant while ball 1 showed a 12% increase in DS as shown in Fig. 4.14. Because the balls showed varying effects, no conclusion could be drawn relating DS performance to repeated impacting.

The change in performance was most likely caused by decay of the foam structure due to fatigue. Residual strain was visibly noticeable in the ball as testing progressed, which indicates that structural damage was occurring. While performance change was evident over time, a significant number of impacts were required. The results support the findings of Duris that repeated impacting (up to 25 impacts per ear) does not significantly change impact performance.

4.5   Summary

A sample of 200 softballs of the same model showed good consistency in performance when tested using standardized procedures. Further experimentation on a single ball revealed a strong dependency of ball performance to both impact speed (60 to 120 mph) and surface geometry (flat and cylindrical). Increasing impact speed tended to increase the absorbed energy, deformation and force of impact. Changing the impact surface from flat to cylindrical increased the absorbed energy and deformation, but decreased force of impact. Alternate methods of calculating momentum suggested a slight decrease in measurement accuracy as speed increased.

A durability test was performed to better understand the effects of repeatedly impacting a ball. Three balls were impacted 50 times at 95 mph on a single ear of the ball. While CCOR decreased for all three balls, two balls showed no change in DS.

4.6   References

ASTM F2845. 2010. Measuring the Dynamic Stiffness (DS) and Cylinderical Coefficient of Restitution (CCOR) of Baseballs and Softballs. s.l. : American Society of Testing and Materials, 2010.

ASTM, F1887-09. 2009. Standard test method for measuring the coefficient of restitution of baseballs and softballs. West Conshohocken, PA : s.n., 2009.

Biesen, E. D. 2006. Prediction of plastic deformation in aluminum softball bats using finite element analysis. *Master's Thesis, Washington State University.* 2006.

Duris, J. G. 2004. Experimental and numerical characterization of softballs. *Master's Thesis, Washington State University.* 2004.

Faber, W. L. 2010. Reducing the effect of ball variation in bat performance measurements. *Master's thesis, Washington State University.* 2010.

Smith, L.V. Ison, A. 2006. Rigid wall effects on softball coefficient of restitution measurements. *The Engineering of Sport 6.* Vol 1, p. 29-34.

5   PU Foam Sample Modeling

5.1   Introduction

Many sport ball models (including baseball, tennis and golf balls) are developed phenomenologically. This involves iteratively adjusting material properties until structural response is duplicated. Models developed in this way have the potential of describing and comparing structural response prior to product fabrication. The following will discuss the development and simulation of two FEA foam material models with material loading responses derived from experimentation in Chapter 3 and phenomenologically developed unloading responses. Simulations of experimental testing from Chapter 3 were performed to allow direct comparison of numerical and experimental results.

5.2   FEA Setup

The instrumented PU foam sample impacts in Chapter 3 were simulated using the dynamic finite element code LS-DYNA (Version 971, LSTC, Livermore, CA). Because the foam cell size ($\approx$ 0.005 inches) was significantly smaller than the specimen diameter (0.42 inches), the foam was assumed to be isotropic and homogeneous.

The PU foam sample, shaded black in Fig. 5.1, was modeled with 2,772 linear, solid elements and two symmetry planes. Length and diameter were similar to the actual foam samples (0.3 and 0.42 inches respectively). The elastically-modeled aluminum striker rod, shaded green in Fig. 5.1, was modeled with 2,709 elements. While the actual striker bar length was 2 inches, the simulated rod length was shortened to 0.1 inches to reduce the number of elements. Density was correspondingly increased to achieve the correct striker bar mass.
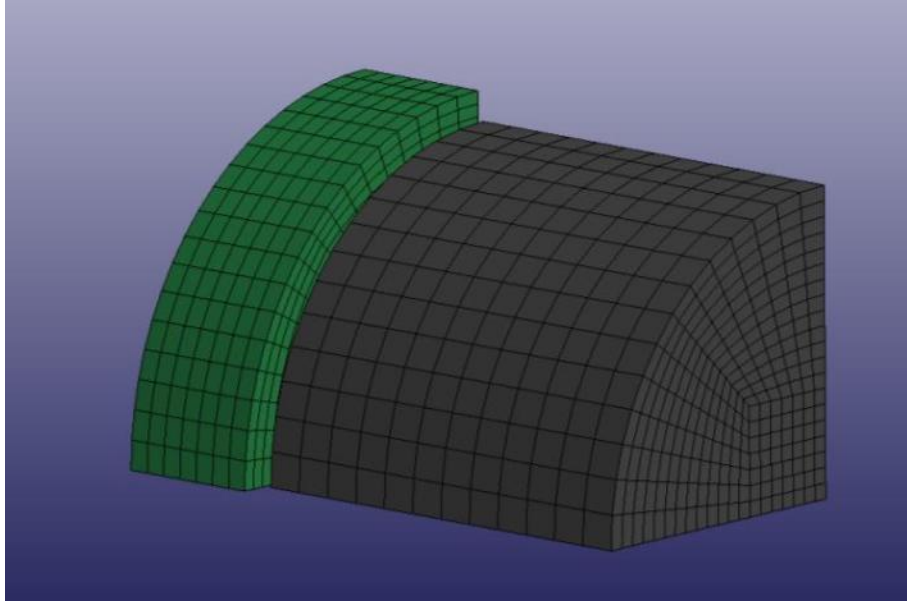
Figure 5.1 FEA setup of an aluminum striker bar (green) colliding into a foam sample (black) using quarter symmetry.

Besides the symmetry boundary conditions, the striker bar was given an initial velocity directed normal to the contact surface, while the foam sample face opposite of the impact was constrained in-plane. A "surface to surface" contact type was used where friction was neglected, as the impact had no obliquity. The addition of frictional effects was found to have no effect on impact performance. An alternate "surface to surface soft" contact option also caused no change in results.

Impact force and sample displacement were measured during the simulation and exported to output files which were subsequently used to quantify foam behavior and produce load-displacement curves. The position history of the striker bar's central node was used to measure both the sample displacement during impact and the rebounding striker bar velocity. Equation 2.2 was used to calculate COR and Eq. 2.8 was used to calculate impulse.

To determine if the simulation results were independent of mesh density, the foam sample was re-meshed with 4864 elements. Simulations with peak strain rates near 2500 s^{-1} (41.4

mph) were compared to that of the 2772 element sample. COR, impulse and maximum

displacement all changed by less than 1%. The coarse mesh was used to shorten solving time.

5.2.1   Simulation Challenges

Various simulating issues were caused by the large deformation of the foam sample.

Especially at higher speeds, the model experienced hourglassing as shown in Fig 5.2. By

assigning fully-integrated elements to both the striker bar and foam sample, hourglassing was

minimized at the cost of an increased solve time. Figure 5.3 shows the well-stabilized node

structure for the fully-integrated foam sample (black) during maximum deflection at the highest

simulated speed of 41.4 mph.
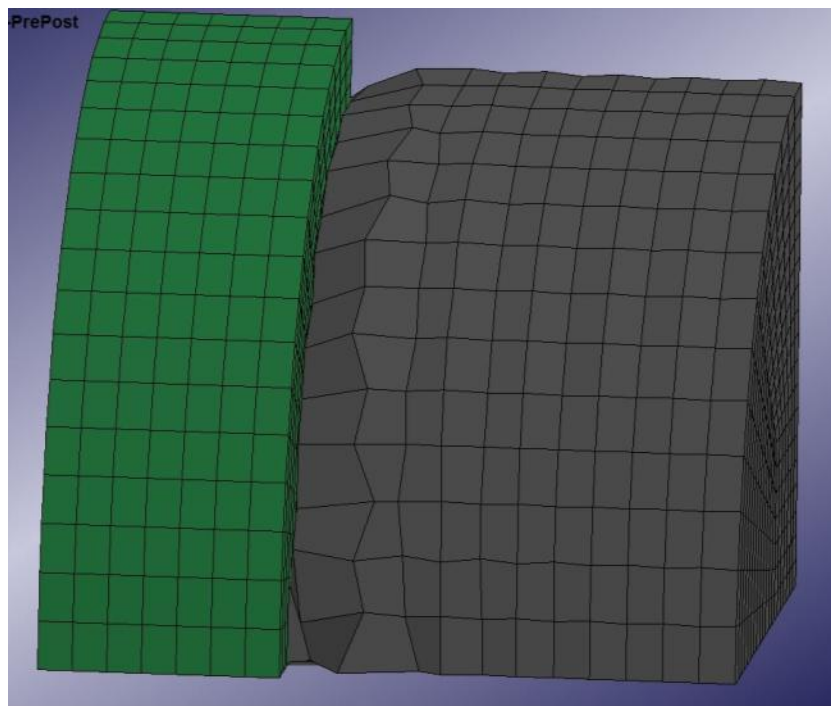
Figure 5.2 Hourglassing caused by high deformations.

Another effect of the large deformation was a tendency of the striker bar to penetrate the

foam sample surface during contact. Two variables affecting this was mesh density and mesh

alignment. Using the same mesh density and diameter for both striker bar and foam sample

caused the surface penetration to increase. Mesh densities of the striker bar and sample were

adjusted such that penetration was minimized as shown in Fig. 5.3.

Surface penetration was also found to be affected by the contact option. Selecting the

entire foam sample and striker bar in defining the "surface to surface" contact option produced

the poorest results, with the striker bar passing far into the foam sample. Penetration was

minimized when the single row of surface nodes was selected for the contact option.
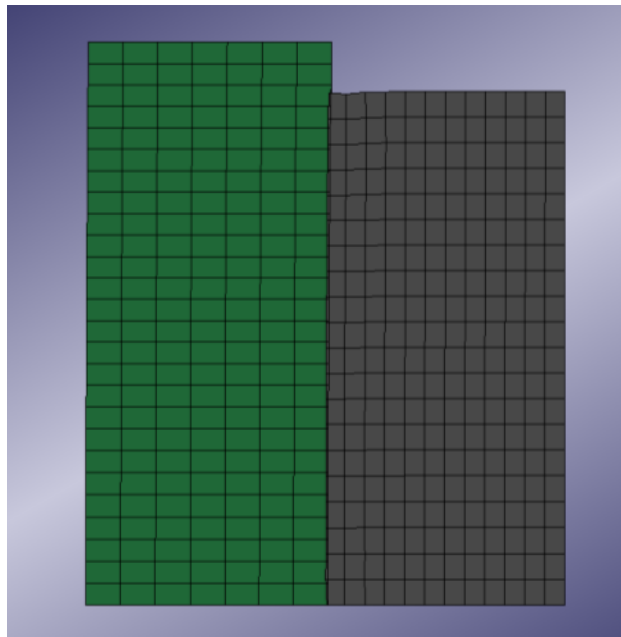
Figure 5.3 Contact penetration between the striker bar (green) and foam sample (black) during peak displacement at the highest simulated speed (41.4 mph) using Mat #57.

5.3   Mat #57 Low Density Foam

Mat #57 was the first of two LS-DYNA foam material models selected to characterize the

PU softball foam. Sambamoorthy investigated numerical simulations of dynamically-loaded PU

foams of varying densities to compare the accuracy of foam material models in LS-DYNA

(Sambamoorthy, 2001). From the results, Mat # 57, as well as Mat # 83 Fu Chang Foam showed

the best correlation with physical testing.

5.3.1 Material Parameters

The master curve developed from impacting foam samples in Chapter 3 was assigned as the nominal stress-strain curve used by Mat #57 to control compressive response. Because only one curve was used, rate effects in loading could not be accounted for. Small adjustments were made to the curve, particularly in the area where the elastic region transitions to the plateau region, to see how the master curve shape effected agreement with experiment. The master curve which produced the best agreement with experiment is shown in Fig. 3.17.

The primary deformation mode in the foam sample was compression. Thus Young's modulus (E), which governed tension, had little effect in the simulation (LSTC, 2010). While the actual material would experience transverse tension during compression due to the Poisson effect, Mat #57 had no Poisson formulation and thus had no transverse expansion when compressed. Young's modulus was set as the initial slope of the master loading curve.

Unloading was controlled by a hysteretic unloading factor, (HU), and a "shape" factor. HU ranged in value between zero and one. Low values of HU shifted the unloading path downward. The lowest value of HU (maximum hysteresis or energy loss) did not sufficiently account for energy loss, so the shape factor was adjusted to increase energy loss by further shifting the unloading curve down. Shape factor values ranged from zero (inactive) to 1000 (above which hysteresis did not change).

Viscous effects were controlled by a "damp" factor. Increasing damp values tended to lower displacement analogous to adding a material damper. The suggested range of damp was between 0.05 and 0.5 (LSTC, 2010). While the damp value which best matched experiment was outside this range (0.75), using values higher than this resulted in elements with negative volumes within the sample which caused the solver to abort. These negative volumes were likely

due to numerical instabilities which are discussed in section 6.3. The non-dimensional values of HU, damp and shape factors were iteratively adjusted to align the model's load displacement curves with experiment. The foam material parameters are summarized in Table 5.1 while all other parameters were left as default.

Table 5.1 Parameters used for the "Material #57 Low Density Foam" material model

Model	ρ (lb s^2/in^4)	E (ksi)	HU	Shape	Damp
Mat #57 PU Foam Sample	3.90E-05	20	0.01	30	0.75

5.3.2 Results

The model was run with initial striker bar speeds of 20.4, 29.7 and 41.4 mph to capture the low, mid-range and upper strain rates typical of play. Selection of these specific speeds also enabled direct comparison with previously-instrumented impacts. The load-displacement response of the numerical model is compared with experiment in Fig. 5.4 and shows good agreement. A notable departure between the model and experiment occurs near the peak strain of each test. The model shows no evidence of viscous softening in this region which suggests an insensitivity to time dependence. Oscillations in the numerical results at small strain magnitudes indicate the presence of elastic waves propagating through the sample. The deformation caused by compression waves, which is typical of dynamic crushing in cellular solids (Gibson, 1999), is shown in Fig. 5.5.
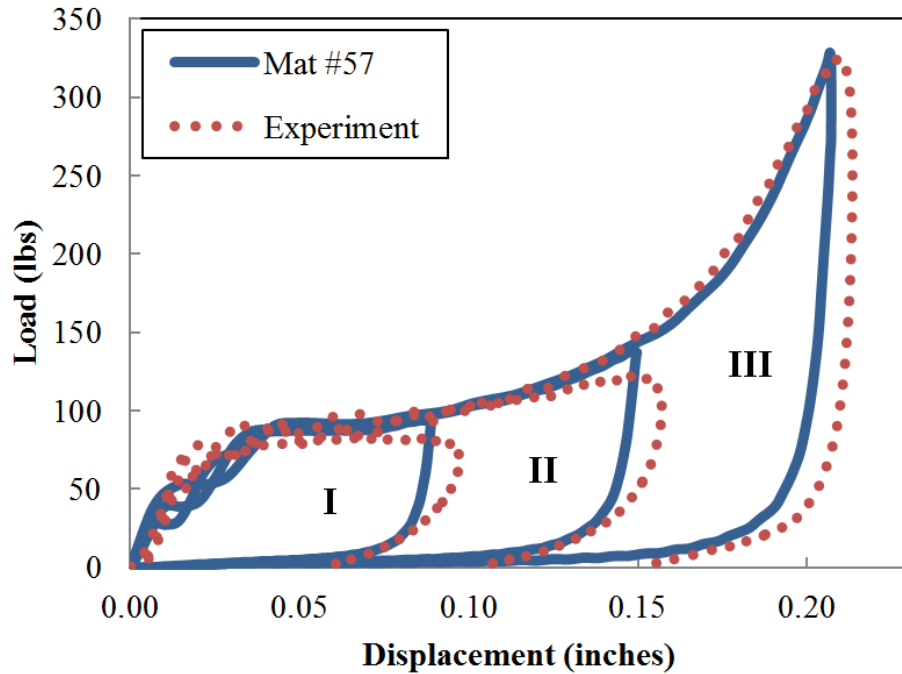
Figure 5.4 Comparison of experimental and numerical load-displacement curves of foam sample impacts at the low, medium, and upper strain rates typical of play conditions: (I) 20.4 mph, (II) 29.7 mph, and (III) 41.4 mph.
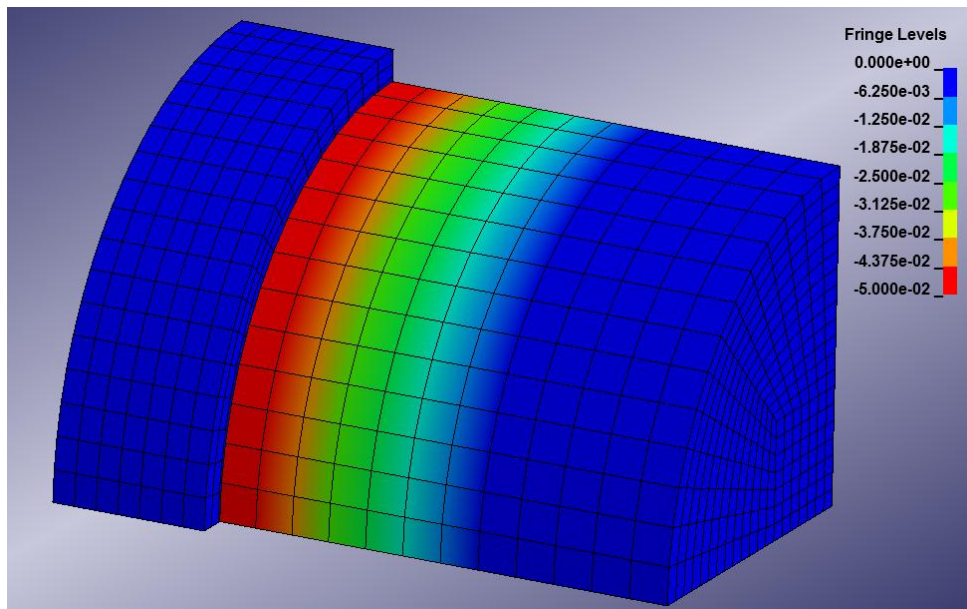
Figure 5.5 Shaded strain magnitudes highlight the localization of deformation initiated just after contact.

The impulse, peak displacement and peak force of the model agreed with experiment on average within 5%, 6% and 4% respectively. The COR from the FEA model is compared with

experiment in Fig. 5.6 and shows numerical COR changing less as a function of speed than was observed experimentally.
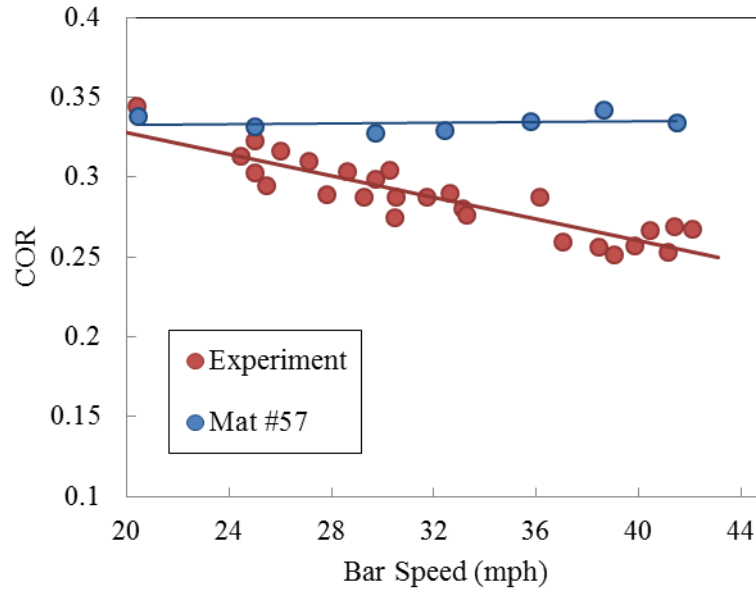
Figure 5.6 Comparison of experimental and numerical COR rate dependence for Mat #57.

5.3.3   COR Rate Dependence Parametric Study

Additional material parameters not listed in Table 5.1, but included in the MAT #57 material model were designed to control rate effects. Young's relaxation modulus and a decay constant, β, were adjusted, but the same effect was produced for all non-zero values. As shown in Fig 5.7, COR rate dependence slightly increased, but hysteresis was reduced to almost zero.
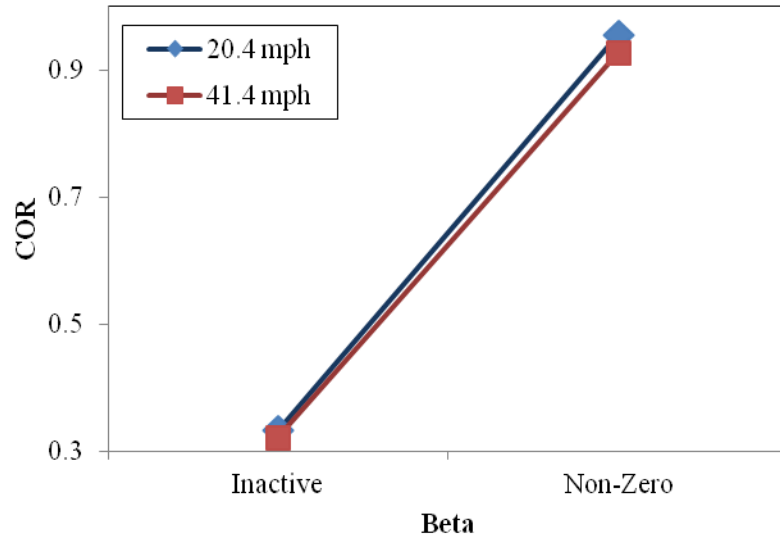
Figure 5.7 Beta, designed to control rate effects, did not significantly improve COR rate dependence.

A parametric study was performed to determine if other parameters affected COR rate dependence. HU, Shape and Damp were separately adjusted within their respective value ranges and simulated at low (20.4 mph) and high (41.4 mph) speeds to compare COR values at differing rates. As shown in Fig 5.8 - 5.10 none of the parameters changed the COR rate dependence. Results were similar for Young's modulus.
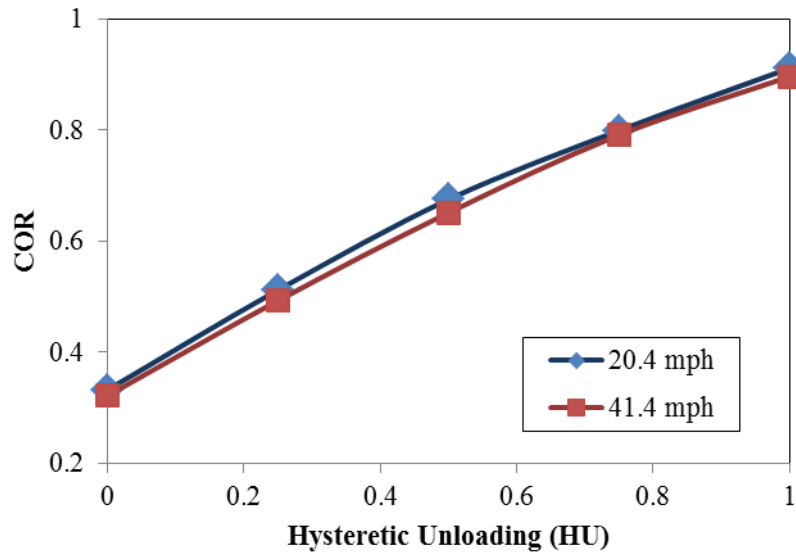
Figure 5.8 The lack of an effect on COR rate dependence is indicated by a similar COR at different speeds for all values of HU.
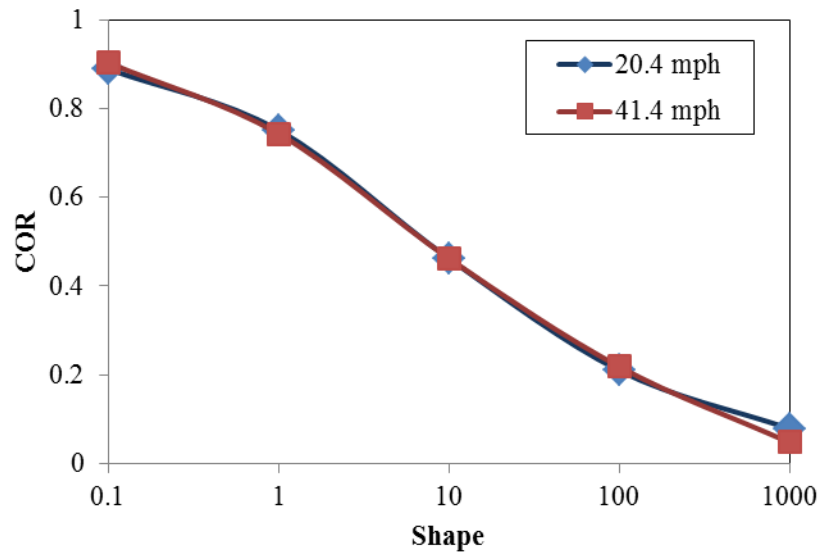
Figure 5.9 The lack of an effect on COR rate dependence is indicated by a similar COR at different speeds for all values of Shape.
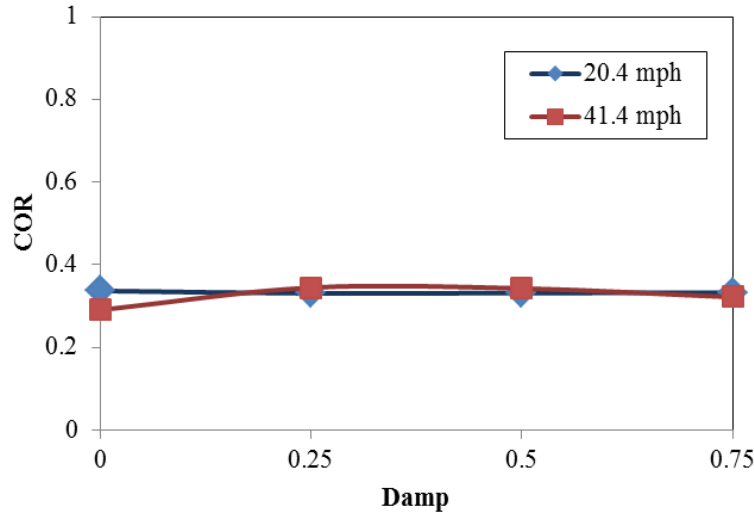
Figure 5.10 The lack of an effect on COR rate dependence is indicated by a similar COR at different speeds for all values of Damp.

5.4   Mat #83 Fu Chang Foam

The previous material model assumed a rate-independent compressive response. Because rate dependence was shown during experimental testing, another foam material designed to incorporate these effects was used. Mat #83 utilized multiple loading curves defined as a function of strain rate. The model internally applied the appropriate curve depending on the simulated loading conditions.

5.4.1   Material Development

To define the rate-dependent loading response, a table was defined which consisted of the stress-strain curves from Fig. 3.29 and their corresponding strain rate. The five curves were adjusted such that no overlapping occurred. Each line was extrapolated to higher stresses, as experimentation could not produce some strain rates at large strain magnitudes. As shown in Fig. 3.25, the stress-strain curve for the strain rate of 2000 ε/s only goes to 0.5 ε. It was assumed that at higher strain magnitudes the curves followed the trends shown at lower strain magnitudes. The LS-DYNA user's manual made no suggestion regarding the number of curves to use. It was found that the simulated loading response changed according to which curves were input.

Various combinations of curves were simulated and it was found that the best experimental agreement occurred when all five curves shown in Fig. 5.11 were used.
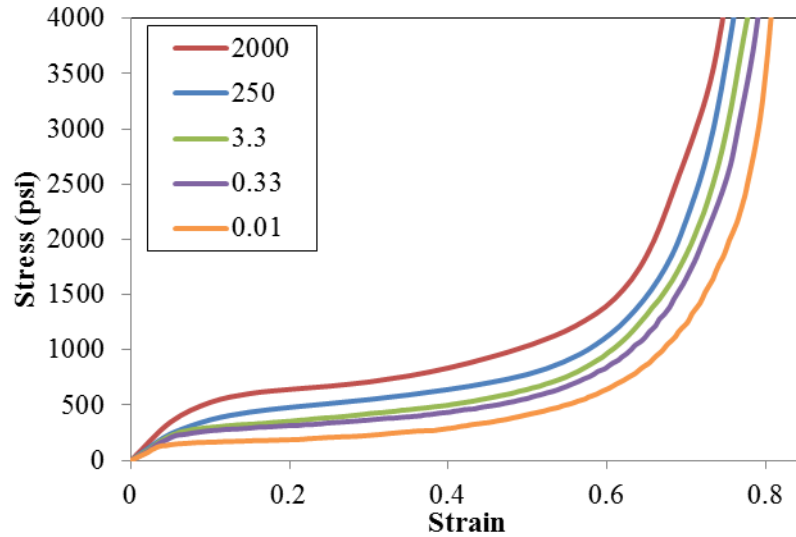
Figure 5.11 Refined stress-strain curves used in the Fu Chang Foam model.

The Fu Chang model had parameters of density, Young's modulus, damp, shape and a hysteretic unloading factor. HU, damp, and shape were adjusted to best match experiment. Similar to Mat #57, the lowest value of HU (maximum energy loss) did not sufficiently account for energy loss, so shape was adjusted to match experimental COR. Parameter values are listed in Table 5.2.The strain rate flag for this material was set to "engineering strain rate" to match the experimental engineering strain measurements.

Table 5.2 Mat #83 parameters which optimized agreement with experiment.

Model	ρ (lb s^2/in^4)	E (ksi)	HU	Shape	Damp
Mat #83 PU Foam Sample	3.90E-05	20	0.01	7.5	0.5

5.4.2 Results

The model was run at various speeds between 20.4 and 41.4 mph to capture strain rates typical of play. COR increased nonlinearly with impact speed, which was contrary to experimental behavior as shown in Fig 5.12. Interestingly, at low impact speeds, COR behaved

correctly, but deviation with experiment increased with impact speed. Theoretically, as impact speed increases, so will the stiffness of the viscous material. Increased material stiffness will lower sample displacement thereby reducing energy loss and increasing COR. This effect was not shown in experiment, but it could possibly explain the increase in COR with impact speed.
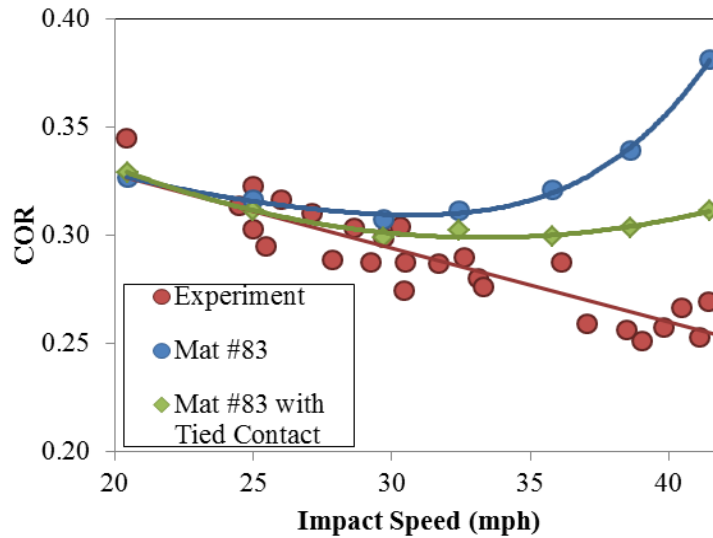
Figure 5.12 COR for Mat #83 showed an uncharacteristic, nonlinear increase in COR with impact speed.

As discussed earlier, mesh density, mesh alignment, and the contact option all affect the contact surface penetration. Re-meshing the PU foam sample from 2772 to 9765 elements resulted in the striker bar penetrating further through the foam sample. Including the second row of nodes in the contact condition also resulted in more surface penetration.

Surface penetration was minimal at low impact speeds but, as seen in Fig 5.13, increased considerably at higher speeds compared to Mat #57 in Fig. 5.3. LS-DYNA's built-in Tied Surface to Surface contact option constrains the slave nodes to move with the master surface thus eliminating surface penetration. At the beginning of the simulation, the nearest master segment for each slave node is located based on an orthogonal projection of the slave node to the master segment (LS-DYNA, 2001). Moving the striker bar closer to the foam sample (gap of 0.001

inches) and using the tied contact option eliminated surface penetration and reduced the non-linear increase in COR as shown in Fig. 5.12.
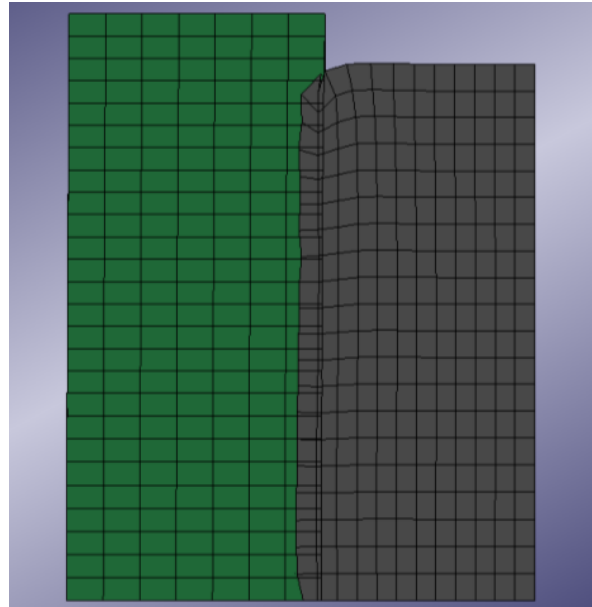
Figure 5.13 Surface penetration for a 41.4 mph impact using Mat #83.

While COR did not completely agree with experiment, the load-displacement curves agreed well as shown in Fig 5.14. An improvement over Mat #57 was shown in the viscous softening near peak displacement. Rate effects were also properly characterized by an increased stiffness at higher rates through the plateau region of loading. Oscillations in the FEA results at small strain magnitudes indicate the presence of elastic waves propagating through the sample.
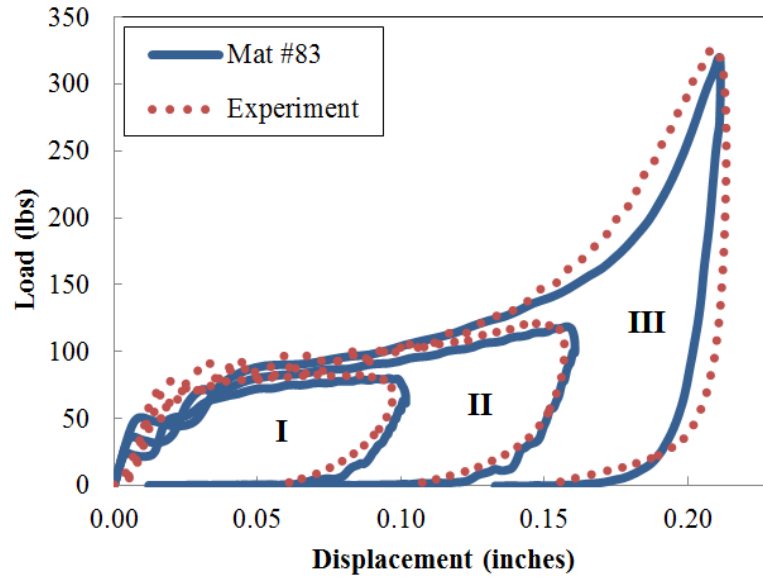
Figure 5.14 Comparison of Experimental load-displacement curves with Mat #83 at speeds of (I) 20.4 mph, (II) 29.7 mph, and (III) 41.4 mph.

5.5   Summary

Two foam material models were developed to simulate the PU foam sample impacts from Chapter 3. Large deformations in the foam sample caused issues with hour glassing and surface contact penetration which were minimized by using fully-integrated elements, and adjusting mesh densities and contact conditions.

Mat #57 showed good agreement with experimental load-displacement curves. However, its inability to account for rate effects was manifest in a lack of viscous softening near peak displacement. COR was shown to have minimal rate dependence which, after a parametric study, could not be attributed to a specific material parameter.

Mat # 83 was better able to describe rate effects in load-displacement curves, as the material allowed for rate-dependent loading characterization. Contact surface penetration was greater compared to Mat #57, causing COR to non-linearly increase with impact speed, which was not typical of experiment.

5.6   References

Duris, J. G. 2004. Experimental and numerical characterization of softballs. *Master's Thesis, Washington State University.* 2004.

Gibson, L. Ashby, M. 1999. *Cellular Solids.* Cambridge, MA : Cambridge University Press, 1999. ISBN: 0521499119.

LS-DYNA, 2001. LS-DYNA Support. [Online]. 2001. [Cited: February 15, 2012] [Online] http://www.dynasupport.com/tutorial/contact-modeling-in-ls-dyna/contact-types

LSTC, 2010. LS-DYNA Keyword User's Manual Volume II Material Models. Version 971/ Rev 5.

Sambamoorthy B, Halder T. 2001. Characterization and component level correlation of energy absorbing (EA) polyurethane foams (PU) using LS-DYNA material models. LS-DYNA Eurpoean Conference.

6   Ball Modeling

6.1   Introduction

To allow direct comparison with experimental results from Chapter 4, softball impacts on cylindrical and flat impact surfaces were simulated in LS-DYNA. The following will discusses results from implementing both foam material models from Chapter 5.

In past research, softball models have been modeled using a linear viscoelastic material. Shortcomings in these models were shown when characterizing impact behavior over changes in impact speed and surface geometry. The following will also compare the impact behavior of the current foam material models to the viscoelastic models of previous studies.

6.2   FEA Setup

The softball and cover were modeled as a single, isotropic, homogeneous sphere as done elsewhere (Duris, 2004), (Faber, 2010). The softball was modeled using 7,168 linear, solid elements and quarter symmetry. Elastically-characterized cylindrical and flat impact surfaces shown in Fig. 6.1 were modeled with 4,864 and 2000 nodes respectively. The base of each impact surface was constrained normal to the line of impact and the contact type was surface to surface. Penetration between the ball and impact surface was negligible compared to the PU foam sample models.

Impact force and ball displacement were measured during the simulation and exported to output files which were subsequently used to calculate ball performance and produce load-displacement curves. The position history of the ball's central node was used to measure both the displacement during impact and the rebounding velocity. The ball was given an initial speed in

the simulation setup and equation 2.2 was used to calculate COR and CCOR. Equation 2.8 was used to calculate impulse.

Equation 2.7 defines DS as a function of ball mass, initial ball velocity and peak impact force. Because numerical ball mass and velocity were set equal to experiment, percent difference in DS values were equal to the square of the percent difference in peak force. Thus, comparison of both DS and peak force was superfluous.

Mesh density was determined to be sufficient, as doubling the number of elements altered impulse, displacement and impact force by only 2%. Interestingly, the mesh alignment between the ball and impact surface was found to have a small effect on impact performance. These effects were, however, minimal compared to those caused by material type and surface geometry.
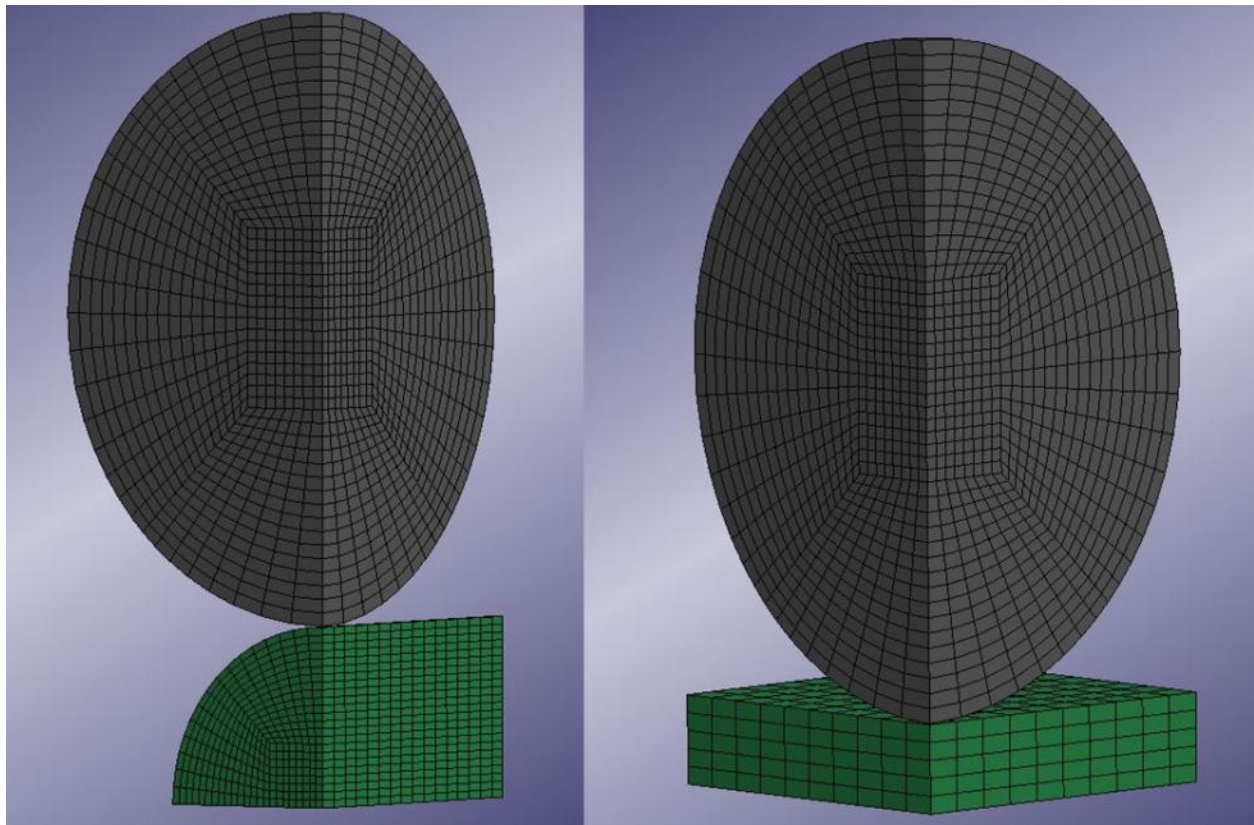
Figure 6.1 Softball model with cylindrical and flat impact surfaces using quarter symmetry.

6.3   Mat #57 Low Density Foam

Applying the material parameters from the PU foam sample model to the softball model resulted in poor agreement with experiment. On the cylindrical surface, impulse, loading stiffness and displacement differed from experiment by 13%, 18% and 15% respectively, while CCOR was 36% lower than experiment. The damp factor was increased and the shape factor was decreased to improve correlation with the loading stiffness and CCOR respectively.

As damp was increased to better match experiment, the solver would abort due to elements with negative volumes. According to LS-DYNA, negative volumes can be caused by using fully integrated elements, which are less robust than a 1-point element when deformation is large. This is because a negative Jacobian can occur at one of the integration points while the element as a whole maintains a positive volume (LS-DYNA, 2003). It was found that using 1-point elements as well as reducing the timestep scale factor below the default value of 0.9 prevented the numerical instabilities and allowed adjustment of the damping values to best match experiment.

Adjustment of damp and shape improved cylindrical performance significantly. Impulse, force, displacement, and CCOR of the modified ball model were, on average, within 3%, 3%, 4% and 4% of experiment respectively. Load displacement curves of Mat #57 shows excellent experimental correlation with respect to curve shape and loading stiffness as shown in Fig. 6.2. Parameters of both the PU foam sample model and softball model are summarized in Table 6.1. Performance values for Mat #57 are listed in Tables A.1 and A.2 in the appendix.
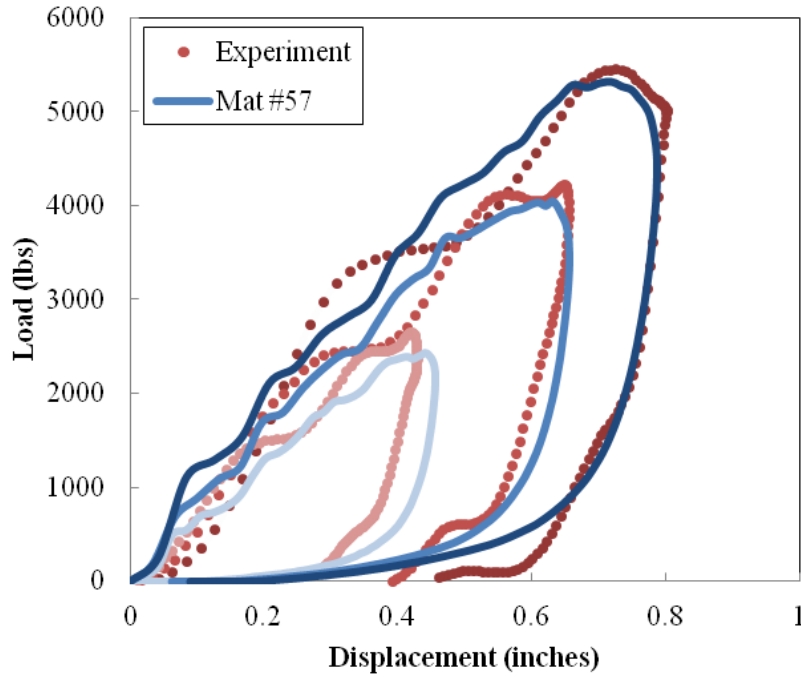
Figure 6.2 Cylindrical impact surface comparison of experimental load-displacement curves with Mat #57. Shades indicate speed at (light) 60mph, (normal) 95 mph, and (dark) 120 mph.

Table 6.1 FEA material model parameters for Mat#57: Density (ρ), Young's modulus (E), hysteretic unloading factor (HU), shape factor, and damp factor.

Model	ρ (lb s²/in⁴)	E (ksi)	HU	Shape	Damp
PU Foam Sample	3.90E-05	20	0.01	30	0.75
Softball	3.90E-05	20	0.01	6	1.8

On a flat surface, peak force, COR, impulse, and displacement all maintained excellent agreement with experiment across the tested speed range (4%, 5%, 5%, 2% average respectively). The flat surface load-displacement curves in Fig. 6.3 show no decrease in the model's exceptional correlation with experiment when surface geometry was altered.
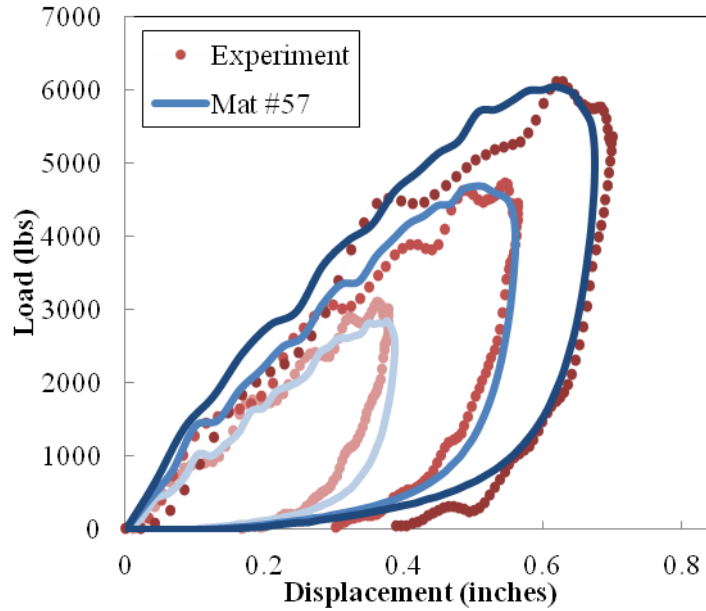
Figure 6.3 Flat impact surface comparison of experimental load-displacement curves with Mat #57. Shades indicate speed at (light) 60mph, (normal) 95 mph, and (dark) 120 mph.

The coefficient of friction between leather and dry metal is approximately 0.5 (Engineering Handbook, 2006). For Mat #57, adding friction to the contact condition at 120 mph increased force 2% but decreased both COR and displacement by 5% and 2% respectively. Friction also lowered CCOR rate dependence by 11%. A soft option in the surface to surface contact condition has been previously used in simulating the felt on tennis balls (Allen, 2008). Interestingly, when active, the soft option actually reversed the effects of surface geometry, causing CCOR to have a higher value than COR.

6.3.1 COR Rate Dependence

Although lower than experiment, the rate dependence of CCOR, as shown in Fig. 6.4, and COR improved over that of the PU foam sample model. The parametric study in Chapter 5 showed that none of the adjustable parameters in Mat #57 improved COR rate dependence. A similar parametric study of the softball simulation revealed that damp, HU, shape and β each affected COR rate dependence (Fig 6.5-8). HU, shape and non-zero values of β improved COR rate dependence at the cost of increasing COR value.
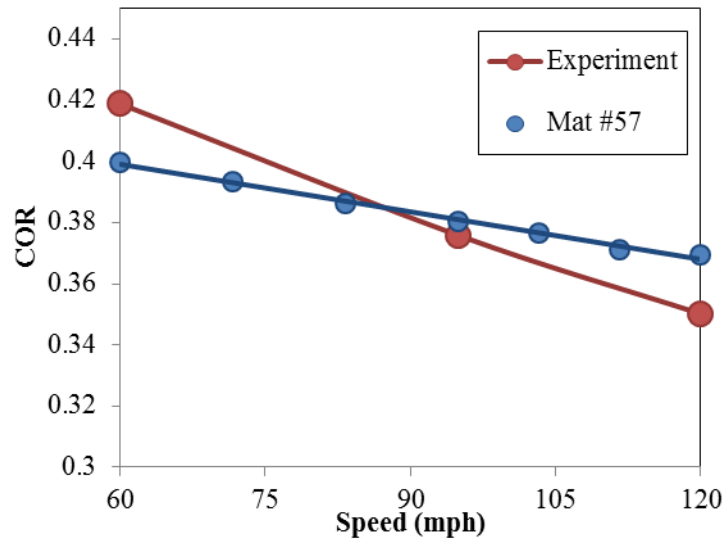
Figure 6.4 Mat #57 CCOR rate dependence was lower than experiment.
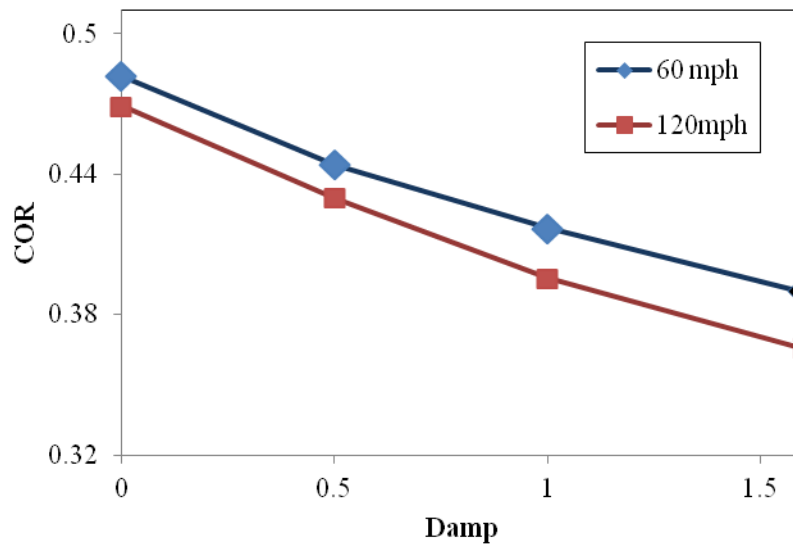
Figure 6.5 The effect of damping factor (damp) on COR rate dependence. Black markers indicate values used in the model.
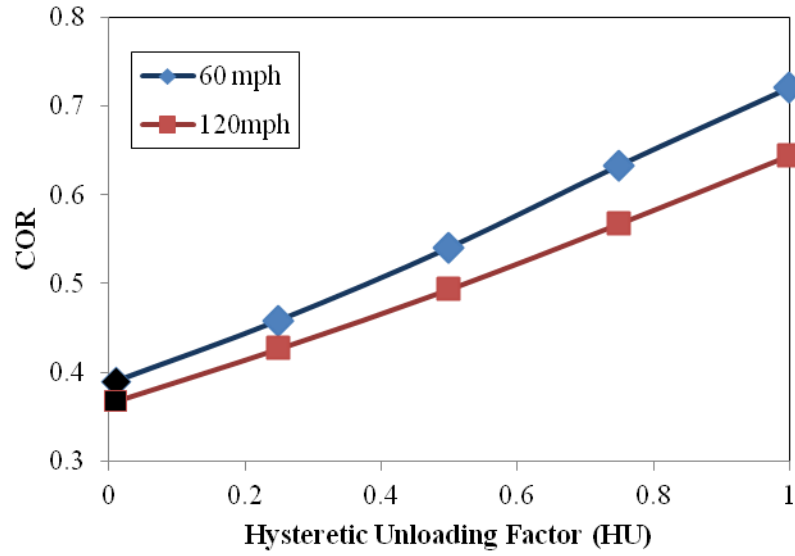
Figure 6.6 The effect of Hysteretic Unloading Factor (HU) on COR rate dependence. Black markers indicate values used in the model.
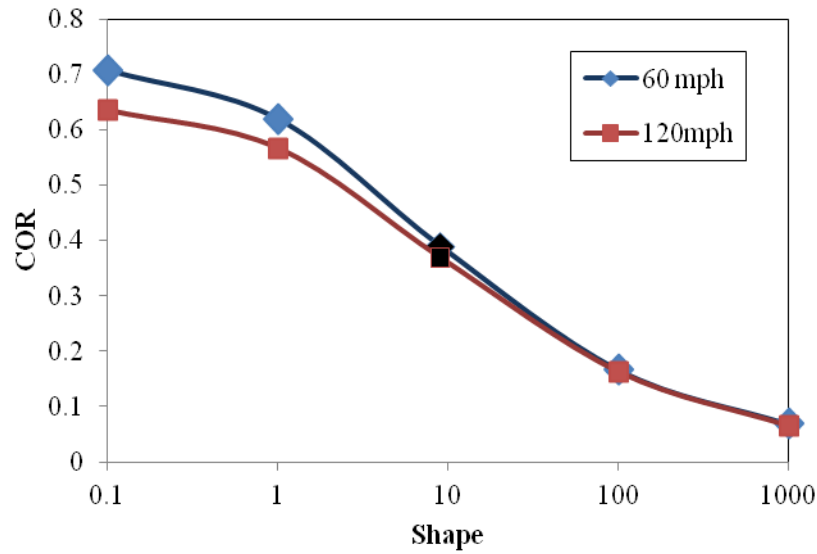
Figure 6.7 The effect of Shape Factor on COR rate dependence. Black markers indicate values used in the model.
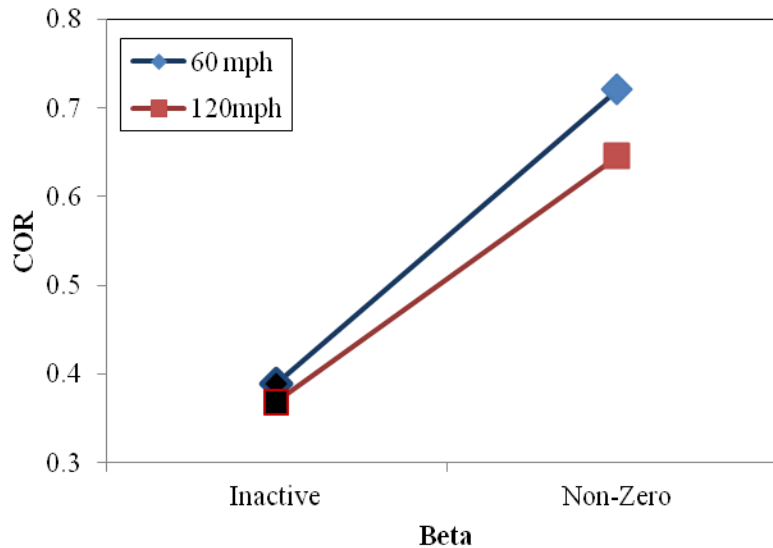
Figure 6.8 The effect of beta on COR rate dependence.

6.3.2 Strain Magnitude and Rate

Strain within the numerical softball was investigated for Mat #57 as it showed good agreement with experimental load-displacement curves. Figure 6.9 shows an increase in both peak strain and the area of the ball with strain magnitudes above the elastic region ($> 0.1\ \varepsilon$) for increasing impact speed. Interestingly, peak strain in the model increased 21% between impacts of 60 and 95 mph, but only 3% between impacts of 95 and 120 mph.

According to the foam structural damage results from chapter 3, regions of the ball shaded green through red in Fig 6.9 should experience permanent residual strain. Impacts at 95 mph clearly have densification strains, however experimental testing in chapter 4 showed no significant change in impact performance for repeated testing at this speed.
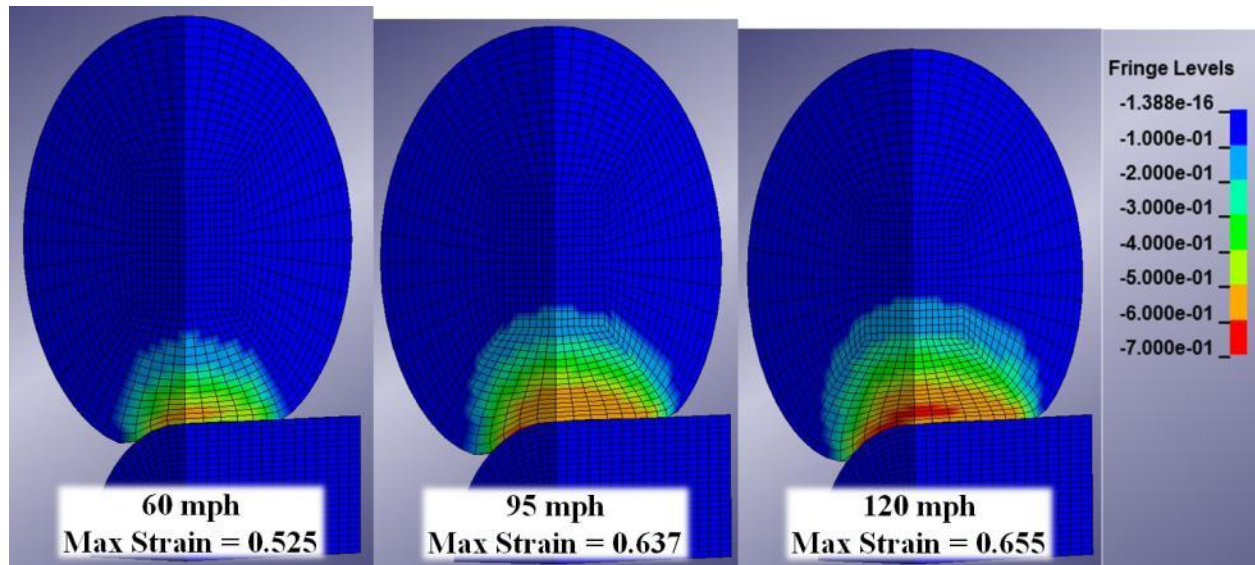
Figure 6.9 Cross sectional strain distribution of Mat #57 at the three instrumented speeds.

Bryson defined the highest strain rate experienced in a 95 mph softball collision to be about 2500 s^{-1} (Bryson, 2009). In his FEA model, this value was measured where the ball first contacted the impact surface. Using a similar location shown in Fig. 6.10, strain rates were measured for Mat #57 and are plotted in Fig. 6.11.
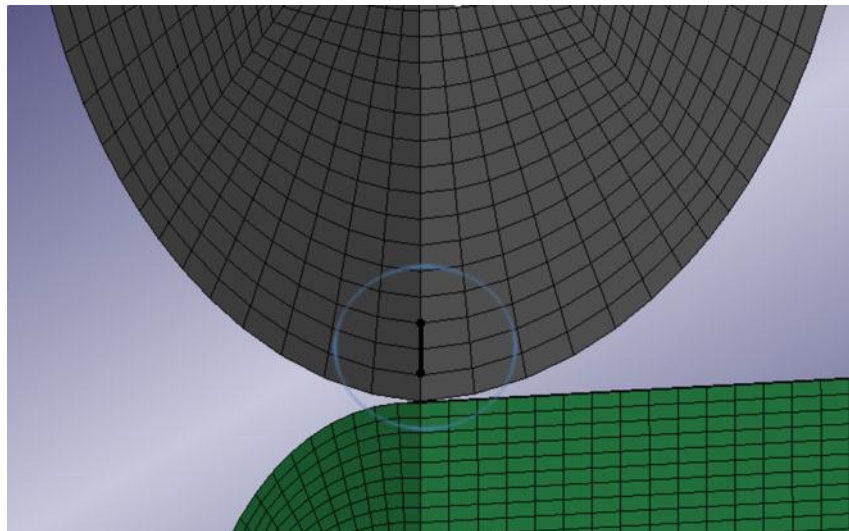
Figure 6.10 Node segment along which peak strain rate was measured.
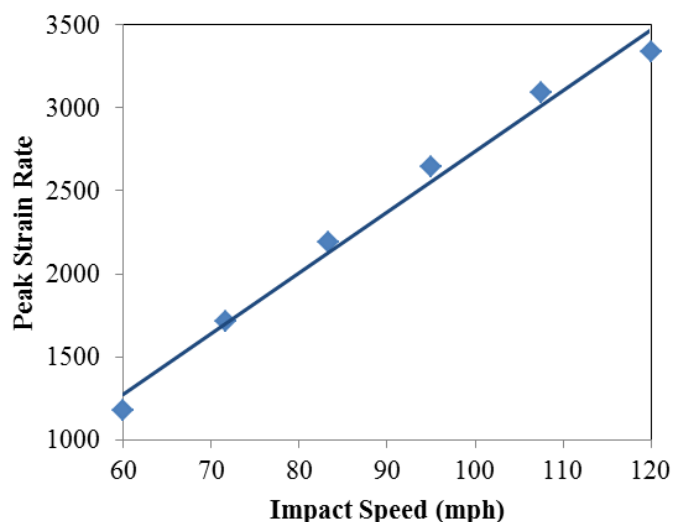
Figure 6.11 Peak strain rate in a softball as a function of impact speed.

As expected, a linear correlation with impact speed was shown. While the peak strain rate at 95 mph matched closely with Bryson's definition, the lower strain rate typical of play listed earlier (1000 s^{-1}) agreed well with the strain rate at 60 mph. Collision velocities above 95 mph, however, can be exceeded at higher levels of play. With bat swing speeds approaching 100 mph for high-level male players (Smith, 2012), and fastpitch pitch speeds above 70 mph (National Pro Fastpitch, 2012), the peak strain rate typical of play should be closer to 3500 s^{-1}.

6.4   Mat #83 Fu Chang Foam

The Fu Chang material model was implemented on both cylindrical and flat impact surfaces. The softball, however, was much too compliant when simulated with parameters from the PU foam sample model. As was done with Mat #57, damp and shape were adjusted to optimize agreement with experiment and are listed in Table 6.2. 1-point elements were used and the timestep scale factor was lowered below default (0.9) to achieve the ideal damp values.

Table 6.2 Material parameters used for Mat#83.

Model	ρ (lb s^2/in^4)	E (ksi)	HU	Shape	Damp
Mat #83 PU foam sample	3.90E-05	20	0.01	7.5	0.5
Mat #83 Softball	3.90E-05	20	0.01	0.57	5.5

Load displacement curves for cylindrical and flat surfaces are shown in Fig 6.12 and 6.13. While initial stiffness closely matched experiment at higher speeds, a softening behavior, indicated by a decrease in stiffness, was shown near peak deformation. The softening caused lower peak forces (16% average) and larger displacements (8% average) than experiment. Performance values for Mat #83 are listed in Tables A.1 and A.2 in the appendix.
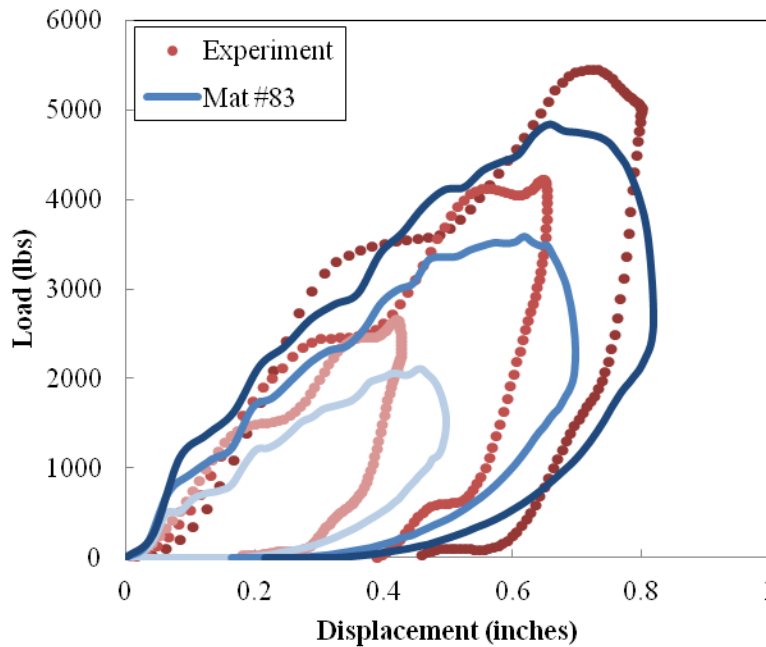
Figure 6.12 Cylindrical surface load-displacement curves for Mat #83. Shades indicate speed at (light) 60mph, (normal) 95 mph, and (dark) 120 mph.
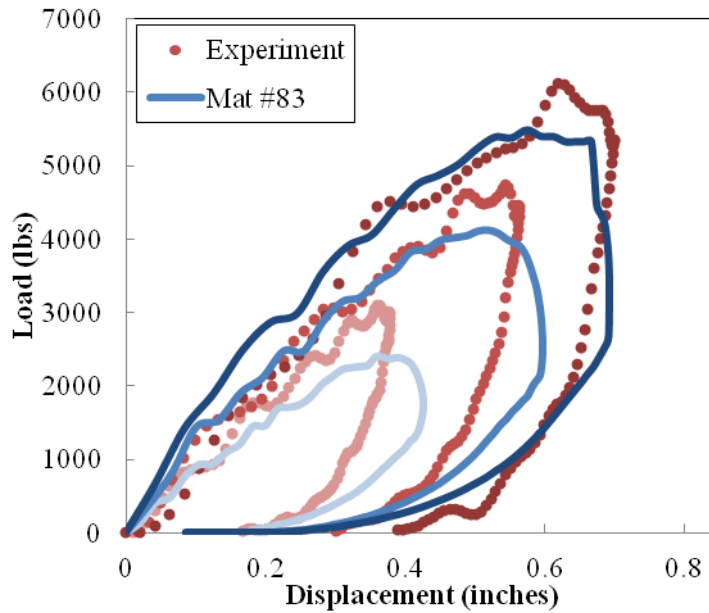
Figure 6.13 Flat surface load-displacement curves for Mat #83. Shades indicate speed at (light) 60 mph, (normal) 95 mph, and (dark) 120 mph.

Mat #83 showed excellent agreement with experimental COR value and rate dependence. On both flat and cylindrical surfaces, COR was consistently within 2% of experiment, while the CCOR rate dependence (the slope in Fig. 6.14) was 2% lower than experiment. COR rate dependence was 4% lower than experiment.
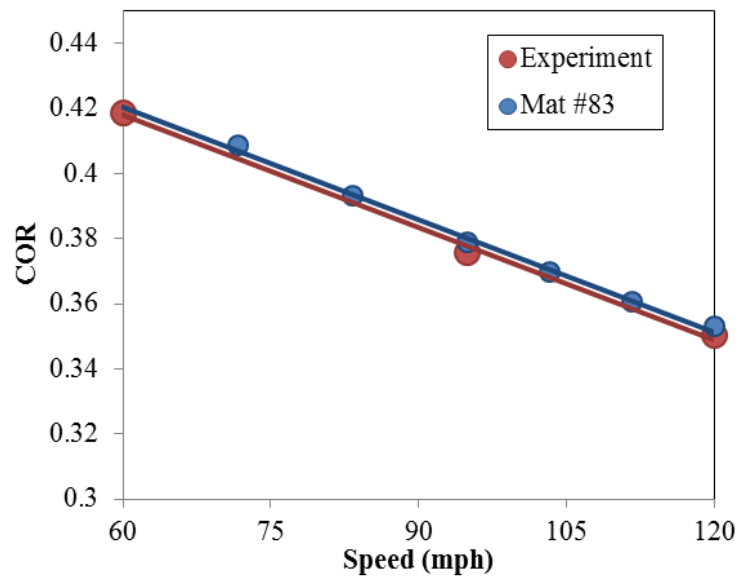
Figure 6.14 Comparison of experimental and numerical CCOR for Mat #83.

Implementing friction into the contact condition for Mat #83 increased peak force 12% at 120 mph but lowered it 2% at 60 mph. Friction decreased COR rate dependence by 4%.

6.5   Linear Viscoelastic Model Comparison

Previous work by Duris, Faber and Bryson produced finite element models of softballs in LS-DYNA using the standard viscoelastic material model (Duris, 2004), (Faber, 2010), (Bryson 2009). The authors each published material parameters for their models as summarized in Table 6.3. Each viscoelastic material was applied to the simulated softball impact and the results were compared to the foam models developed in this study. Performance values for the viscoelastic models are listed in Tables A.1 and A.2 in the appendix.

Table 6.3 FEA material parameters from previous viscoelastic softball models: density (ρ), bulk modulus (K), instantaneous shear modulus (G0), long term shear modulus ($G\infty$) and decay constant (β).

Model	ρ (lb s^2/in^4)	K (psi)	G_0 (psi)	G_∞ (psi)	β (Hz)
Duris	3.90E-05	1E7	1E4	700	68000
Faber	3.90E-05	1E5	2E4	1000	68000
Bryson	3.90E-05	1E6	3500	400	40000

The load-displacement cylindrical surface response of the foam and viscoelastic models is compared at 95 mph in Fig. 6.15. The loading stiffness, peak displacement and peak force of Mat #57 agreed best with experiment. Mat #57 also most accurately matched the unloading shape. All three viscoelastic models displayed a generally oval-shaped curve; indicating a different mechanism of deformation than occurs with foam. Mat #83 showed a linear loading response similar to Mat #57, but had a more oval unloading shape similar to the viscoelastic models. A similar comparison, but of a flat surface impact is shown in Fig. 6.16. Mat #57 again shows the best agreement with experiment. A clear difference was again shown between the linear loading of the foam models and the oval-shaped viscoelastic curves.
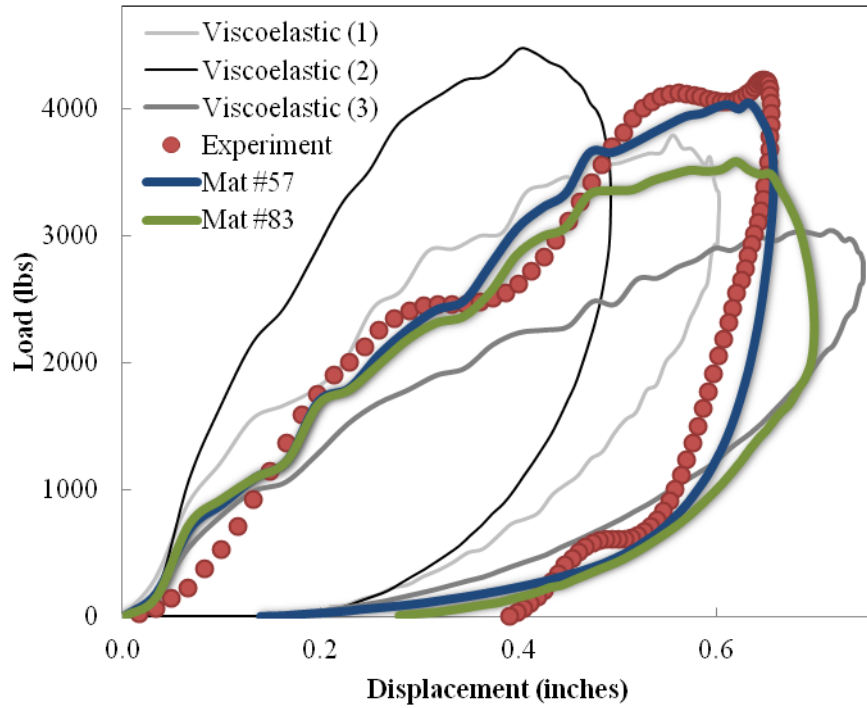
Figure 6.15 Cylindrical surface, load-displacement curves at 95 mph. Viscoelastic models from previous studies are compared to the foam models developed in this study. Viscoelastic models are from (1) Duris, (2) Faber, and (3) Bryson.
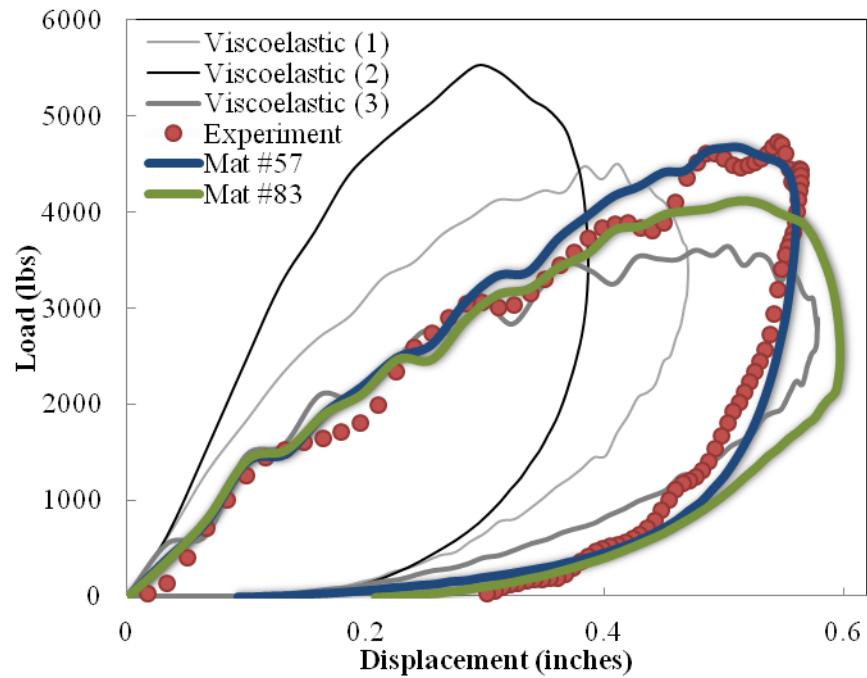
Figure 6.16 Flat surface, load-displacement curves at 95 mph. Viscoelastic models from previous studies are compared to the foam models developed in this study. Viscoelastic models are from (1) Duris, (2) Faber, and (3) Bryson.

95 mph COR and CCOR from the FEA models is compared with experiment in Figure 6.17. Since impacts on a flat surface have less ball deformation and less energy loss, the COR should be greater than the CCOR. Both foam models correctly reflected the effect of surface geometry on COR, whereas all three viscoelastic models show CCOR greater than COR. The magnitude of COR and CCOR of both foam modes were closer to experiment than any of the viscoelastic models.
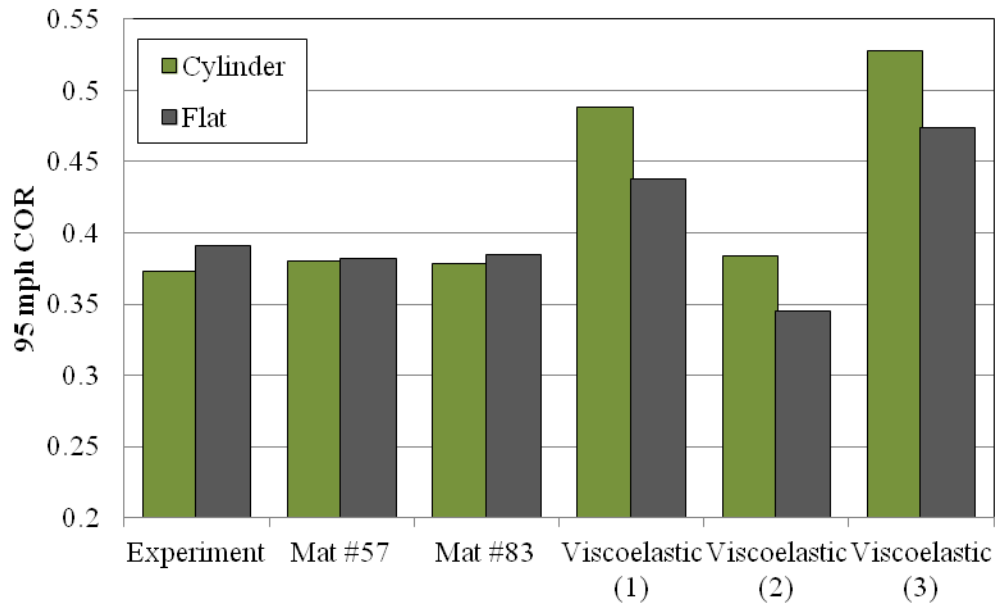
Figure 6.17 COR value as a function of surface geometry. Previous viscoelastic models are compared to the foam models developed in this study. Viscoelastic models are from (1) Duris, (2) Faber, and (3) Bryson.

The dependence of COR and CCOR on impact speed was observed to be linear in Table 4.2. The slope of numerical COR and CCOR (as a function impact speed) is compared with experiment in Figure 6.18. Mat #83 better matched experimental COR and CCOR rate dependence than any other model. Interestingly, all models correctly described the higher rate dependence of the flat surface impacts over the cylindrical impacts. The lack of sensitivity to time dependence in Mat #57 has been manifest throughout this study and Fig 6.18 is no exception.
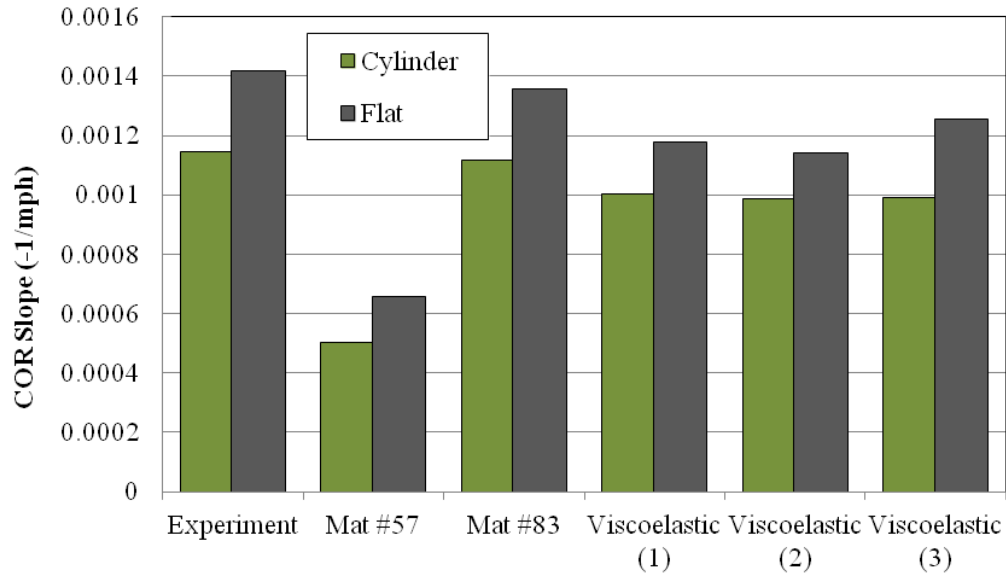
Figure 6.18 COR rate dependence as a function of surface geometry. Previous viscoelastic models are compared to the current foam models. Viscoelastic models are from (1) Duris, (2) Faber, and (3) Bryson.

Dynamic stiffness was compared for each material model at 95 mph in Fig 6.19. While Mat #57 did not best match either flat or cylindrical DS, it outperformed all models when both cylindrical and flat DS were considered across all speeds (11% average). DS for Mat #83 was lower than most models, which was due to the previously-discussed softening behavior at lower strain rates. Faber's single objective for his model was to accurately emulate CCOR and DS on a cylindrical surface at 95 mph (Faber, 2009). While his model had the most accurate cylindrical DS at 95 mph, the model had the poorest match with experimental DS on a flat surface.
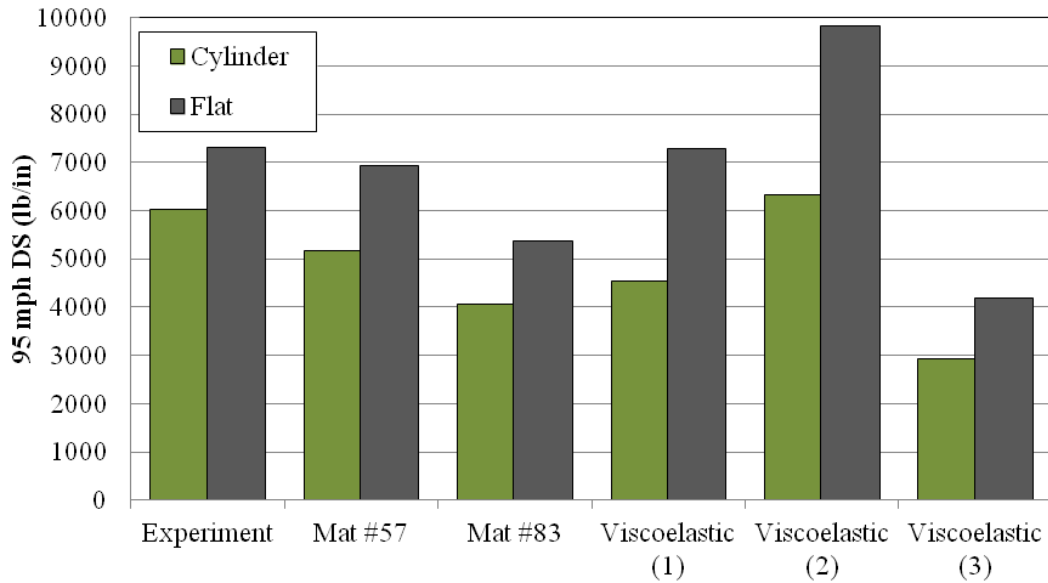
Figure 6.19 Comparison of dynamic stiffness. Viscoelastic models are from (1) Duris, (2) Faber, and (3) Bryson.

A comparison of DS rate dependence is shown in Fig 6.20. Mat #57 was the only model to correctly emulate a lower rate dependence of DS on a flat surface compared to a cylindrical surface. Mat #57 also best matched DS rate dependence on both impact surfaces.
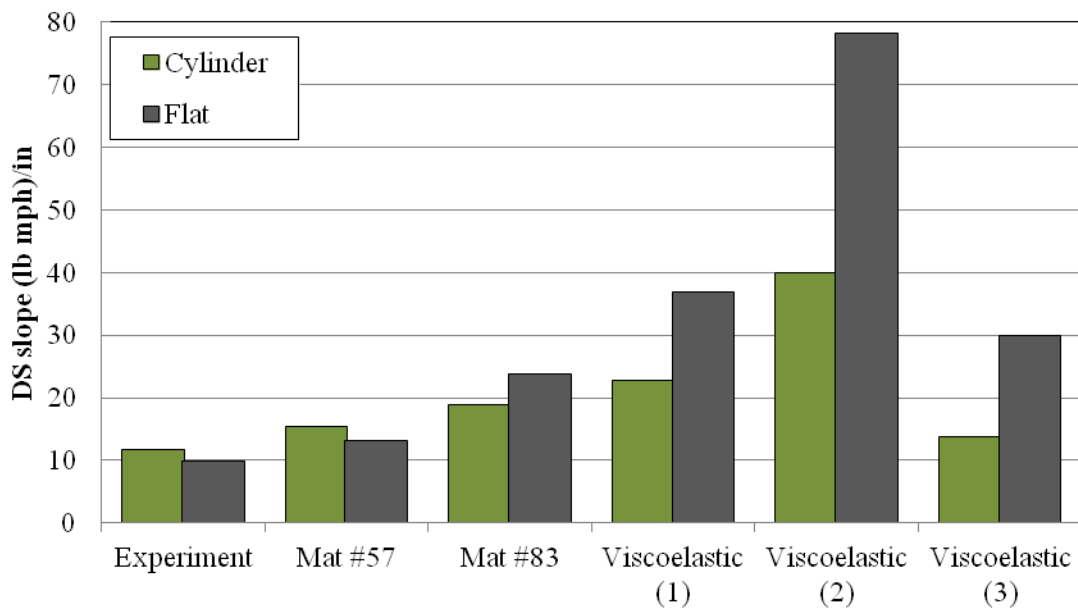
Figure 6.20 DS rate dependence as a function of surface geometry. Viscoelastic models are from (1) Duris, (2) Faber, and (3) Bryson.

6.6 Summary

The two foam material models developed in Chapter 5 were used in simulated softball impacts on flat and cylindrical surfaces. Speeds identical to experiment in Chapter 3 were used to directly compare load-displacement curves. Surface penetration and hour glassing were found to affect the simulation less than the PU foam sample model in Chapter 5.

Mat #57 showed the best agreement with experimental load-displacement curves and DS across variations in both impact speed and surface geometry. The material's COR rate dependence improved over the PU foam sample model, but was still below experiment. A parametric study revealed that COR rate dependence improved slightly as parameters were adjusted to lower energy loss. Cross-sectional strain distributions showed peak strain magnitudes occurring near the collision surface with strain magnitudes well into the densification region of compressive foam response for typical impact speeds.

Mat #83 best agreed with experimental COR and CCOR rate dependence compared to any existing model. A softening behavior was shown as loading rate decreased. This is likely a result of the material's time-dependent formulation.

Comparison with viscoelastic material models from previous studies showed key improvements. Both foam models correctly characterized the effect of surface geometry on COR, whereas previous viscoelastic models did not. The oval shaped load-displacement curves of the viscoelastic models incorrectly characterized the softball's linear loading which was well-defined for both foam material models.

6.7   References

Allen, T. Goodwill, S. R and Haake, S. J. 2008. Experimental validation of a tennis ball finite-element model for different temperatures. *The engineering of sport 7.* Springer, 125-133.

Bryson, A. J. 2009. Impact response of polyurethane. *Master's thesis, Washington State University.* 2009.

Duris, J. G. 2004. Experimental and numerical characterization of softballs. *Master's Thesis, Washington State University.* 2004.

Faber, W. L. 2010. Reducing the effect of ball variation in bat performance measurements. *Master's thesis, Washington State University.* 2010.

LS-DYNA, 2003. LS-DYNA Support. [Online]. 2003. [Cited: February 9, 2012]

http://www.dynasupport.com/howtos/material/negative-volume-in-soft-materials

National Pro Fastpitch. 2012. Fastpitch Facts. [Online] 2012. [Cited: January 24, 2012.]

http://www.profastpitch.com/fanz/facts/

Smith, L.V. 2012. Field Measurements of Softball Player Swing Speed. *9th Conference of the International Sports Engineering Association.*(Unpublished)

7   Summary

The foregoing has been concerned with improving numerical predictions of solid sport ball impacts. Desired improvements over previous ball models included a rate dependent response and characterization across impact surfaces of varying geometry. A key distinction from previous models, which involved viscoelastically-characterized materials, was approaching the softball as a structural foam.

A new test method was developed to characterize the ball material at strain rates and magnitudes representative of play conditions. Results of this method showed a material response that is consistent with structural foam. Impacting PU foam softball samples with varying masses at multiple speeds resulted in compressive stress-strain curves which were used in two different numerical foam material models.

Numerical softball impacts were directly compared with experiment. An air cannon was used to fire softballs at both cylindrical and flat impact surfaces across a range of speeds typical of play (60 to 120 mph). Impact properties including COR, DS, impulse, peak force and displacement were measured and later used to both optimize and assess numerical agreement. Experimental COR linearly decreased with increasing impact speed while impulse, force, displacement and DS increased. The cylindrical impact surface had higher displacement but lower COR, force and DS than the flat impact surface.

In optimizing the foam material models, numerical simulations of the impacted PU foam softball samples were compared to experiment. Mat #57, which had no formulation to implement rate effects, showed good load-displacement agreement but lacked the temporal dependence of COR typical of experiment. Mat #83 used multiple curves from different loading rates to successfully characterize an increase in loading stiffness with impact speed. Surface penetration

was, however, more significant than with Mat #57, resulting in a nonlinear increase in COR with impact speed.

Incorporating the foam material models into softball simulations impacting flat and cylindrical surfaces significantly improved correlation with measured ball response compared to previous viscoelastic models. Optimal agreement was only achieved, however, when the foam material parameters were tailored to the measured ball response. Mat #57 was able to describe the time and surface geometry dependence of load-displacement curves, as well as the dynamic stiffness response, better than any other material model. Both foam models correctly emulated the effect of a changing impact surface on COR as well as a softball's linear loading behavior. Mat #83 better emulated COR and CCOR rate dependence than any other material model.

7.1   Future Work

Obtaining an appropriate description of the ball remains the primary impediment to modeling sports ball impacts with high energy dissipation. While progress in this area continues to be made, the models have not evolved to the point where they can be used ubiquitously in product development or design.

Although Mat #57 was able to describe load and displacement well on both flat and cylindrical surfaces, its lack of rate dependent formulation weakened the material's overall robustness. Future work could be done to investigate other foam material models which incorporate rate effects. A potential foam model in LS-DYNA is Mat #73, which uses one stress-strain loading curve similar to Mat #57, but incorporates a relaxation curve for rate effects. An improved description of time dependence will be key to future improvements of solid ball impacts using foam material models.

Mat #83 incorporated rate effects well, but was unable to match experimental stiffness near the climax of collision. Improvement in low-rate characterization could possibly be achieved through more rigorous experimentation.

Both Mat #57 and Mat #83 outperformed the viscoelastic models with contrasting behaviors which lends both materials to specialized uses in future simulations. Mat #57 closely emulated experimental stiffness and forces which are critical for simulating collisions with objects which sustain structural damage. Impacts with safety equipment or testing of bodily injury would be well suited. Mat #83 best characterized the ball's rebounding rate dependence and would be best applied where rebounding properties are critical. Simulations of bat-ball collisions or other equipment performance testing would be ideal.

Appendix A

Table A.1 Cylindrical surface performance of each model.

	Experiment	Mat #57	Mat #83	Duris	Faber	Bryson
60 mph						
COR	0.419	0.400	0.428	0.516	0.416	0.539
Impulse (lb s)	1.74	1.67	1.71	1.83	1.70	1.89
Force (lbs)	2576	2434	2106	2149	2478	1742
Disp (inches)	0.425	0.456	0.498	0.453	0.371	0.566
DS (lb/in)	5487	4914	3794	3928	5086	2805
95 mph						
COR	0.376	0.380	0.379	0.471	0.374	0.515
Impulse (lb s)	2.68	2.60	2.61	2.83	2.63	2.92
Force (lbs)	4132	4047	3585	3790	4476	3041
Disp (inches)	0.631	0.657	0.698	0.603	0.494	0.748
DS (lb/in)	6027	5782	4617	5104	7119	3510
120 mph						
COR	0.350	0.370	0.353	0.445	0.352	0.480
Impulse (lb s)	3.28	3.26	3.23	3.52	3.27	3.62
Force (lbs)	5297	5325	4842	5036	6055	4037
Disp (inches)	0.780	0.788	0.819	0.694	0.569	0.860
DS (lb/in)	6192	6257	5211	5610	8259	3813

Table A.2 Flat surface model performance comparison of percent difference from experiment.

	Experiment	Mat #57	Mat #83	Duris	Faber	Bryson
60 mph						
COR	0.442	0.409	0.435	0.454	0.359	0.473
Impulse (lb s)	1.80	1.68	1.72	1.77	1.65	1.82
Force (lbs)	2996	2856	2396	2785	2944	2041
Disp (inches)	0.378	0.388	0.426	0.360	0.296	0.446
DS (lb/in)	7236	6473	4553	6153	6874	3305
95 mph						
COR	0.391	0.382	0.385	0.403	0.312	0.431
Impulse (lb s)	2.72	2.61	2.61	2.71	2.53	2.78
Force (lbs)	4805	4681	4117	4800	5576	3638
Disp (inches)	0.568	0.560	0.596	0.470	0.387	0.578
DS (lb/in)	7319	6935	5363	7291	9841	4189
120 mph						
COR	0.357	0.370	0.367	0.374	0.292	0.394
Impulse (lb s)	3.34	3.25	3.24	3.36	3.14	3.43
Force (lbs)	6286	6053	5489	6496	7637	5074
Disp (inches)	0.687	0.674	0.693	0.536	0.440	0.658
DS (lb/in)	7828	7268	5976	8369	11568	5106

Appendix B

Operation Procedures for the Impactor Device

Boot up

1. Power strip located on the back of the frame should be ON.

2. Turn the computer on and allow it to boot up.

3. Make sure the black switch located on the right front leg is in the on position.

4. Twist the red safety switch on.

5. Make sure the load cell signal conditioner, the pressure regulator located behind the left

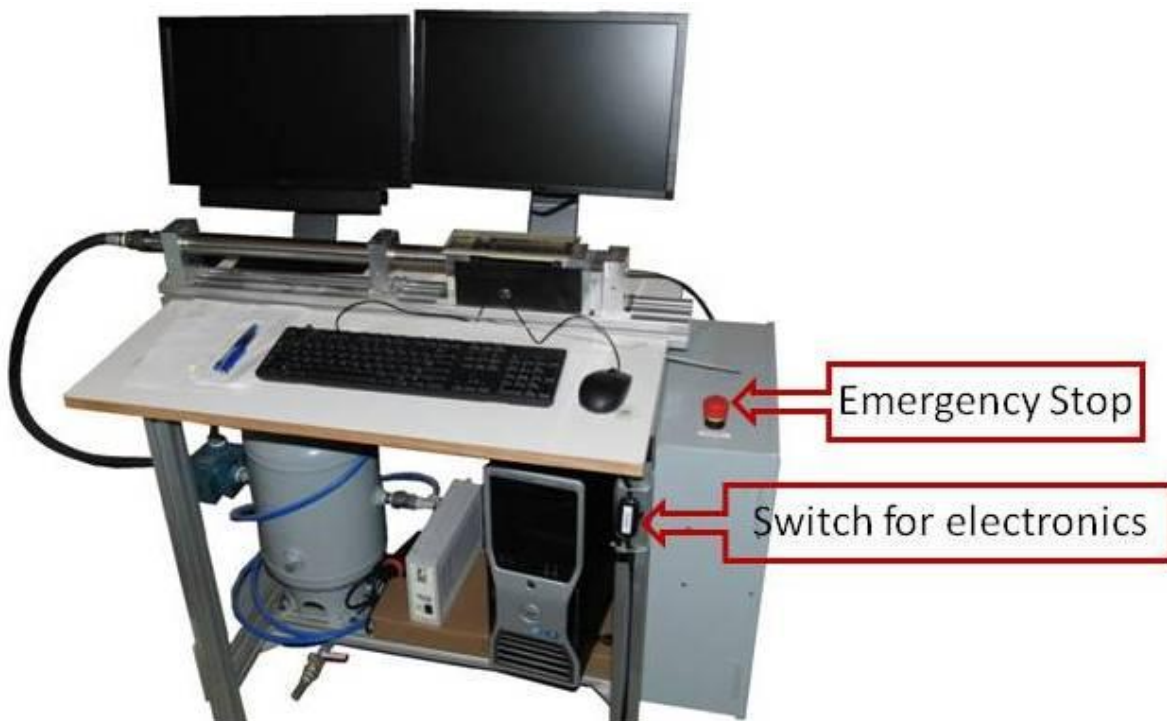   monitor, and the infrared sensors located in the electronics box are on.

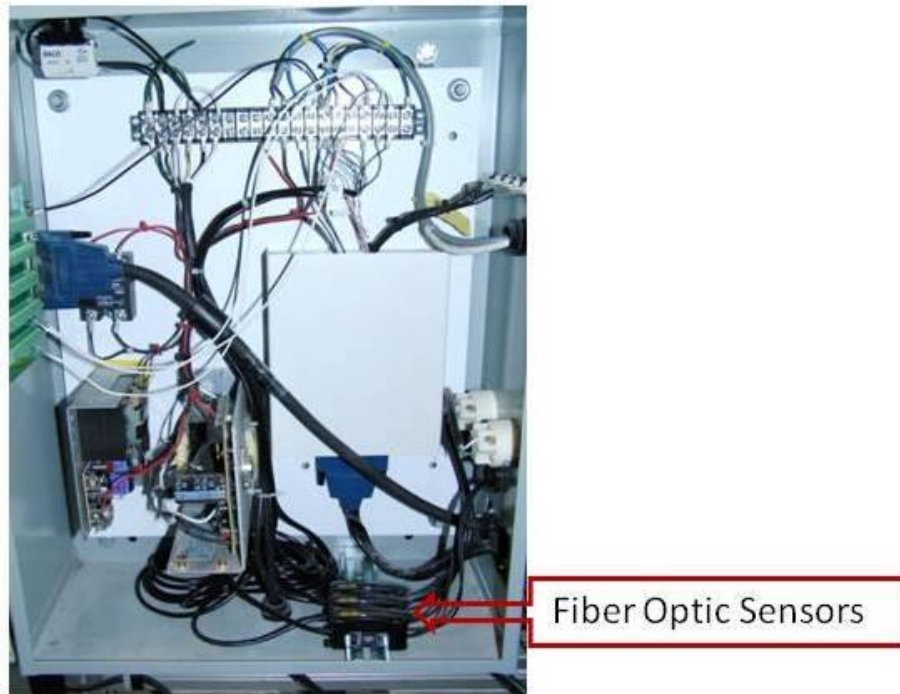**Figure B.1 Impactor device and startup switches.**

Figure B.2 Electronics box.

LabView Front Panel Operation

1. Open LabView and select "Scott's Impactor.vi" from the list of recently opened vi's, or double click it's icon on the desktop and run it. The **Controls** box is used to set up the impact and is highlighted blue, as in Fig B.3, before pressing the **Fire** button.

2. The VI has the ability to either physically fire the cannon, or read previously-written output files and re-process the impact. The **Data From** vertical toggle switch between the **Fire** and **Stop** buttons in the **Controls** box determines which of the two operations is executed when the **Fire** button is pushed. Figure B.4 shows the **Controls** box changes associated with the vertical toggle switch.

Figure B.3 Front panel and showing the blue Controls box used before firing. Graphs of load-time (top right), stress-strain (bottom right) and strain (center) are updated after firing the cannon.

Figure B.4 Two different operations are available for the Controls box: importing a previous impact file (left) and firing the cannon (right).

Option 1: Data from File

1. Switch the **Data From** toggle switch down. The **Fire** button should be bordered in black.

2. Select the desired file from the **Force In** selection box in the **Data Recording** section. The file must have the same name as when it was created. File names are produced by the program as follows: *strain rate_striker bar speed_bar length_(sample length, sample diameter)_ note*.

3. The directory for a **Summary** file can be set in the **Data Recording** section. The summary file saves impact results including date, comment, strain rate, max strain, COR, impulse, bar velocity, and sample diameter and length. The summary file content is displayed in the table below the **Controls** box. The **Wave Out** indicator shows the directory and filename of the last saved file.

4. Under **DAQ Parameters,** the **File Name Offset** is used to properly offset the file name characters so bar speed, sample length etc. can be read from the file name. Adjust its value so that the characters in **Strain Rate** matches the strain rate in the file name in the **Force In** selection box.

5. Make a comment in the **Note** text box if desired. The **Count** number is an automated increment for repeated impacts with the same **Note**. If you want an incremented number to follow the note, set **Count** to 1 and it will automatically increment and be included in the note. Set **Count** to zero to deactivate it.

6. Press the **Fire** button. The cannon will not fire.

Option 2: Fire the Cannon

1. Switch the **Data From** toggle switch up, which will turn it yellow. The **Fire** button will be bordered in yellow.

2. Select the appropriate **Load Cell** (500 lbs default).

3. Select **Length** for the **Impact Bar** section. Bar weight is automatically assigned according to bar length and can only be changed in the rear panel. Load the striker bar into the end of the barrel and use a rod to push it to the back of the barrel.

3. Set the desired **Line Pressure** (suggested between 4-10 psi). Overly high pressures will max out and damage the load cell.

4. Define the **Length** and **Diameter** in the **Sample** section. Apply a thin layer of grease to the sample and mount it to the load cell. Close the clear protection lid.

6. The **DAQ Parameters** section control how the load cell is read. After the cannon is fired, the program waits a period of time set by **Delay**, and then records a number of **Samples** at the specified **Frequency.**

7. In the **Data Recording** section, the directory for a **Summary** file can be set. The summary file saves impact results including date, comment, strain rate, max strain, COR, impulse, bar velocity, and sample diameter and length. The summary file content is displayed in the table below the **Controls** box. The **Wave Out** indicator shows the directory and filename of the last saved output file which includes time, load and sample displacement.

8. Make a comment in the **Note** text box if desired. The **Count** number is an automated increment for repeated impacts with the same **Note**. If you want an incremented number to follow the note, set **Count** to 1 and it will automatically increment with each impact and be included in the note. Set **Count** to zero to deactivate it.

9. Press the fire button.

After Pressing the Fire button

1. The **Controls** box will turn grey and the **Load Indexing** box will turn blue (Fig B.5).

2. The program tries to automatically crop the force signal to isolate the impact. A suggested **Start Index** and **Length** of the impact is displayed along with the corresponding force-time graph. Manually refine **Start Index** and **Length** as needed to show the desired force-time and stress-strain curves.

3. To save impact data, click the **Write File** button to say "yes" and then push **Done.** If the **Write** file says "no", then no data is recorded. The data saved includes the **Summary** file of impact performance and the **Wave Out** file of time, load and sample displacement. A text file of tabulated stress-strain values is also saved to the following directory by default:
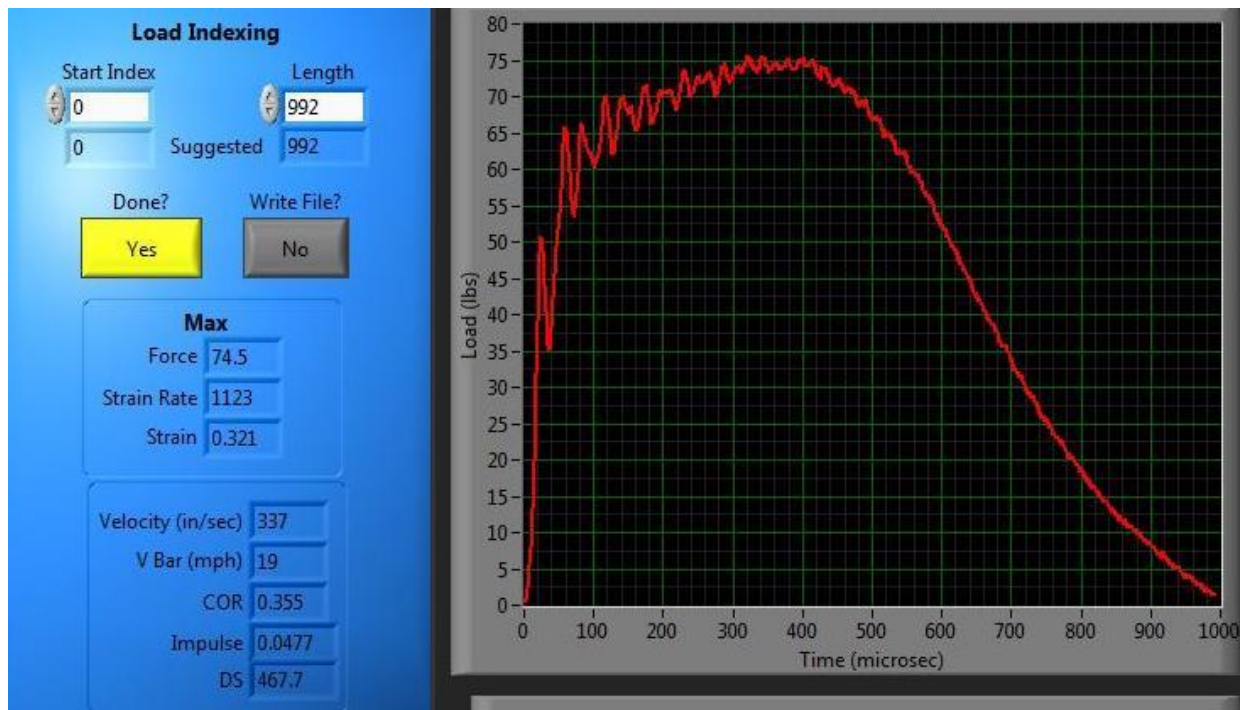
C:\Users\Power User\Desktop\Impactor Files\Old tests.

Figure B.5 Load Indexing Box and force-time curve.